Passive Open Planar Microwave Circuit Analysis by Enhanced Spectral Domain Method †

Hasan Huseyin Balik

December 1997

†A thesis submitted to the University of Bristol in accordance with the requirements for the degree of Doctor of Philosophy in the Faculty of Engineering, Department of Electrical and Electronic Engineering

Abstract

Passive planar microwave circuits and planar antennas are essential components of electronic communication systems utilising the microwave region of the electromagnetic spectrum. This thesis is concerned with the development of a method which allows efficient mathematical modelling to be obtained, giving the interactive design tool capability of the simpler techniques but with the accuracy of the rigorous methods. The Spectral Domain Method (SDM), which is shown in the literature to be an efficient technique for the analysis of components and discontinuities of the passive planar microwave circuits, has been chosen to meet these requirements. SDM requires a set of basis functions to be defined for the unknown current distribution and the choice of this set is crucial to the efficiency of the technique. The solution of this problem is presented in this research in the form of precalculated basis functions and of the application of sub–gridding.

The SDM is a frequency domain technique and requires repeated calculation of the impedance matrix at each frequency point of interest. Special techniques to reduce the number of the impedance matrix elements, which need to be calculated, and to speed up the two–dimensional continuous integration have been introduced. The adaptive integration technique, which consists of an adaptive integration range and an adaptive integration step, has been introduced to limit the two dimensional continuous integration over an infinite surface to finite computer resources. The use of the asymptotic functions and of the location vector calculation are discussed. The symmetry in both the Green's function and the impedance matrix has also been exploited.

The method described in this thesis has been widely verified against both alternative techniques and measured data for realistically complex circuits. The reduction in computation time achieved is such as to make viable the interactive design of the open planar microwave circuits and planar antennas with a full–wave rigorous technique.

In memory of my grandfather
Huseyin BALIK
1910–18 October 1997

Acknowledgements

I would like to express my gratitude to all the people who have made completion of this thesis possible. In particular I would like to thank Professor Joe McGeehan, Professor Aydin Dumanoglu, Sefa Akpinar for the opportunity of undertaking a Ph.D. at Bristol and their support and encouragement over the years. Financial support, for which I am extremely grateful, has been provided by Karadeniz Technical University in Turkey. I am also most grateful to my supervisor, Dr. Chris Railton, who has been invaluable in the role of advisor throughout the course of this work

I have very much enjoyed working as part of the Centre for Communications Research (CCR). I would especially like to acknowledge Steave Meade, Ian Craddock, K. M. Krishnaiah. I would like to thank Naci Kayaoglu and Ross Wilkinson for reading my thesis, and providing some valuable suggestions. I am also very gratwful to all my friends specially Halil Ibrahim Okumus and Yusuf Baltaci for their friendships and encouragements. I am very much indebted to Sefa Akpinar, Rifat Yazici and Cahit Altan for being my financial guarantors.

Last but not least, thanks to my wife, Dilek, for her unfailing love and support. I express my deepest gratitude. I also thank my father, Osman, my mother Azime, my sister, Hatice, and my brother, Ahmet, for their endless support over the years.

Author's Declaration

Unless otherwise acknowledged, the content of this thesis is the original and sole work of the author. No portion of the work in this thesis has been submitted by the author in support of an application for any other degree or qualification, at this or any other university or institute of learning. The views expressed in this thesis are those of the author, and not necessarily those of the University of Bristol.

Hasan Huseyin Balik

Copyright

Contents

List of Figures

List of Tables

List of Abbreviations

EFIE	Electric Field Integral Equation
FDTD	Finite Difference Time Domain
FFT	Fast Fourier Transform
HF	High Frequency
IEM	Integral Equation Method
MFIE	Magnetic Field Integral Equation
MIC	Microwave Integrated Circuit
MoM	Method of Moments
MPIE	Mixed Potential Integral Equation
MMIC	Monolithic Microwave Integrated Circuit
SDM	Spectral Domain Method
TE	Transverse Electric
TEM	Transverse Electromagnetic
TM	Transverse Magnetic
TLM	Transmission Line Matrix
UHF	Ultra High Frequency

List of Symbols

E	Electric filed intensity
D	Electric flux intensity
H	Magnetic field intensity
B	Electric flux intensity
J	Electric current density
ρ	Electric charge density
ϵ	Permittivity
μ	Permeability
σ	Conductivity
k_x, k_z	Fourier transform variables
G	Dyadic Green's function
G^{∞}	Asymptotic form of the Green's function
Z	Impedance matrix
V	Excitation vector
π	Pi
λ	Wavelength
k_n	Propagation constant or wave number
k_o	Free space wave number
w	Weighting function

List of Notations

ψ	Any function (possibly a vector) in the space domain
$\boldsymbol{\psi}$	Any function (possibly a vector) in the spectral domain
A	Any matrix in the space domain
$\mathbf{A}$	Any matrix in the spectral domain
A^T	Transpose of A
$\nabla \cdot \psi$	Divergence of vector function ψ
$\nabla \times \psi$	Curl of vector function ψ

List of Publications

Hasan H. Balik and C. J. Railton, "Sub–gridding in the spectral domain method for the analysis of planar circuits and antennas," in *Proceedings of TELSIKS - 97*, (Nis, Yugoslavia), p.592–595, University of Nis, October 1997.

Hasan H. Balik and C. J. Railton, "Adaptive numerical integration technique for the analysis of open planar circuits and antennas," in *Proceedings of* 3^{rd} *High Frequency Postgraduate Student Colloquium*," (Leeds, U.K), p.100–105, University of Leeds, September 1997.

Hasan H. Balik and C. J. Railton, "Effective excitation mechanism for open planar microwave circuits" in *Proceedings of Spring Research Conference - 97*, (Bristol, UK), p.14, University of Bristol, April 1997.

Chapter 1

Introduction

1.1 Introduction

Improvements in technology have always affected society as well as their standards of living. The last few decades have witnessed advances in communication and computer technology (referred to collectively as information technology). These developments have transformed society from the *industrial* to the so-called *information* society [1, chapter 1].

One of the key technologies in an information society is the means of information exchange. All means of modern communication rely on the modulation of electromagnetic waves which are broadcast around the world through the atmosphere or transmitted along the cable from one point to another.

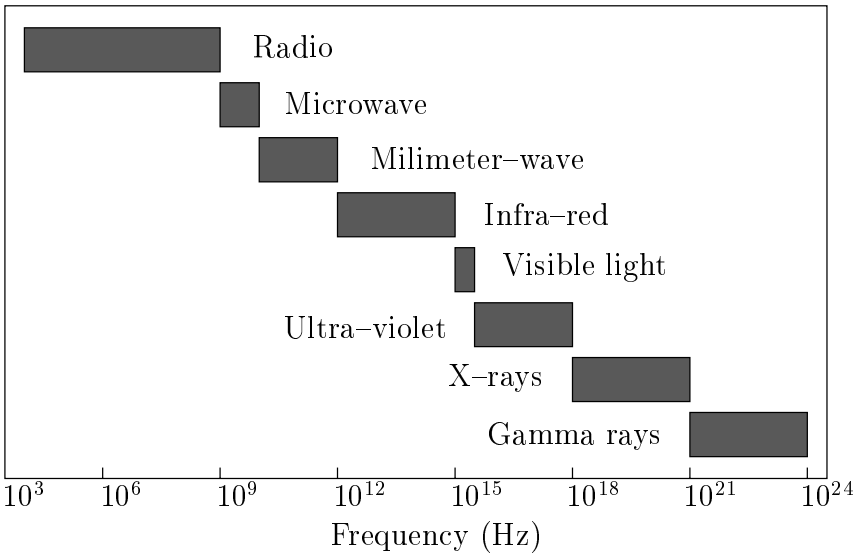

Figure 1.1: The electromagnetic spectrum

An electromagnetic wave, which is a completely intangible phenomenon that propagates at extremely high speed through space, is generally described in terms of its frequency (number of cycles per second) or its wavelength (distance between two cycles). The most common subdivisions of the electromagnetic spectrum, which is continuous from less than 1 Hz to greater than 10^{24} Hz, are shown in figure 1.1.

Frequency Band	Designation	Typical service
3–30 kHz	Very low frequency (VLF)	Navigation, sonar
30–300 kHz	Low frequency (LF)	Radio beacons, navigational aids
300 kHz–3 MHz	Medium frequency (MF)	AM broadcasting, maritime radio, Coast Guard communication, direction finding
3–30 MHz	High frequency (HF)	Telephone, telegraph
30–300 MHz	Very high frequency (VHF)	Television, FM broadcast, air–traffic control, police, taxicab mobile radio, navigational aids
300 MHz–3 GHz	Ultra high frequency (UHF)	Television, satellite communication, radiosonde, surveillance radar, navigational aids
3–30 GHz	Super high frequency (SHF)	Airborne radar, microwave links, common–carrier land mobile communication, satellite communication
30–300 GHz	Extreme high frequency (EHF)	Radar, experimental

Table 1.1: Frequency band designation

There are a number of classification schemes in use to designate frequency bands in the electromagnetic spectrum. These classification schemes are summarised in table 1.1.

The lower frequency bands can provide only a limited amount of spectrum and are already heavily used. The increase in demand for data transmission necessitated communication systems to be moved upward to less–used frequency bands with more available bandwidth. Although the frequencies above 3 MHz were considered useless [2, chapter 6] in 1912 at the Radiotelegraph Conference in London, available cellular mobile telephone services now operate in Europe at around 900 MHz and latest generation of services (DCS1800 system) operates at 1.8 GHz.

The frequency region of interest in this thesis is the microwave region. The definition of the microwave region varies. It is used for those wavelengths in the range 30 cm–0.3 mm which correspond to the frequency range $10^9 - 10^{12}$ Hz in [3, chapter 1], whereas

in [4, chapter 1] microwaves are defined as those wavelengths in the range 1 cm–1 mm.

At low frequencies, the complicated equations of electromagnetism can be simplified to straightforward circuit theory. As the frequency increases up to the microwave frequencies, the assumptions of traditional circuit theory are no longer valid. Thus in order to characterise microwave circuits, the fundamental concepts of electric and magnetic field have to be considered.

Communications, heating and remote sensing are common areas which utilise the microwave frequency range. Microwave heating has become very popular in both domestic and industrial environments. However, the communications industry has been continuing a rapid growth in demand for the use of the microwave frequency range. The spread of satellite communications and television broadcasting is an evident use of the microwave frequencies. Furthermore, mobile communications networks are expected to continue to grow rapidly in coverage, with new systems using the microwave frequencies.

The rapid increase of higher frequency usage over recent years has created a demand for accurate design tools. A design tool which allows "right first time" prediction is invaluable to the realisation of cost–effective research and development. The accuracy of the design tool is often balanced against the computational effort required. Existing packages allow rapid design, but their accuracy is not sufficient for today's applications. Alternatively there are highly–accurate analysis tools available, but they require a large amount of computer resources. For example, software packages such as Linmic and Sonnet are available, which utilise results from more rigorous electromagnetic analysis [5, 6] but are restricted by the inherent computational overheads.

The demands of the design engineer require a technique which is accurate, yet retains the interactive design capabilities of the simpler techniques. High speed computers do

not solve the problem, because the complexity of the circuits to be designed and the computational overhead required for accurate modelling will outstretch any development in computer technology. Therefore a design tool, which reverses the trend for the requirement of ever–increasing computer resources, is required. Throughout this thesis, fast accurate numerical microwave circuit analysis techniques will be sought.

1.2 A Brief Review of Electromagnetism

The problem of electromagnetic analysis is actually a problem of solving Maxwell's equations, subject to given boundary conditions. In other words, electric and magnetic fields, which vary with time, are governed by physical laws described by a set of equations. Initially these equations were derived from experiments carried out by several investigators.

Maxwell's equations, which are a set of fundamental equations governing all electromagnetic phenomena, can be written in both integral or differential forms, but here they are only presented in their differential forms. For the time-varying fields, Maxwell's equations in differential forms can be written as

$$\nabla \times E + \frac{\partial B}{\partial t} = 0 \quad \text{(Faraday's law)} \tag{1.1}$$

$$\nabla \times H - \frac{\partial D}{\partial t} = J \quad \text{(Maxwell–Ampere's law)} \tag{1.2}$$

$$\nabla . D = \rho \quad \text{(Gauss's law)} \tag{1.3}$$

$$\nabla . B = 0 \quad \text{(Gauss's law–magnetic)} \tag{1.4}$$

where

E = electric field intensity (volt/metre)

D = electric flux intensity (coulomb/metre^2)

H = magnetic field intensity (ampere/metre)

B = magnetic flux intensity (weber/metre^2)

J = electric current density (ampere/metre^2)

ρ = electric charge density (coulomb/metre^3)

Another fundamental equation, which is known as the *equation of continuity* and satisfies the conservation of charge, is given by;

$$\nabla.J = -\frac{\partial \rho}{\partial t} \tag{1.5}$$

Only three of (1.1)–(1.5) are independent, and then called *independent* equations, the other two equations can be derived from the chosen independent equations, and thus are called *auxiliary* or *dependent* equations. The three selected independent equations amongst Maxwell's four equations and the equation of continuity are less than the number of unknowns. These equations are called *indefinite* and must be transformed to *definite* by seeking constitutive relations. These relations are,

$$D = \epsilon E \tag{1.6}$$

$$B = \mu H \tag{1.7}$$

$$J = \sigma E \tag{1.8}$$

where the constitutive parameters ϵ, μ, σ are the permittivity (farad/metre), permeability (henry/metre) and conductivity (siemens/metre) of the medium. The above equations are general, in that the media can be *nonhomogeneous, nonlinear*, and *nonisotropic*. These are the fundamental equations of electromagnetism.

The electromagnetic field at the boundary of two different media must satisfy a set of equations called *boundary conditions*. In the electromagnetic problem involving two or more media, Maxwell's equations together with the boundary conditions are required to be simultaneously satisfied.

1.3 Basic Concepts of Microwave Circuits

The physical implementations of modern microwave systems generally take the form of MIC (Microwave Integrated Circuits) [7, 8]. This family can be subdivided into hybrid MIC and MMIC (Monolithic Microwave Integrated Circuits). The latter are completely integrated circuits where planar transmission lines, distributed elements and active devices are formed on the same substrate. In contrast, the active devices of the hybrid MIC are separate packages bonded to the integrated circuit. Although, MMICs have many advantages such as the small package size and economics of scale in manufacture, the hybrid MIC is inherently simpler to manufacture due to separate fabrication of active devices.

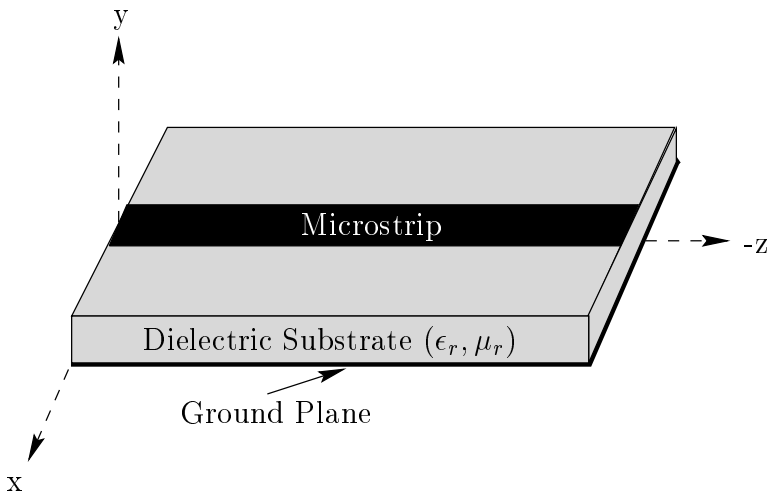

Figure 1.2: The geometry of a microstrip line

The microwave integrated circuits of interest in this thesis are passive open planar microwave circuits. The term *passive* implies that the circuits of interest contain no active devices and the term *planar* implies that the circuit has a planar metallisation surface with arbitrary shape. Moreover, the circuits of interest are completely open and hence contain no side walls. Planar antennas may also be included within this description. The basic element in the planar microwave circuit is a transmission line, known as *microstrip*. This microstrip line consists of a grounded conducting plane,

an insulating sheet, which is a dielectric substrate, and a conducting strip as shown in figure 1.2.

Although microstrip is very simple and useful in the design of microwave miniature and integrated circuits, its theoretical treatment is more complicated. Since the dielectric material does not completely surround the conducting strip, consequently the fundamental mode of propagation is not a pure TEM–mode [7, 9]. For a single infinite transmission line, a diagram of the E and H field is shown in figure 1.3. The fringing field is evident in figure 1.3, and there is an inherent non-zero component of E and H in the direction of propagation. Of course at low frequencies, the mode can be approximated as *a quasi*–TEM, but in this research, this approximation is not applicable to compact integrated circuits operating at microwave frequencies.

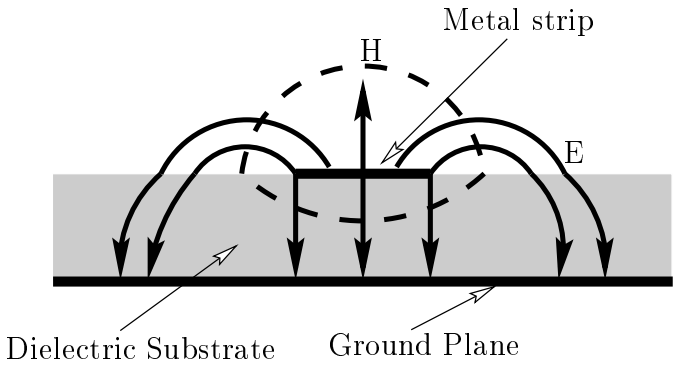

Figure 1.3: Illustration of electromagnetic field associated with a microstrip transmission line

The corresponding surface current density on the microstrip has singularities at the strip edges [10]. As the edge is approached, the current in the direction of propagation is singular and the current in the direction perpendicular to the propagation tends to zero, as illustrated in figure 1.4. The inclusion of the edge conditions is a fundamental part of the research presented in this thesis.

The modelling of infinite microstrip line problems is necessary in order to find the guided wavelength, propagation constant and surface current distribution. These

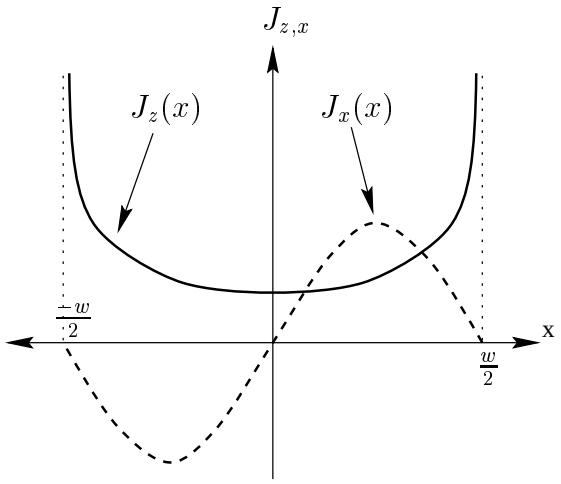

Figure 1.4: Illustration of typical microstrip current distributions

parameters will be discussed and used to speed up microstrip circuit calculations. However this thesis is primarily concerned with the modelling of finite passive open microwave circuits which consist of several discontinuities such as open–ends, gaps, corners and changes in width. These are fundamentally constructed as a finite section of microstrip line, the junctions of which form such discontinuities as shown in figure 1.5.

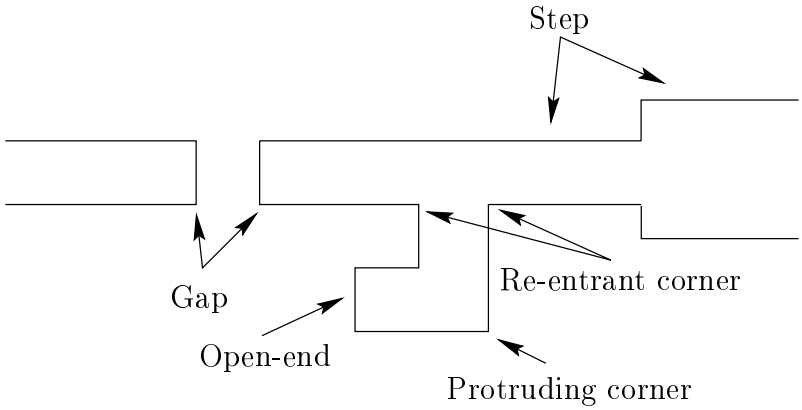

Figure 1.5: Illustration of microstrip singularities and discontinuities

Jackson has calculated the current distribution for microstrip open–end and gap discontinuities in [11]. Re-entrant and protruding corners have been predicted the quasi–

static current distribution by Van Bladel *et al* [12] and Marchetti *et al* [13]. The actual current distribution is more complex than that predicted by [12, 13]. For example, frequency–dependent behaviour and coupling between discontinuities are not taken into account. However, the inclusion of these current distributions in the numerical analysis will greatly increase the convergence of the technique.

To reduce the computational overheads of circuit analysis is the core of this research. Functions which include *a priori* knowledge of the current distribution of these corners have been derived in [14, chapter 4] for shielded planar microwave circuits and, in this research are adapted to open planar microwave circuits.

1.4 Thesis Outline and Summary

This thesis is concerned with the efficient mathematical modelling of passive open planar microwave circuits. The purpose is to develop a design tool which allows realistically complicated metallisation patterns to be defined and to be solved using modern computing resources at a desired accuracy. The techniques are presented in this thesis which are used to design an interactive tool capable of allowing the rapid analysis of complex microwave circuit problems.

In chapter 1, the area of research for this thesis has been introduced and an outline of the following chapters is given.

In chapter 2, a brief summary of alternative techniques is given and the basic philosophy of each technique is highlighted together with its advantages and disadvantages within the context of its application to passive planar microwave circuits. The chosen Spectral Domain Method is introduced and discussed in the context of alternative techniques. The historical development is reviewed and fundamental theory is presented for a general formulation.

In chapter 3, the choice of current basis functions as introduced in chapter 2 is described in detail. Variants of the present choice of basis functions are compared to those commonly used by other researchers. A technique is presented for the derivation of functions which allows the efficient inclusion of *a priori* knowledge of the current distribution and sub–gridding of the metallisation due to discontinuity. Examples are given to illustrate and verify the proposed enhancements.

Chapter 4 discusses enhancements to reduce the computational overheads of the impedance matrix calculation and the number of impedance matrix elements to be calculated at each frequency point. An adaptive integration technique, which consists of an adaptive integration range and an adaptive integration step, is introduced to speed up numerical integration of the impedance matrix elements. The asymptotic form of the Green's function, which splits the impedance matrix into two parts is applied for open structures. A location vector calculation is also proposed to reduce the number of impedance matrix elements to be calculated for the same size of the impedance matrix. Special techniques for numerical integration of the impedance matrix are presented to further reduce the numbers of the impedance matrix elements to be calculated in one dimension to speed up overall integration. The effects of the loss in dielectric substrate are also taken into account and details are given. Numerical examples are given to illustrate the numerical convergence and the effects of loss in substrate.

Chapter 5 introduces the derivation of network parameters, which is required to present the main results in this thesis. The results are presented in the forms of S–parameters and examples are given to highlight the efficiency of the excitation model. This method is also compared with other available models and the improvement in the accuracy is emphasised.

Chapter 6 presents results for the analysis of realistically complex open microwave circuits compared to measured data and numerical results of other techniques. Features of the enhancements in this thesis are discussed in the context of the circuits

modelled.

In chapter 7, the derivation of the Green's function for multilayer structures is discussed and the immitance approach is given in detail. The asymptotic form of the Green's function, which is proven to be effective to calculate the impedance matrix in chapter 4 for two–layer circuits, is derived by the use of the immitance approach for multilayer structures. To verify the accuracy of the immitance approach, a simple microstrip line is modelled by the two dimensional version of the technique and compared with published data. The effects of the order of dielectric substrates in the microstrip structures are illustrated by modelling the multilayer microstrip line and resonator.

Chapter 8 summarises the research implemented in the preceding chapters and suggests potentially rewarding directions for future investigation.

References

[1] I. J. Croddock, *Enhanced Numerical Techniques for Time Domain Electromagnetic Analysis*. PhD thesis, University of Bristol, October 1995.

[2] M. Paetsch, *Mobile Communications in the U.S. and Europe*. Artech House, 1993.

[3] R. Chatterjee, *Elements of Microwave Engineering*. Ellis Horwood Ltd., 1986.

[4] R. E. Collin, *Foundations for Microwave Engineering*. McGraw-Hill, 1992.

[5] R. H. Jansen, "The spectral–domain approach for microwave integrated circuits," *IEEE Transaction on Microwave Theory and Technique*, vol. 33, pp. 1043–1056, October 1985.

[6] J. C. Rautio and R. F. Harrington, "An electromagnetic time–harmonic analysis of shielded microstrip circuits," *IEEE Transaction on Microwave Theory and Technique*, vol. 35, pp. 726–729, August 1987.

[7] Y. Konishi, *Microwave Integrated Circuits*. Marcel Dekker Inc., 1991.

[8] D. B. Shorthouse, *The CAD and Analysis of Passive Monolithic Microwave Integrated Circuits by the Finite Difference Time Domain Technique*. PhD thesis, University of Bristol, June 1992.

[9] P. Lorrain, D. R. Corson, and F. Lorrain, *Electromagnetic Fields and Waves : Including Electric Circuits*. W. H. Freeman and Company, 1988.

[10] T. Itoh, *Numerical Techniques for Microwave and Millimeter–Wave Passive Structures*. John Willey and Sons, 1989.

[11] R. W. Jackson and D. M. Pozar, "Full–wave analysis of microstrip open–end and gap discontinuities," *IEEE Transaction on Microwave Theory and Technique*, vol. 33, pp. 1036–1042, October 1985.

[12] R. D. Smedt and J. G. V. Bladel, "Field singularities near aperture corners," *in IEE Proceedings Pt.*, vol. 134, pp. 694–698, 1987.

[13] S. Marchetti and T. Rozzi, "H–field and J–current singularities at sharp edges in printed circuits," *IEEE Transaction on Antennas and Propagation*, vol. 39, pp. 1321–1331, September 1991.

[14] S. A. Meade, *The Rapid and Rigorous Mathematical Modelling of Passive Planar Microwave Circuits*. PhD thesis, University of Bristol, March 1994.

Chapter 2

Available Full–Wave Analysis Techniques

2.1 Introduction

For the last two decades, the high–speed computer has influenced the computation of electromagnetic problems, to the point that most practical computations of fields are now done numerically on computers. This is because most of the practical problems in electromagnetics can be solved numerically but cannot be solved analytically. As a result, the science of computational electromagnetics is a mixture of electromagnetic theory, mathematics and numerical analysis.

Most of the early numerical analysis methods for microwave integrated circuits were based on either *quasi*–static or magnetic wall approximations, in which only the TEM–mode of propagation was taken into account. At operating frequencies high enough to fulfil contemporary demands for spectrum space, it becomes necessary to use full–wave analysis to include effects like coupling due to surface waves and discontinuities. This chapter introduces modelling techniques which allow a rigorous full–wave analysis to be achieved. In this context the descriptive term *full–wave* is used to define the set of numerical techniques which include all field components and thus allow rigorous analysis of dispersive structures, where coupling between circuit's elements cannot be ignored in the microwave frequency band of interest.

Currently there are several available methods which fulfil these requirements. The Spectral Domain Method (SDM) has been chosen to analyse open planar microwave circuits. It is a very popular method but has been criticised for being computationally intensive, due to the need for the formation and inversion of a large matrix. Another criticism is that SDM is severely limited in the complexity of the metallisation patterns which it can handle. The results of this research overcome the limitations mentioned above and allow an interactive design tool to be developed for the computer aided design of passive open planar microwave circuits as well as planar antennas.

To present a cross–section of the more commonly used methods with which SDM is compared, a brief summary is given concerning alternative techniques in section 2.2.

The basic philosophy of each technique is highlighted together with its advantages and disadvantages. All criticism of alternative approaches is given within the context of the application to passive planar microwave circuits. The techniques considered are,

- Finite–Difference Time–Domain Method (FDTD)
- Transmission Line Matrix (TLM)
- Integral Equation Method (IEM)

The above techniques do not include all available methods. FDTD and TLM have minimal analytical preprocessing and are therefore applicable to a wide variety of applications, but require a large amount of computer resources for complex circuits. IEM is quite similar to the SDM, therefore it is included and given in relatively more detail than the others to make SDM easy to understand. SDM and IEM are both based on solving integral equations, but in different domains. The majority of the calculations of IEM take place in the space domain, in contrast to the spectral domain where all SDM calculations take place. Both require relatively large overheads in analytical preprocessing, but the results may be yielded very quickly for certain classes of problems with efficient implementations. It is proposed in this thesis that open planar microwave circuits fit into the class of problems suitable for analytical preprocessing without restricting the application to unrealistically simple structures.

The basic philosophy of SDM is summarised in section 2.3 along with the historical background of the present implementations. The choice of SDM for the fast rigorous modelling of open planar microwave circuits is justified in comparison to the alternative techniques mentioned above. The general formulation of SDM is included for open planar circuits. This chapter is intended to provide sufficient background knowledge to follow the enhancements in the following chapters.

2.2 Available Full–Wave Analysis Techniques

2.2.1 Finite–Difference Time–Domain Method (FDTD)

The Finite–Difference Time–Domain Method is a full–wave numerical technique in which Maxwell's time dependent electromagnetic curl equations are replaced by difference equations. The original FDTD algorithm proposed by Yee [1] in 1966 is specifically designed to solve electromagnetic problems in a rectangular co–ordinate system and it assumes a lossless, isotropic and nondispersive medium. It uses the linear central difference approximations for the time and space derivatives of the electric and magnetic fields directly to replace the differential operators of the curl equations.

The Finite Difference Time Domain Method has been applied to a wide variety of electromagnetic problems including electromagnetic scattering [2], the analysis of various planar transmission lines and discontinuities [3, 4], dielectric waveguides [5], planar circuits [6, 7], microstrip filters and couplers [8], active [9] and passive [10] antennas and medical electronics [11].

The calculation of an electric field vector at a particular point in time and space depends upon the value of that field at the previous time, plus a function of the surrounding perpendicular magnetic fields. Similarly, the magnetic field depends upon the previous value in time plus a function of the surrounding perpendicular electric fields. As the electric field and magnetic field vectors are calculated in turn, the electric fields are calculated a half time step out of sequence with the magnetic values. Numerical boundary conditions are required for limit infinite open structures to finite computer resources. The frequency response can be obtained by taking the Fourier transform of the resulting time–domain transient response.

FDTD is inherently computationally intensive because of the general nature of the model with minimal analytical preprocessing. Advances have been made to include *a*

priori knowledge of the field behaviour at metallic edges by including the singularities in the iterative calculation [12]. Although improved boundary conditions and non–uniform mesh [13] have reduced the computational overhead, FDTD still remains an analysis tool instead of an interactive design tool, due to the relatively long run–times required. FDTD is best suited to more complex structures than the planar geometry of interest in this thesis.

2.2.2 Transmission Line Matrix (TLM)

The Transmission Line Matrix, which was developed by P. B. Johns and his co–workers [14, chapter 8] represents a computer simulation of electromagnetic fields in three–dimensional space and time. TLM is based on the discrete model of Huygen's principle which is an alternative form of Maxwell's equations, whereas the Finite–Difference Time–Domain Method (FDTD) is a discrete form of Maxwell's equations. Therefore TLM is similar to FDTD and can be derived directly from Maxwell's equations using differencing [15, 16]. Celuch and Gwarek demonstrated the equivalence of the two methods in [17]. As a results, FDTD and TLM share the same limitations and advantages.

The underlying principle of the Transmission Line Matrix Method is a mesh of discrete nodes connected by transmission lines, with the solution derived in the time domain. In common with FDTD, the main advantage of TLM is that it is possible to include time–dependent parameters in the algorithm and the ease with which most complicated structures can be evaluated. The main disadvantage of the method is that it is limited by the amount of memory storage required, which depends on the complexity of the structure and the nonuniformity of the field [14]. The technique is not optimised for planar structures thus it is computationally intensive compared to the optimised Spectral Domain Method [18].

2.2.3 Integral Equation Method (IEM)

The Integral Equation Method is one of the full–wave techniques used to analyse microwave and millimetre–wave integrated circuits, and is reviewed by Mosig [14, chapter 3]. It is based on solving the integral equation which is also used by the Spectral Domain Method. The majority of the calculations take place in the space domain, in contrast to the spectral domain. The spectral domain is used only during the calculation of the Green's functions, then inverse transforms are taken and the integral equation is solved in the space domain. Due to this similarity, this technique is given here in relatively more detail to facilitate the comparison to SDM

Katethi and associated authors [19–22] used IEM to analyse microstrip discontinuities for open and shielded structures. The Integral Equation Method has been enhanced by several authors and hence called with some extra names to suit different applications. The Singular Integral Equation Method is used to determine the normal modes of propagation in general transmission lines taking finlines as example in [23], whereas in [24] the Boundary Integral Equation Method is proposed for the full–wave analysis of suspended planar transmission line with finite metallisation thickness. Morisue *et al* have launched the Lorentz Gauge vector potential formulation for the Boundary–IEM in [25]. The application of the IEM to anisotropic inhomogeneous waveguides has been presented by Urbach [26]. A Volume–Surface IEM is published in [27] to enable the calculation of electromagnetic fields in complicated 3–D models.

The formulation of the integral equation can be written in different ways. The more common one is the electric field integral equation (EFIE) formulation where the fundamental unknown is the surface electric current flowing on the conductor. Alternative formulations are the magnetic field integral equation (MFIE) and mixed potential integral equation formulations (MPIE) [14, chapter 3]. However the magnetic field integral equation is not suitable for microstrip integrated circuits. This is because, it is numerically unstable when the embedded conductors are thin and it fails completely

for zero–volume conductors [14, page 139].

To demonstrate the basic philosophy of the Integral Equation Method, the formulation is summarised for the electric field and surface current (Electric Field Integral Equation, EFIE). An electric field integral equation which relates the surface current and electric field is defined via a dyadic Green's function in the space domain.

$$\begin{aligned}\iint [G_{zz}(x-x^{'},y,z-z^{'})J_z(x^{'},z^{'})+G_{zx}(x-x^{'},y,z-z^{'})J_x(x^{'},z^{'})]dx^{'}dz^{'} &= E_z(x,z)\\ \iint [G_{xz}(x-x^{'},y,z-z^{'})J_z(x^{'},z^{'})+G_{xx}(x-x^{'},y,z-z^{'})J_x(x^{'},z^{'})]dx^{'}dz^{'} &= E_x(x,z)\end{aligned} \tag{2.1}$$

No convenient form of the Green's function exits in the space domain for the planar circuit configurations of interest [18]. The most efficient technique formulates the Green's function in the spectral domain, and therefore is closely related to the SDM, where x, z replaced by their spectral counterparts k_x, k_z according to the double Fourier transform. It is therefore the spectral domain which is used during the calculation of the Green's functions, and then inverse transforms are taken. This procedure is one of the main disadvantages of IEM as it is computationally intensive.

Equation 2.1 contains four unknowns, namely J_x, J_z, E_x and E_z. At least two unknowns must be eliminated. In common practice, the Method of Moments (MoM) is used to solve equation 2.1. The first step of the analysis is to expand the unknown current distribution on the metallisation of the circuit as a set of known basis functions with unknown coefficients. Basis functions which are defined as non–zero only on the metallisation are given by;

$$J_s(x,z) = \sum_{n=1}^{N} a_n J_{sn}(x,z), \qquad s = x,z \tag{2.2}$$

The basis functions (J_{sn} in equation 2.2) must be chosen to approximate the unknown current distribution on the metallisation of the circuit. Note that in equation 2.2, the

Fourier transform of the basis functions is not required, as the algorithm operates in the space domain.

After application of the Method of Moments using weighting functions, equation 2.1 becomes the matrix equation,

$$[Z][I] = [V] \tag{2.3}$$

where Z is the impedance matrix and I is the vector of the coefficients (a_n in equation 2.2) and V is the excitation vector defined as zero everywhere except for sources. If current basis and weighting functions are the same, then the procedure is called Galerkin's.

By solving matrix equation 2.3 for the unknown current coefficients, the unknown current distribution of the metallisation of the circuit can be determined for a set of excitation vectors and the S–parameters can be derived.

Equation 2.3 shows that the inverse of Z is required for the final solution. The choice of the current basis function is crucial, since if a large number of basis functions are used, the size of the matrix to be inverted will be large. Thus special care must be taken to minimise the size of the set of current functions for a given problem. This problem is also shared by SDM. The major drawback of the method is that it requires the inverse transform of the spectral domain Green's functions, which must be performed numerically.

2.3 Introduction to Spectral Domain Method

2.3.1 Choice of SDM

The purpose of the work described in this thesis is to develop an efficient full–wave design tool for open planar microwave circuits. The Spectral Domain Method is chosen as it is believed to be capable of meeting these requirements. Although FDTD and TLM have minimal preprocessing, significant analytical preprocessing is not their basic philosophy, therefore redundancies often exist when applied to the planar structures of interest. These redundancies have been reduced to a minimum in SDM by using significant enhancements which will be explained in the following chapters.

Both SDM and IEM are based on solving integral equations, but in different domains. No convenient form of the Green's functions for the planar circuits of interest exist in the space domain, where the majority of the calculations of IEM take place. The most efficient way to find the Green's function is to use an inverse transform from the spectral domain into the space domain. This is computationally intensive and the major drawback of IEM. The principal advantage of using SDM is that the integral equation in the space domain is transformed into an algebraic formulation after Fourier transformation of the convolution form.

The SDM is numerically efficient at the cost of significant analytical preprocessing. This feature imposes certain restrictions on the applicability of the technique. One of the limitations is that SDM normally assumes an infinitesimal thickness for the strip conductor. It is also difficult to analyse circuits with a strip having finite conductivity. No discontinuities are allowed in the substrate in the directions in which Fourier transforms are taken. In spite of these limitations, SDM is one of the most popular and widely used numerical techniques.

The efficiency of SDM will be highlighted throughout the thesis. The existing SDM

is enhanced to allow its use as interactive design tool. The computer run–time will be reduced for circuits including those which are realistically complex. The following sections are devoted to the description of the general formulation on which the present implementation is based.

2.3.2 Historical Developments of Spectral Domain Method

Although it would be impossible to include all works concerning the Spectral Domain Method, even when restricting interest to implementations for planar microwave circuits, it is hoped to present a guide to the historical background which inspired the development of this project.

The analysis in the Fourier transform domain was first introduced by Yamashita and Mittra [28] in 1968 for the computation of the characteristic impedance and the phase velocity of an open microstrip. It was based on *a quasi*–TEM approximation which is a low frequency simplification that neglects the longitudinal electric and magnetic fields supported by the microstrip.

Increasing of the operating frequency has led numerical techniques towards full–wave analysis, because effects such as coupling due to surface waves and discontinuities become significant at high frequencies. Denlinger [29] solved the integral equation using the Fourier transform technique. The solution by his method, however, is strongly dependent on the assumed current distribution on the strip. To avoid this difficulty and allow systematic improvements of the solution for the current components to a desired degree of accuracy, Itoh and Mittra [30] introduced the Spectral Domain Approach, otherwise called the Spectral Domain Method in 1973 for open microstrip lines and enhanced for shielded microstrip lines in [31]. The unknown current distribution on the strip is defined as a set of known current basis functions with unknown coefficients and Galerkin's Procedure is used to yield a homogeneous system of equations to determine the propagation constant and amplitude of current distribution.

The application of the method to a general three–dimensional structure required the introduction of a more advanced formulation. The move in this direction is presented by Itoh [32] with the modelling of a microstrip resonator. In 1980, Itoh introduced a formulation process called the immitance approach [33] for a easy formulation of multilayer structures. This approach is based on the transverse equivalent circuit concept as applied in the spectral domain. An application of the immitance approach was presented by Itoh and Menzel [34] which allowed the analysis of planar resonator antennas for the complex resonant frequency. The historical progress of the Spectral Domain Method until 1984 was summarised by Jansen [35].

A full–wave analysis of microstrip open–end and gap discontinuities in SDM was presented by Jackson [36]. In his analysis, the results were presented for the reflection and transmission coefficients derived with a source formulation of SDM. A time–harmonic electromagnetic field analysis method related to SDM, which allows the modelling of shielded arbitrary shaped planar discontinuities, was presented by Rautio and Harrington [37]. Similarly, Jackson [38] formulated SDM for open irregular microwave circuit discontinuities with semi–infinite feedlines, although Jackson calls his technique as Finite Element Method.

Numerous authors have contributed to the development of SDM. A generalised spectral domain Green's function was described by Das and Pozar [39] in terms of suitable components of the vector electric and magnetic potentials. The works by Railton *et al* who described the asymptotic form of the Green's function in [40] and re–arranged the characteristic equation by making use of its asymptotic properties in 1992 in [41] are seen by the author to be particularly significant. Precalculated current basis functions have been used by Meade [42] to reduce the number of current basis functions required and to include *a priori* knowledge of the current distribution at discontinuities. It can be noticed that the historical development of SDM has been summarised until 1994 which is the starting date of this project. Existing SDM has been improved by the enhancements introduced in this thesis. Meanwhile Tsai *et al* [43] has developed the Mixed Potential Integral Equation Method (MPIEM) in the spectral domain and Kuo

et al [44] has formulated the hybrid–mode Spectral Domain Approach to investigate the dispersion nature of multiple coupled microstrip lines with arbitrary metallisation thickness. General analytical solutions of static Green's functions for shielded and open arbitrary multilayered media have been presented by Li *et al* in 1997.

2.3.3 General Formulation

A general formulation of the Spectral Domain Method for the passive open planar microwave circuits of interest is presented. The following is based on references quoted above. Before formulating this process, the types of equations obtained by SDM and those obtained by a typical space domain formulation are compared. In the space domain, a microwave circuit can be analysed by solving the coupled integral equation given as,

$$\begin{aligned}\iint [G_{zz}(x-x^{'},y,z-z^{'})J_z(x^{'},z^{'})+G_{zx}(x-x^{'},y,z-z^{'})J_x(x^{'},z^{'})]dx^{'}dz^{'} &= E_z(x,z)\\ \iint [G_{xz}(x-x^{'},y,z-z^{'})J_z(x^{'},z^{'})+G_{xx}(x-x^{'},y,z-z^{'})J_x(x^{'},z^{'})]dx^{'}dz^{'} &= E_x(x,z)\end{aligned} \tag{2.4}$$

where

G_{st} is the dyadic Green's function (dependent on frequency, ω),

E_s is the electric field at the air–dielectric interface,

J_s is the current distribution on the metallisation.

Equation 2.4 can be solved if G_{st}, etc., are given . The Green's functions G_{zz}, etc., however, are not available in closed form for the nonhomogeneous structures. The following algebraic equations (2.5), instead of the coupled integral equations (2.4), are obtained in the spectral domain formulation. These equations are Fourier transforms

of the coupled integral equations (2.4).

$$\begin{aligned}\mathbf{G}_{zz}(k_x,d,k_z,\omega)\mathbf{J}_z(k_x,k_z)+\mathbf{G}_{zx}(k_x,d,k_z,\omega)\mathbf{J}_x(k_x,k_z)=\mathbf{E}_z(k_x,d,k_z)\\ \mathbf{G}_{xz}(k_x,d,k_z,\omega)\mathbf{J}_z(k_x,k_z)+\mathbf{G}_{xx}(k_x,d,k_z,\omega)\mathbf{J}_x(k_x,k_z)=\mathbf{E}_x(k_x,d,k_z)\end{aligned} \tag{2.5}$$

where the **bold** quantities are the Fourier transform of corresponding quantities and d is the thickness of the dielectric substrate. The two dimensional Fourier transform is defined as,

$$\boldsymbol{\phi}(k_x,k_z)=\int_{-\infty}^{\infty}\int_{-\infty}^{\infty}\phi(x,z)e^{j(k_x x+k_z z)}dxdz \tag{2.6}$$

Equation 2.5 can also be written in a matrix form as follows,

$$\begin{bmatrix}\mathbf{G}_{zz} & \mathbf{G}_{zx}\\ \mathbf{G}_{xz} & \mathbf{G}_{xx}\end{bmatrix}\begin{bmatrix}\mathbf{J}_z\\ \mathbf{J}_x\end{bmatrix}=\begin{bmatrix}\mathbf{E}_z\\ \mathbf{E}_x\end{bmatrix} \tag{2.7}$$

where

$\mathbf{G}(k_x,d,k_z,\omega)$ is the dyadic Green's function in the spectral domain,

$\mathbf{J}_z$ is the Fourier transform of the z–directed surface current density,

$\mathbf{J}_x$ is the Fourier transform of the x–directed surface current density,

$\mathbf{E}$ is the Fourier transform of the electric field.

Spectral Fourier transforms have been taken in the x and z directions, therefore the dielectric must extend to infinity in both the x and z directions. This is a disadvantage of the SDM formulation, but a layered dielectric structure is considered general enough to fit a wide variety of applications.

Derivations of the spectral domain forms of the Green's functions ($\mathbf{G}_{zz}$, etc. in equations 2.5 and 2.7) are widely available in the literature for single dielectric layer [30, 31]. Derivation of the dyadic Green's function for multiple dielectric layers will be discussed in detail in chapter 7.

Equations 2.5 and 2.7 contain four unknowns which are $\mathbf{J}_z, \mathbf{J}_x, \mathbf{E}_z$ and $\mathbf{E}_x$. At least two unknowns must be eliminated to solve the equations. The Method of Moments [18] is applied to eliminate the Fourier transformed electric fields from the formulation. The first step to the solution is to expand the unknown surface current as a set of known basis functions with unknown coefficients.

$$\mathbf{J}_s(k_x, k_z) = \sum_{n=1}^{N} a_{sn}\mathbf{J}_{sn}(k_x, k_z) \qquad s = x, z \tag{2.8}$$

where $\mathbf{J}_{sn}$ is the n^{th} basis function with coefficient a_{sn}.

The basis functions ($\mathbf{J}_{sn}$) must be chosen to approximate the unknown current distribution on the metallisation of the circuit. The choice of basis functions is crucial to the efficiency of the technique. If they are not chosen to represent the actual current distribution closely, then a large number of functions will be required for convergence. The choice of current basis functions will be discussed in detail in chapter 3.

To eliminate the Fourier transformed electric fields ($\mathbf{E}_z, \mathbf{E}_x$ in equation 2.7), a set of weighting functions ($\mathbf{w}_t$) are required. The weighting functions ($\mathbf{w}_t$) are chosen to be identical to the set of current basis functions. Two more weighting functions are also required for the problem with excitation, the definition of these functions is described in chapter 5.

After application of the Method of Moments, equation 2.7 becomes

$$\begin{bmatrix} \mathbf{Z}_{zz} & \mathbf{Z}_{zx} \\ \mathbf{Z}_{xz} & \mathbf{Z}_{xx} \end{bmatrix} \begin{bmatrix} a_z \\ a_x \end{bmatrix} = \begin{bmatrix} \mathbf{V_z} \\ \mathbf{V_x} \end{bmatrix} \tag{2.9}$$

where the elements of the impedance matrix $\mathbf{Z}$ are given by

$$\mathbf{Z}_{st} = \int_{-\infty}^{\infty}\int_{-\infty}^{\infty} \mathbf{w}_t(k_x, k_z)\mathbf{G}(k_x, k_z, d, \omega)\mathbf{J}_s(k_x, k_z)dk_x dk_z \qquad s, t = x, z \tag{2.10}$$

and the excitation vector is given by

$$\mathbf{V}_t = \int_{-\infty}^{\infty}\int_{-\infty}^{\infty} \mathbf{w}_t(k_x, k_z)\mathbf{E_t}(k_x, k_z)dk_x dk_z \qquad t = x, z \tag{2.11}$$

By solving equation 2.9 for the unknown current coefficients, the unknown current distribution of the metallisation of the circuit can be determined. For the sourceless eigenvalue problem, the excitation vector ($\mathbf{V}_t$) is identically zero. This can be verified using Parseval's theorem [14, page 341].

Note that the method is formulated for spot frequencies, that is the final matrix equation is repeatedly solved for each frequency of interest. Thus minimisation of the order of the matrix equation is very important for the efficiency of the technique. For the Method of Moments, the order of the matrix is twice the total number of basis functions plus two, therefore the critical choice of the basis functions is highlighted.

2.4 Summary

Three alternative numerical techniques have been discussed along with their advantages and disadvantages. All criticism of above techniques were presented within the context of the application of passive planar microwave circuits. Although these are not inclusive, it is believed that they represent a cross–section of the more commonly used methods. The choice of the Spectral Domain Method and highlighted reasons why SDM is more suited to the application of passive planar circuits have also been discussed in this chapter. The historical background of the SDM implementation has been outlined and the general formulation has been presented.

References

[1] K. S. Yee, "Numerical solution of initial boundary value problems involving Maxwell's equations in isotropic media," *IEEE Transactions on Antennas and Propagation*, vol. Ap–14, pp. 302–307, May 1966.

[2] A. Taflove and K. R. Umashankar, "The finite–difference time–domain (FD–TD) method for numerical modelling of electromagnetic scattering," *IEEE Transactions on Magnetics*, vol. 25, pp. 3086–3091, July 1989.

[3] C. J. Railton and J. P. McGeehan, "An analysis of microstrip with rectangular and trapezoidal conductor cross sections," *IEEE Transaction on Microwave Theory and Technique*, vol. 38, pp. 1017–1022, August 1990.

[4] X. Zhang and K. K. Mei, "Time–domain finite difference approach to the calculation of the frequency–dependent characteristics of microstrip discontinuities," *IEEE Transaction on Microwave Theory and Technique*, vol. 36, pp. 1775–1787, December 1988.

[5] C. J. Railton, E. M. Daniel, D. L. Paul, and C. J. McGeehan, "Optimized absorbing boundary conditions for the analysis of planar circuits using finite difference time domain method," *IEEE Transaction on Microwave Theory and Technique*, vol. 41, pp. 290–297, February 1993.

[6] P. Mezzanotte, M. Mongiardo, L. Roselli, R. Sorrentino, and W. Heinrich, "Analysis of packaged microwave integrated circuits by FDTD," *IEEE Transaction on Microwave Theory and Technique*, vol. 42, pp. 1796–1801, September 1994.

[7] D. M. Sheen, S. M. Ali, M. D. Abdouzahra, and J. A. Kong, "Application of the three–dimensional finite-difference time–domain method of the analysis of planar microstrip circuits," *IEEE Transaction on Microwave Theory and Technique*, vol. 38, pp. 849–857, July 1990.

[8] D. L. Paul, E. M. Daniel, and C. J. Railton, "Fast finite difference time domain method for the analysis of planar microstrip circuits," in *21st European Microwave Conference*, pp. 303–308, September 1991.

[9] B. Toland, J. Lin, B. Houshmand, and T. Itoh, "FDTD analysis of an active antenna," *IEEE Microwave and Guided Wave Letters*, vol. 3, pp. 423–425, November 1993.

[10] E. M. Daniel and C. J. Railton, "Fast finite difference time domain analysis of microstrip patch antennas," *IEEE Antennas and propagation Symposium Digest*, pp. 414–417, 1991.

[11] N. M. Pothecary and C. J. Railton, "Finite difference time domain modelling of hyperthermia applicators for cancer therapy," *IEEE MTT–S Digest*, pp. 1151–1154, 1993.

[12] D. B. Shorthouse and C. J. Railton, "The incorporation of static field solution into the finite difference time domain algorithm," *IEEE Transaction on Microwave Theory and Technique*, vol. 40, pp. 986–994, May 1992.

[13] E. M. Daniel and C. J. Railton, "An improvement second order radiating boundary condition for use with non–uniform grids in the finite difference time domain method," in *21st European Microwave Conference*, pp. 547–552, September 1991.

[14] T. Itoh, *Numerical Techniques for Microwave and Millimeter–Wave Passive Structures*. John Willey and Sons, 1989.

[15] J. L. Vetri and N. R. S. Simons, "A class of symmetrical condensed node TLM methods derived directly from Maxwell's equations," *IEEE Transaction on Microwave Theory and Technique*, vol. 41, pp. 1419–1428, August 1993.

[16] M. Krumpholz and P. Russer, "On the dispersion in TLM and FDTD," *IEEE Transaction on Microwave Theory and Technique*, vol. 42, pp. 1275–1279, July 1994.

[17] M. Celuch-Marcysiak and W. K. Gwarek, "Formal equivalence and efficiency comparison of the FD–TD, TLM and SN methods in application to microwace CAD programs," in *21st European Microwave Conference*, pp. 199–204, September 1991.

[18] S. A. Meade, *The Rapid and Rigorous Mathematical Modelling of Passive Planar Microwave Circuits*. PhD thesis, University of Bristol, March 1994.

[19] P. B. Katehi and N. G. Alexopoulos, "Frequency–dependent characteristics of microstrip discontinuities in millimeter–wave integrated circuits," *IEEE Transaction on Microwave Theory and Technique*, vol. 33, pp. 1029–1035, October 1985.

[20] L. P. Dunleavy and P. B. Katehi, "Shielding effects in microstrip discontinuities," *IEEE Transaction on Microwave Theory and Technique*, vol. 36, pp. 1767–1773, December 1988.

[21] W. P. Harokopus and P. B. Katehi, "Characterisation of microstrip discontinuities on multilayer dielectric substrates including radiation losses," *IEEE Transaction on Microwave Theory and Technique*, vol. 37, pp. 2058–2066, December 1989.

[22] T. G. Livernois and P. B. Katehi, "A simple method for characterizing planar transmission line discontinuities on dissipative substrate," *IEEE Transaction on Microwave Theory and Technique*, vol. 39, pp. 368–370, February 1991.

[23] A. S. Omar and K. Schunemann, "Formulation of the singular integral equation technique for planar transmission lines," *IEEE Transaction on Microwave Theory and Technique*, vol. 33, pp. 1313–1321, December 1985.

[24] L. Zhu and E. Yamashita, "Full–wave boundary integral equation method for suspended planar transmission lines with pedestals and finite metallisation thickness," *IEEE Transaction on Microwave Theory and Technique*, vol. 41, pp. 478–483, March 1993.

[25] T. Morisue and T. Yajima, "The Lorentz Gauge vector potential formulation for the boundary integral equation method," *IEEE Transaction on Magnetics*, vol. 30, pp. 3032–3035, September 1994.

[26] H. P. Urbach and E. S. A. M. Lepelaars, "On the domain integral equation method for anisotropic inhomogeneous waveguides," *IEEE Transaction on Microwave Theory and Technique*, vol. 42, pp. 118–126, January 1994.

[27] J. Nadobny, P. Wust, M. Seebass, P. Deuflhard, and R. Felix, "A volume–surface integral equation method for solving Maxwell's equations in electrically inhomogeneous media using tetrahedral grids," *IEEE Transaction on Microwave Theory and Technique*, vol. 44, pp. 543–554, April 1996.

[28] E. Yamashita and R. Mittra, "Variational method for the analysis of microstrip lines," *IEEE Transaction on Microwave Theory and Technique*, vol. 16, pp. 251–255, April 1968.

[29] E. J. Denlinger, "A frequency dependent solution for microstrip transmission lines," *IEEE Transaction on Microwave Theory and Technique*, vol. 19, pp. 30–39, January 1971.

[30] T. Itoh and R. Mittra, "Spectral–domain approach for calculating the dispersion characteristics of microstrip lines," *IEEE Transaction on Microwave Theory and Technique*, pp. 496–499, July 1973.

[31] T. Itoh and R. Mittra, "A technique for computing dispersion characteristics of shielded microstrip lines," *IEEE Transaction on Microwave Theory and Technique*, pp. 896–898, October 1974.

[32] T. Itoh, "Analysis of microstrip resonators," *IEEE Transaction on Microwave Theory and Technique*, vol. 22, pp. 946–952, November 1974.

[33] T. Itoh, "Spectral domain immitance approach for dispersion characteristics of generalized printed transmission lines," *IEEE Transaction on Microwave Theory and Technique*, vol. 28, pp. 733–736, July 1980.

[34] T. Itoh and W. Menzel, "A full–wave analysis method for open microstrip structures," *IEEE Transactions on Antennas and Propagation*, vol. 29, pp. 63–67, January 1981.

[35] R. H. Jansen, "The spectral–domain approach for microwave integrated circuits," *IEEE Transaction on Microwave Theory and Technique*, vol. 33, pp. 1043–1056, October 1985.

[36] R. W. Jackson and D. M. Pozar, "Full–wave analysis of microstrip open–end and gap discontinuities," *IEEE Transaction on Microwave Theory and Technique*, vol. 33, pp. 1036–1042, October 1985.

[37] J. C. Rautio and R. F. Harrington, "An electromagnetic time–harmonic analysis of shielded microstrip circuits," *IEEE Transaction on Microwave Theory and Technique*, vol. 35, pp. 726–729, August 1987.

[38] R. W. Jackson, "Full–wave, finite element analysis of irregular microstrip discontinuities," *IEEE Transaction on Microwave Theory and Technique*, vol. 37, pp. 81–89, January 1989.

[39] N. K. Das and D. M. Pozar, "A generalised spectral–domain Green's function for multilayer dielectric substrates with application to multilayer transmission lines," *IEEE Transaction on Microwave Theory and Technique*, vol. 35, pp. 326–335, March 1987.

[40] C. J. Railton and T. Rozzi, "Complex modes in boxed microstrip," *IEEE Transaction on Microwave Theory and Technique*, vol. 36, pp. 865–873, May 1988.

[41] C. J. Railton and S. A. Meade, "Fast rigorous analysis of shielded planar filters," *IEEE Transaction on Microwave Theory and Technique*, vol. 40, pp. 978–985, May 1992.

[42] S. A. Meade and C. J. Railton, "Efficient implementation of the spectral domain method including precalculated corner basis functions," *IEEE Transaction on Microwave Theory and Technique*, vol. 42, pp. 1678–1684, September 1994.

[43] M.-J. Tsai, D. Flaviis, O. Fordham, and N. G. Alexopoulos, "Modelling planar arbitrary shaped microstrip elements in multilayered media," *IEEE Transaction on Microwave Theory and Technique*, vol. 45, pp. 330–337, March 1997.

[44] J. Kuo and T. Itoh, "Hybrid–mode computation of propagation and attenuation characteristic of parallel coupled microstrips with finite metalisation thickness," *IEEE Transaction on Microwave Theory and Technique*, vol. 45, pp. 274–280, February 1997.

Chapter 3

Current Basis Functions

3.1 Introduction

The choice of current basis functions for the Method of Moments solution is crucial to the efficiency of the technique. To obtain an efficient numerical solution, which converges for a small number of basis functions, the set of basis functions must represent the actual current distribution as closely as possible. If they are not chosen carefully, then a large number of basis functions would be required for convergence. However this criterion must not sacrifice the range of the metallisation patterns which can be analysed.

The basic SDM formulation can be applied to simple structures in an efficient way, but problems exist in the application of the method to complex circuits. An entire domain basis function which is valid on the entire metallisation of the circuit can be used to define the unknown current distribution of simple structures such as an infinite microstrip line [1, 2], a microstrip resonator [3] or a hairpin resonator [4]. However the implementation of an arbitrary metallisation pattern requires sub–domain basis functions which are valid on a portion of the metallisation. It has been shown and commonly used that the rooftop function [5,6] as a sub–domain current basis function allows an irregular shaped microwave circuit's current to be defined. But, the use of the rooftop functions to define the unknown current distribution on the metallisation of the circuit results in a large number of basis functions for convergence. As the size of the impedance matrix to be calculated for each spot frequency is proportional to double of the number of basis functions, it is therefore very important to minimise the set of basis functions required.

It was proposed by Railton and Meade [4, 5] that precalculated basis functions be used to reduce the number of basis functions required. They applied the proposed technique to complex shielded planar microwave circuits showing that inclusion of *a priori* knowledge of the current distribution for realistically complex structures reduces the size of the impedance matrix to be calculated. The precalculated basis

function is derived from the sub–domain basis functions, which are identical apart from a shift in origin, to exploit the benefit of using the FFT. In addition the number of rooftop functions plus 1 in both directions must be an integer power of 2. These conditions restrict the geometry of the circuit and the size of the rooftop function.

The present implementation applies all available enhanced current basis functions in the literature. The effectiveness of rooftop functions is improved by introducing sub–gridding in the spectral domain. The sub–gridding is used in the sense that sizes of the rooftop functions are defined as functions of their locations. The precalculated function is derived in this thesis from two different precalculations. It can be either a linear combination of rooftop functions with precalculated coefficients, or a current wave with a precalculated wave number as explained in section 3.5.4. In both cases, there is no restriction of geometry. This chapter also describes the combination of sub–gridding, precalculation and re–mapping of the precalculated functions.

To measure the performance of the present implementation, a simplified two–dimensional version of SDM is used to derive the dispersion characteristics of infinite microstrip lines, for which numerical results are shown in section 3.7. This allows the calculation of the surface current distribution of the microstrip line, which is going to be used in the full three–dimensional version of the technique. In addition, complex three–dimensional circuits are analysed by using the proposed technique and numerical results are compared with available measurements and published data in section 3.8.

3.2 Classes of Current Basis Functions

- Entire domain : A basis function which is valid for an entire metallisation of the circuit, for example the resonant mode of a microstrip hairpin resonator [4].
- Sub–domain : This is the smallest current basis function used in this thesis. The piecewise linear rooftop is preferred and defined as a product of two separable

functions, a step function in the direction perpendicular to current flow and a triangle function in the direction of current flow.

- Region : A basis function is defined for a section of the metallisation which is bigger than a sub–domain but smaller than an entire domain.
- Transfer : This is a special case of a region basis function and used to join neighbouring regions. Transfer functions can be either sub–domain basis functions which overlap into neighbouring regions or a precalculated basis function.

Throughout this thesis, the above classes of current basis functions are used to define the unknown current distribution of an arbitrary shaped metallisation pattern. Further details of each class of basis function are given in following sections.

3.3 Entire Domain Basis Function

An entire domain current basis function is a function which is valid over the entire metallisation of the circuit. The definition of the unknown current distribution for a simple circuit can be possible by using just a single entire domain function, but the implementation of an arbitrary metallisation pattern requires sub–domain current basis functions. Therefore the entire domain basis function is only mentioned very briefly in this thesis.

3.4 Sub–domain Basis function

3.4.1 Definition of Sub–domain Basis function : Rooftop Basis Function

The definitions of known basis functions which are non–zero only on the metallisation of the circuit of interest in the space domain and of which analytical Fourier transforms exist are required for the Method of Moments solution. The same set is also used as a set of weighting functions ($\mathbf{w}_t$ in equations 2.10 and 2.11) for metallisation. The choice of basis functions is very important for the efficiency of the technique and they must approximate the unknown current distribution as closely as possible.

Arbitrary shaped planar microwave circuits have been modelled using rooftop functions as sub–domain basis functions by numerous authors [4–6]. The geometry of a rooftop function is illustrated in figure 3.1 and is defined in space domain by :

$$J_{xn}(x,z) = \begin{cases} 1 - \frac{|x-x_n|}{l_x} & x_n - l_x \leq x \leq x_n + l_x \\ & z_n - l_z \leq z \leq z_n + l_z \\ 0 & \text{otherwise} \end{cases} \tag{3.1}$$

$$J_{zn}(x,z) = \begin{cases} 1 - \frac{|z-z_n|}{l_z} & x_n - l_x \leq x \leq x_n + l_x \\ & z_n - l_z \leq z \leq z_n + l_z \\ 0 & \text{otherwise} \end{cases} \tag{3.2}$$

where x_n and z_n are the coordinates of the centre of the n^{th} rooftop and l_x, l_z are the sizes of the grid where the rooftop function is located. The rooftop function is defined by two separable functions: a triangle function in the direction of current flow and a step function in the direction perpendicular to current flow. Figure 3.1 shows a rooftop function to model current flow in the z–direction as two separable functions, the step function which is $2l_x$ wide and the triangle function which is $2l_z$ wide. Thus the function overlaps in both directions.

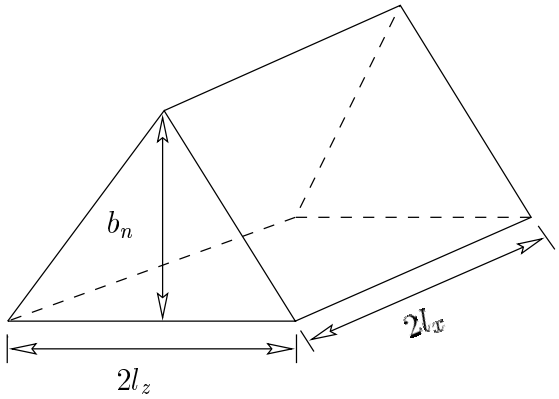

Figure 3.1: Z–directed rooftop function

The two–dimensional Fourier transform of the rooftop function as defined in equation 2.6 and derived in appendix A.1, is given by :

$$\mathbf{J}_{xn}(k_x, k_z) = \frac{4}{k_x^2 k_z l_x}(1 - \cos(k_x l_x)) \sin(k_z l_z) e^{j(k_x x_n + k_z z_n)} \tag{3.3}$$

$$\mathbf{J}_{zn}(k_x, k_z) = \frac{4}{k_x k_z^2 l_z} \sin(k_x l_x)(1 - \cos(k_z l_z)) e^{j(k_x x_n + k_z z_n)} \tag{3.4}$$

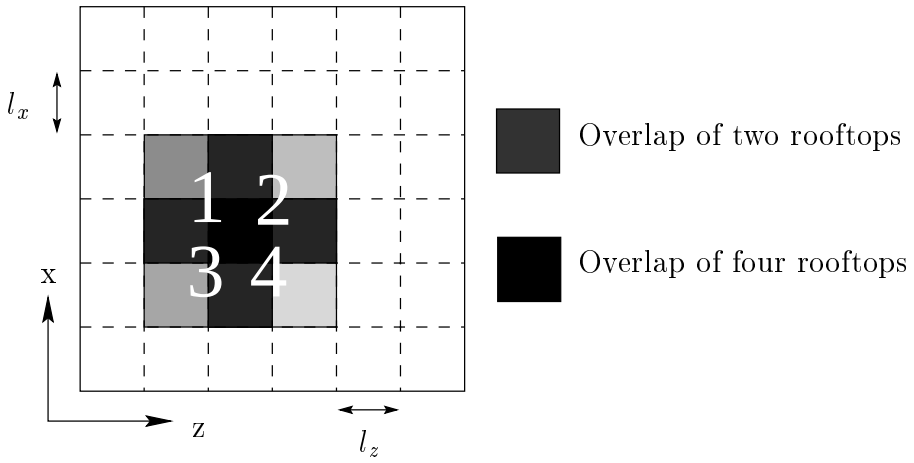

Figure 3.2: Illustration of sub–domain basis function gridding

The rooftop functions define an area of metallisation of the circuit by forming a grid of overlapping rectangular sub–domains as illustrated in figure 3.2. Each function overlaps in its neighbouring rooftops in both directions. Therefore the x and z–

directed components are co–located and are defined on the same grid.

3.4.2 Sub–gridding

The unknown current distribution on an arbitrary shaped metallisation can be defined as a combination of the rooftop functions, but this approach results in a large number of rooftop functions for convergence. The modelling of a corner singularity shown in figure 3.3 requires even more rooftop functions in order to get accurate results for the entire circuit if all rooftop functions are defined identical, apart from a shift in origin. This is because, fine rooftops are required to model the singularity and the same sized rooftops must be used to model the entire circuit. In this case, unnecessarily fine rooftops would be used in the region where no discontinuity exists. This is a major drawback of the technique and a reduction in the number of basis functions required would be an improvement.

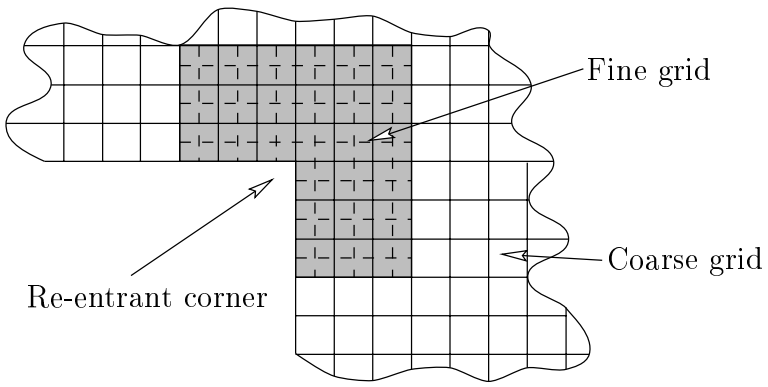

Figure 3.3: Illustration of sub–gridding

In contrast to the formulation for boxed structures [4], the FFT is not employed for the calculation of the impedance matrix elements in this implementation. The restrictions for the FFT usage no longer apply and alternative calculation methods are introduced in chapter 4. The author has defined the size of the rooftop function in [7] as a function of its location, allowing sub–gridding. Fine rooftops are used where

rapid change in current distribution occurs and a coarse size where only slow changes in current distribution occur, as illustrated for the re–entrant corner discontinuity in figure 3.3. The fine grid is located next to the discontinuity and a coarse grid is defined where the current distribution is less dependent on position.

It must be emphasised that the ratio of the fine and coarse grid size, unlike sub–gridding in FDTD, can be any arbitrary number. It is not necessary to have this ratio as an integer number. The discontinuity region is treated individually and only fine rooftops are used to connect the fine grid region to adjacent coarse grid regions as illustrated in figure 3.4.

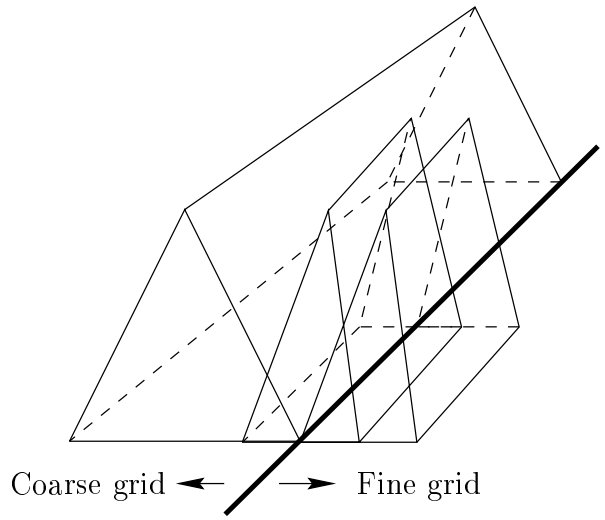

Figure 3.4: Connection of coarse and fine grids

3.4.3 Comparison with other Implementations

In common with this implementation, sub–domain basis functions are used to allow the definition of an arbitrary shaped metallisation of the circuit in [4–6, 8–10]. The methods generally use a rectangular gridding system to define the location of the sub–domain function. There are two forms of rectangular grid basis functions implemented, piecewise linear [4–6, 8] and piecewise sinusoid [9, 10]. Both are referred to

as *rooftop* functions, but in this research this term is reserved for the previous piecewise linear definition. The later piecewise sinusoidal sub–domain rooftop functions are commonly used in the space domain Integral Equation Method (IEM), because the Fourier transform is not required. The piecewise linear rooftop functions are more suited to the spectral domain formulation, because the Fourier transform of the piecewise linear rooftop function is simpler than its piecewise sinusoidal contourpart.

As mentioned in section 3.4.1, a rooftop function is defined as two separable functions: a triangle function in the direction of current flow and a step function in the direction perpendicular to current flow (see in figure 3.1). As illustrated in figure 3.2, a rooftop function in this thesis is $2l_x$ wide (l_x is the grid size in x direction which is the direction perpendicular to current flow) compared to l_x in [6,8]. The rooftop function overlaps in both directions identical to [4,5] and in contrast to [6,8] in which it overlaps only in the direction of current flow.

A novel feature of this implementation is that, the size of the rooftop function is defined as a function of its location as explained in section 3.4.2. To the author's knowledge this method has not been used elsewhere, for example in [4,5], the grid sizes must be identical to exploit the benefit of using the Fast Fourier transform (FFT).

3.5 Region Basis Functions

3.5.1 Division of A Circuit into Region

Following [11], the analysis of an arbitrary shaped metallisation pattern is based on dividing a complex metallisation into regions. In each region, a set of basis functions which are called *region basis functions* are defined . The division of the metallisation of the circuit into regions is central to the form of the set of basis functions and hence

the criteria governing this is crucial to the efficiency and feasibility of the method.

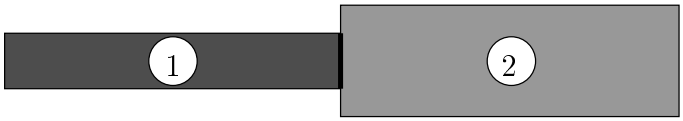

(a) Microstrip step in width

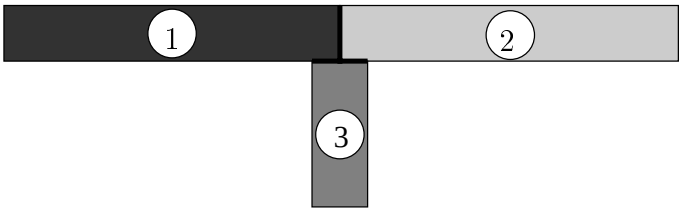

(b) Microstrip stub

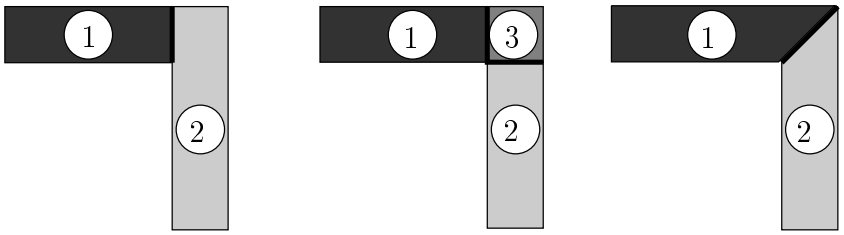

(c) 90^o bend

Figure 3.5: Illustration of division into regions

The division of a metallisation into regions is such that a region is defined between each discontinuity. This is illustrated by example microstrip circuits in figure 3.5. The rules of division are not strict and can be adjusted to fit each specific example. As shown in figure 3.5(a), the discontinuity has been sandwiched between two regions for a microstrip step. If more than two regions are neighbours of a discontinuity, a "T" junction is produced by the position of the stubs as shown in figure 3.5(b). For a 90^o bend discontinuity, three possible sub–divisions have been illustrated in figure 3.5(c). A special case of basis functions is used to join two regions and can be either rooftop functions, or precalculated current basis functions as described in detail in section 3.6.

3.5.2 Definition of Region Basis Function

The inclusion of *a priori* knowledge of the surface current distribution is essential to the efficiency of the technique. A technique which allows precalculated basis functions to be used was presented by Railton in [4] for shielded microstrip structures and is applied to the open planar structures in this present implementation of SDM.

Railton [4] introduced the concept of precalculated basis functions for the modes of a microstrip resonator. This was extended by Meade [5] to allow a set of arbitrary basis functions to be defined as,

$$\mathbf{J}(r) = \sum_{m=1}^{M} a_m \boldsymbol{\psi}_m(r) \tag{3.5}$$

where $\boldsymbol{\psi}_m(r)$ is the current distribution of m^{th} region basis function. A precalculated region basis function ($\boldsymbol{\psi}_m(r)$ in equation 3.5) is defined in [4,5] as a linear combination of the rooftop functions which are identical apart from a shift in origin as,

$$\boldsymbol{\psi}_m(r) = \sum_{n=1}^{N} b_{mn} \mathbf{R}_n(r) \tag{3.6}$$

In addition, the number of rooftop functions (N in equation 3.6) plus 1 must be chosen to be an integer power of 2 to allow use of the FFT [11, page 32]. These limitations restrict the geometry of the circuit. Since the FFT is not applicable to open structures, the rooftop functions are defined in this thesis as functions of their locations, allowing sub–gridding in the region where rapid changes occur in the current distribution. Some precalculated basis functions are also produced from an analytical current wave function with precalculated propagation constants. Details of this procedure are given in section 3.5.4. The final set of current basis functions for an arbitrary shaped metallisation pattern ($\mathbf{J}(r)$ in equations 3.5) are any combination of region and rooftop functions.

3.5.3 Re–mapping of Precalculated Basis Function

The use of precalculated basis functions and the inclusion of *a priori* knowledge reduce the number of basis functions which are required to define the unknown current distribution on the complex metallisation of the circuit. An arbitrary shaped metallisation pattern is analysed by dividing the metallisation into regions for which basis functions are easy to determine. The region basis functions are calculated and stored in the library to be used in the full–wave analysis. In some cases, the dimensions of the region to be modelled by the precalculated basis function can be slightly different from the region for which the stored function is previously calculated. In this case, new precalculated basis functions are required to be calculated, which is computationally intensive.

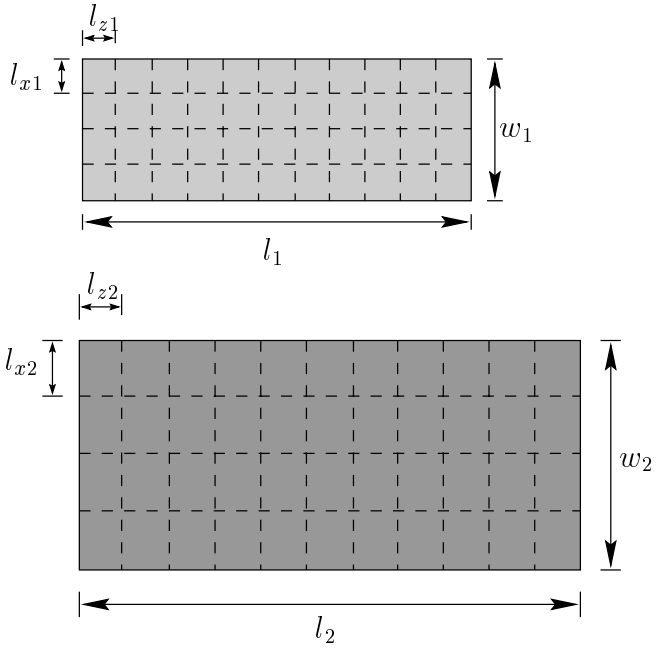

Figure 3.6: Illustration of re–mapping

It is proposed and illustrated in figure 3.6 that scaling of the function from one grid size to another one in either the x or z direction may be used to avoid the need to re–calculate new basis functions. However the accuracy of the procedure is inversely proportional to the variation in length. The adaptation of the mapping is possible to more complicated regions, but care must be taken in its application to complex

regions.

3.5.4 Microstrip Line Region Basis Function

A straight microstrip line with no discontinuity is the simplest region and its basis function is the simplest region basis function. The standing current wave set up on a microstrip line can be modelled by a set of line modes [11]. In this case, the variation of the current distribution in the space domain is given by

$$J_z(x,z) = J_z(x) \overbrace{\left(\sum_{n=0}^{N} a_n^{'} \cos\left(\frac{n\pi z}{L}\right) + \sum_{n=1}^{N} a_n^{''} \sin\left(\frac{n\pi z}{L}\right) \right)}^{J_z(z)} \tag{3.7}$$

$$J_x(x,z) = J_x(x) \overbrace{\left(\sum_{n=0}^{N} b_n^{'} \sin\left(\frac{n\pi z}{L}\right) + \sum_{n=1}^{N} b_n^{''} \cos\left(\frac{n\pi z}{L}\right) \right)}^{J_x(z)} \tag{3.8}$$

where L is the length of the microstrip line and $J_s(x)(s = z, x)$ is the current distribution along the line perpendicular to current flow and precalculated by using the two–dimensional version of the technique given in detail in appendix B. The Fourier transform of the current basis function in the direction perpendicular to current flow ($\mathbf{J}_s(k_x)$) is a sum of the Fourier transforms of the corresponding rooftop functions with precalculated coefficients. The Fourier transforms of the line modes in the direction of current flow as defined in equations 3.7, 3.8 and derived in appendix A.2 are given by:

$$\begin{aligned} \mathbf{J}_z(k_z) = & \sum_{n=0}^{N} a_n^{'} \frac{2(-1)^n \frac{n\pi}{L}}{k_z^2 - (\frac{n\pi}{L})^2} \cos\left(\frac{k_z L}{2}\right) + \\ & j \sum_{n=1}^{N} a_n^{''} \frac{2(-1)^n k_z}{k_z^2 - (\frac{n\pi}{L})^2} \cos\left(\frac{k_z L}{2}\right) \end{aligned} \tag{3.9}$$

$$\begin{aligned} \mathbf{J}_x(k_z) = & j \sum_{n=0}^{N} b_n^{'} \frac{2(-1)^n k_z}{k_z^2 - (\frac{n\pi}{L})^2} \cos\left(\frac{k_z L}{2}\right) + \\ & \sum_{n=1}^{N} b_n^{''} \frac{2(-1)^n \frac{n\pi}{L}}{k_z^2 - (\frac{n\pi}{L})^2} \cos\left(\frac{k_z L}{2}\right) \end{aligned} \tag{3.10}$$

Each line mode can be represented by a precalculated basis function with x and z components. The number of modes required to fully describe a given length of line are restricted by the minimum guide wavelength (λ_{min}) to be modelled. Therefore the minimum line mode wavelength (λ_N) must be less than the minimum microstrip guide wavelength required.

$$\lambda_N < \lambda_{min} \tag{3.11}$$

where λ_N is the wavelength of the highest order line mode and the wavelength of the n^{th} line mode is given by

$$\lambda_n = \frac{2L}{n} \tag{3.12}$$

The microstrip guide wavelength (λ_{min} in equation 3.11) is taken as the wavelength for an infinite microstrip line and calculated by using the two–dimensional version of SDM (see appendix B). This allows the user to specify the maximum operating frequency and from this, the number of modes and the related line mode current basis functions are automatically calculated.

At high frequencies, a large number of line modes are needed to accurately model the unknown current distribution of a microstrip line. For this reason, a wave function is proposed in the direction of current flow as a current basis function for the microstrip line of interest and given in the space domain by:

$$J_z(z) = \begin{cases} e^{-jk_n z} & \frac{L}{2} \leq z \leq \frac{L}{2} \\ 0 & \text{otherwise} \end{cases} \tag{3.13}$$

$$J_x(z) = \begin{cases} e^{-jk_n (z-\frac{\pi}{2})} & \frac{L}{2} \leq z \leq \frac{L}{2} \\ 0 & \text{otherwise} \end{cases} \tag{3.14}$$

where k_n is the precalculated wave number of an infinite microstrip line, where the width is identical to the microstrip line region, and L is the length of the microstrip

line region. The precalculation of k_n is carried out by the two–dimensional version of the technique which is given in appendix B. The same precalculated transverse basis functions ($J_z(x), J_x(x)$ in equations 3.7 and 3.8) are used in the direction perpendicular to current flow. The Fourier transforms of equations 3.13 and 3.14 derived in appendix A.3 are given by:

$$\mathbf{J}_z(k_z) = \frac{2}{(k_z - k_n)} \cos(k_z - k_n) \tag{3.15}$$

$$\mathbf{J}_x(k_z) = \frac{j2}{(k_z - k_n)} \cos(k_z - k_n) \tag{3.16}$$

Note that the centre of the microstrip line region is located at the origin and can be shifted by multiplying the Fourier transforms by $e^{jk_z z_{off}}$, where z_{off} is the offset from the origin.

3.5.5 Resonant Modes

A microstrip resonator shown in figure 3.7 is another special case of the region basis function which includes *a priori* knowledge of the end effect on the current distribution. This microstrip line is open–circuited at both ends and can be completely modelled by a set of resonant modes. The variation of the current distribution for the microstrip resonator in the space domain is given by

$$J_z(x,z) = J_z(x) \sum_{n=1}^{N} a_n \cos\left(\frac{n\pi z}{L}\right) \tag{3.17}$$

$$J_x(x,z) = J_x(x) \sum_{n=1}^{N} b_n \sin\left(\frac{n\pi z}{L}\right) \tag{3.18}$$

where L is the length of the microstrip resonator and $J_s(x)(s = z, x)$ is the transverse current distribution, calculated by the two–dimensional version of the technique (see appendix B). The Fourier transform of the current basis function in the direction perpendicular to current flow ($\mathbf{J}_s(k_x)$) is also a sum of the Fourier transforms of

the corresponding rooftop functions with precalculated coefficients, as mentioned in section 3.5.4. The Fourier transforms of the resonance modes in the direction of current flow as defined in equations 3.17, 3.18 are given by:

$$\mathbf{J}_z(k_z) = \sum_{n=1}^{N} \frac{2(-1)^n \frac{n\pi}{L}}{k_z^2 - (\frac{n\pi}{L})^2} \cos\left(\frac{k_z L}{2}\right) \tag{3.19}$$

$$\mathbf{J}_x(k_z) = \sum_{n=1}^{N} j\frac{2(-1)^n k_z}{k_z^2 - (\frac{n\pi}{L})^2} \cos\left(\frac{k_z L}{2}\right) \tag{3.20}$$

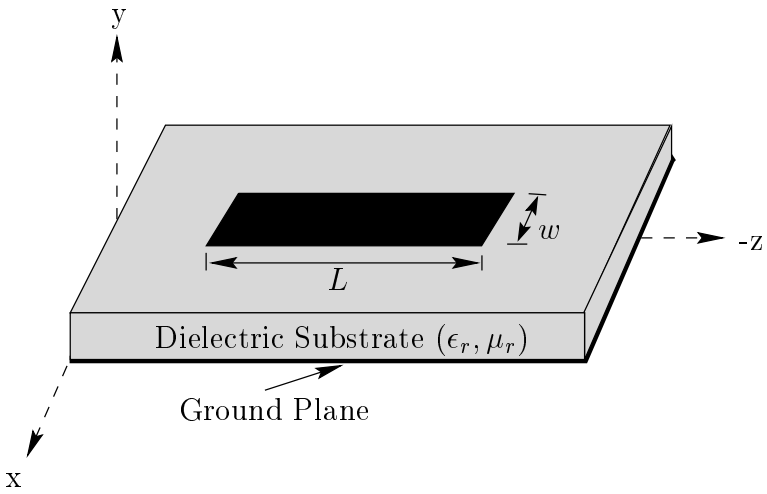

Figure 3.7: Microstrip resonator

The maximum number of the resonant modes is determined by the criterion given for line modes in equation 3.12. The origin is in the centre of the resonator and can be shifted by multiplying by $e^{jk_z z_{off}}$, where z_{off} is the offset from the origin.

3.5.6 Precalculated Discontinuity Function

The set of line modes and resonator modes are not sufficient to model an arbitrary shaped metallisation pattern including several discontinuities. It is possible to add extra rooftop functions in the area of the discontinuity, similar to [6], but this requires a relatively high number of basis functions. Moreover, the effect of a discontinuity can

be significant along a large portion of a circuit. Therefore, Meade and Railton [5] have introduced precalculated corner basis functions for shielded structures, to include *a priori* knowledge of the edge and corner singularities in the set of basis functions. In this section, the basic philosophy of the calculation of the precalculated discontinuity functions is given in brief. Further details can be found in [5] and [11, chapter 4].

This technique has been developed to "extract" the required function from a spot frequency solution for the current distribution of a region, by comparing this with the current distribution for a similar region which does not contain any discontinuity. It has been found by Meade [5] that a single function is required to model the discontinuity over the entire frequency band of interest.

The precalculated discontinuity function depends only on the geometry of the corner itself, not on the surrounding circuitry. Moreover, the function is also independent of substrate thickness, permittivity and permeability. It is not limited to the exact circuit for which it was originally defined, only the relative dimensions of the region and the adjacent metallisation pattern of interest. This reduces the necessity to define new functions for new circuits.

3.6 Transfer Function

The transition of the current between neighbouring regions is achieved by using either rooftop functions or a set of precalculated current basis functions. The microstrip stub (shown in figure 3.5(b)) has been taken as an example and rooftop functions which overlap into adjacent regions are defined for the "T" shaped area. This is illustrated in figure 3.8, which shows the location of the transfer functions and of the area of overlap into neighbouring regions.

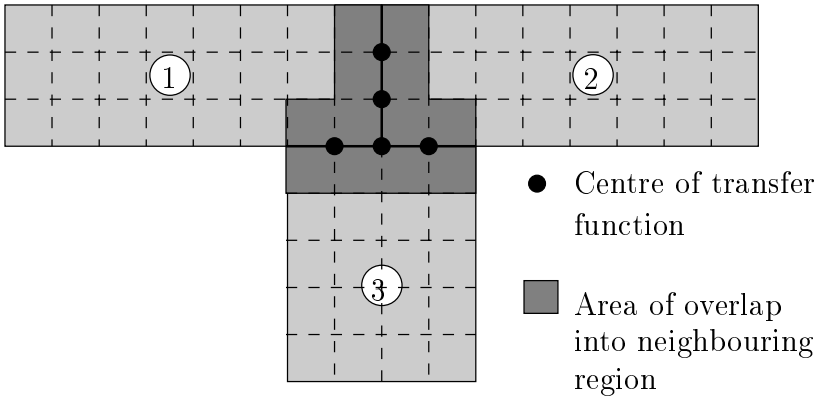

Figure 3.8: Illustration of transfer functions for T–shaped junction

3.7 Two–Dimensional Numerical Examples

3.7.1 Introduction

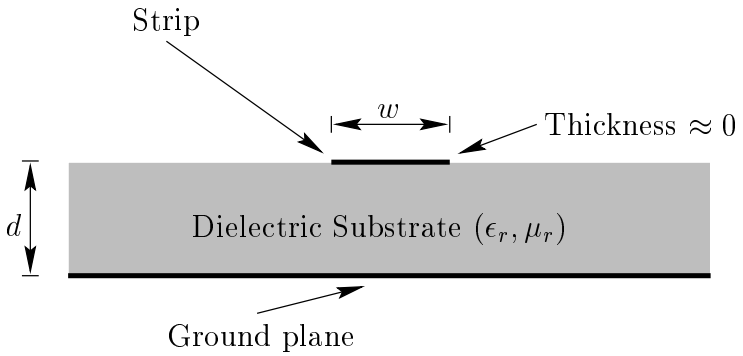

Figure 3.9: Infinite microstrip line for two–dimensional version of SDM

Numerical considerations are introduced in this section with the aid of results from the two–dimensional version of the technique, for which the formulation is given in detail in appendix B. The two–dimensional version of SDM is formulated as an eigenvalue problem to calculate the propagation constant (k_z) of infinite microstrip lines of the form in figure 3.9. From this solution, the effective permittivity, the current distribution in the transverse direction, the guide wavelength and the characteristic impedance can be derived. In this two–dimensional analysis, overlapping rooftop

functions (given section 3.4.1) are used.

3.7.2 Dispersion Characteristics of Infinite Microstrip Line

Dispersion characteristics for microstrip lines are commonly presented as the effective permittivity (ϵ_{eff}) versus frequency is defined as

$$\epsilon_{eff} = \left(\frac{k_z}{k_o}\right)^2 \tag{3.21}$$

Also, the concept of microstrip guide wavelength is used where

$$\lambda_g = \frac{2\pi}{k_z} \tag{3.22}$$

where k_z is the propagation constant.

As an initial test of confidence, the dispersion characteristics for a simple infinite microstrip line are calculated. The tested microstrip line is completely open and of width 1.27 mm, on a substrate of thickness 1.27 mm and of relative permittivity 20. Figure 3.10 is a plot of effective permittivity for a frequency range of 0.1 GHz to 20 GHz. The results are compared to the published results of Itoh [1]. A series of curves are also plotted for different number of basis functions. A convergence to the calculated reference data [1] can be noted.

3.8 Three–Dimensional Numerical Examples

3.8.1 Introduction

In this section, three–dimensional example structures are analysed, to illustrate and verify the theoretical discussions in the proceeding sections. The numerical results

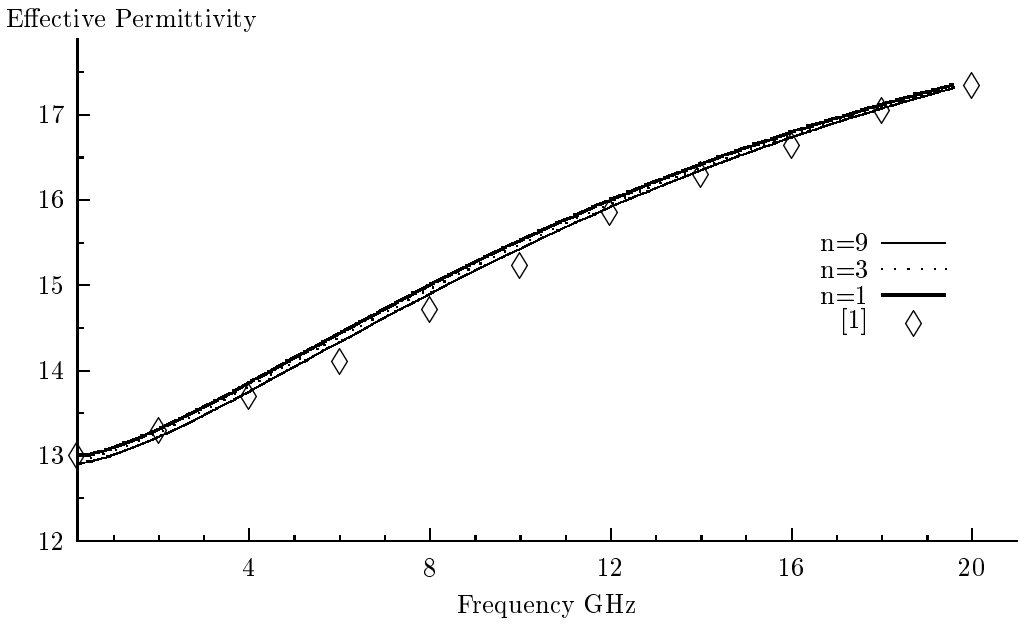

Figure 3.10: Dispersion characteristics for the open infinite microstrip line

are presented in the forms of resonant frequencies and of scattering parameters. The derivation of the resonant frequency is given in [3, 12] and of scattering parameters is described in chapter 5. In the three–dimensional analysis, non–overlapping rooftop functions in the direction perpendicular to current flow are not favoured and only overlapping rooftop functions (see section 3.4.1) in both directions are used to analyse complex metallisation patterns.

3.8.2 Precalculated Transverse Basis Function

Inclusion of *a priori* knowledge of the current distribution reduces the size of the impedance matrix to be calculated. The precalculated transverse function is the first step to include *a priori* knowledge of the current distribution. It is derived by applying the two–dimensional version of SDM given in appendix B, at a spot frequency and assumed to be valid over a wide frequency band. The choice of the spot frequency is arbitrary, but in practice it is in the middle of the intended operating frequency

range. The spot frequency has been chosen here to be 5 GHz. The Fourier transform of the precalculated transfer function is derived from the sum of the Fourier transform of the rooftop functions with precalculated coefficients. In this section, the practical similarity of the results given by a set of rooftop functions and the precalculated transverse basis function is verified. The precalculated function is made up of the same number of rooftop functions in the direction perpendicular to current flow.

3.8.2.1 Microstrip Resonator

The microstrip resonator is the first example used to test the similarity of the results given by precomputed transverse basis function and a set of rooftop functions. This is a useful integrated circuit component at microwave and millimetre–wave frequencies for building filters, oscillators, etc. Before presenting the numerical results to compare published results and experimental data, it should be noted that the structures used in [3] for both numerical computations and experiments are scale models of millimetre–wave integrated circuits. Because in practice after a circuit is designed and tested at low frequency, a miniature structure for millimetre–wave integrated circuits may be obtained by reducing all dimensions of the circuit structure while keeping the ratios of all the dimensions to the wavelength constant. The value of the relative dielectric constant of the substrate is assumed to be unchanged in these two frequency ranges. Since the field distributions in both the scale model and the actual structure are the same, the field problem of millimetre–wave integrated circuit structures is being solved even though the actual operating frequency is in the UHF range.

To test the accuracy of the two approaches, the first resonant frequency of the microstrip resonator on a substrate of thickness 1.27 cm and of relative permittivity 3.82 is calculated. The calculation of the resonant frequency is given in [3, 12]. In the analysis, a set of rooftop functions and a precalculated transverse basis function, in which the same number of rooftop functions are used for precalculation using the

two–dimensional version of the technique, are used in the direction perpendicular to current flow to test the similarity in accuracy. Both models are compared with experimental and published data [3]. For the first model, a total of 48 rooftop functions as current basis functions are required, whereas the number of basis functions required are reduced to 16 by the use of the precalculated transverse basis function for the same definition ($l_x = w/4$ and $l_z = L/9$).

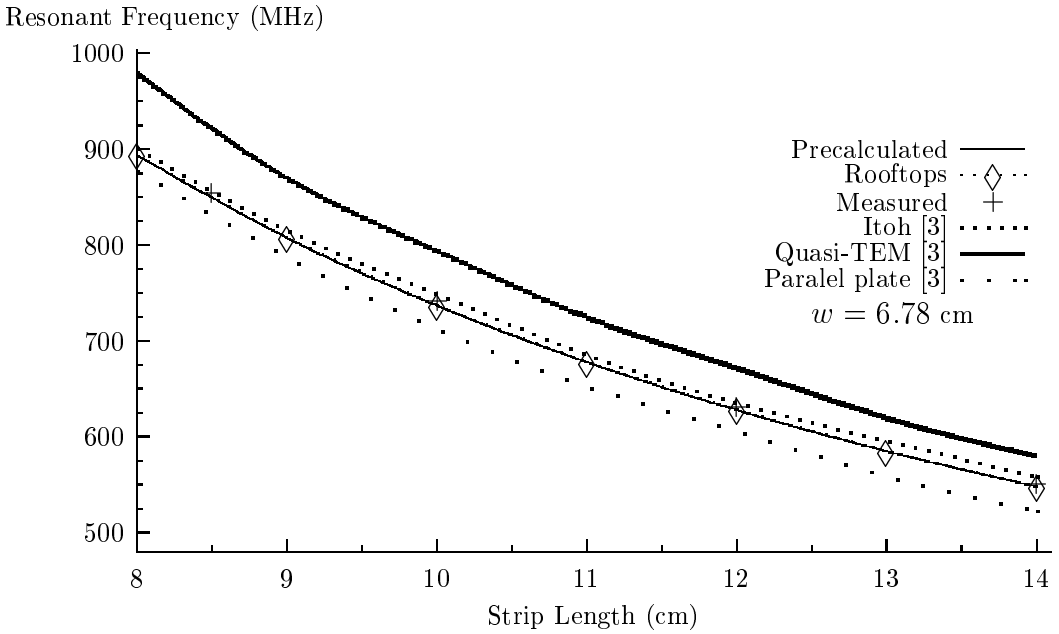

Figure 3.11: Comparison of the results from the present method with those obtained from experiments and other methods

The first resonant frequency versus length of the resonator is plotted in figure 3.11, in which the results obtained by using the precalculated transverse basis function and those obtained using a set of rooftop functions are almost identical. Other theoretical results are based on the Spectral Domain Method by using entire domain basis function, *quasi*–TEM and parallel–plate transmission line models. The experiments were conducted by Itoh [3], using a strip of thickness 0.254 mm which is negligibly small compared to other dimensions. As seen in figure 3.11, the results for the two kinds of current basis functions are indistinguishable on the graphical figure and the agreements between experimental data and the results computed by the proposed

technique are extremely good.

3.8.2.2 Microstrip Gap

In order to further prove that a precalculated transverse basis function is valid for a wide frequency band and gives similar results to a set of rooftop functions, the microstrip gap discontinuity consisting of two identical end–coupled microstrip lines as shown in figure 3.12 is modelled. The dimensions of the circuit are given in figure 3.12.

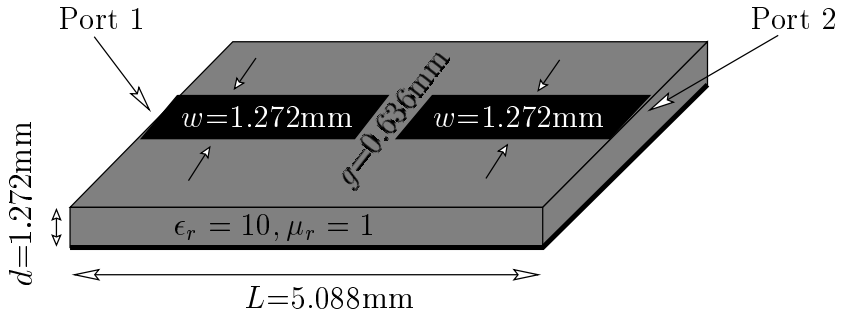

Figure 3.12: Microstrip gap layout

72 basis functions in total (36 x and 36 z components) are required for the sub–domain analysis for the definition ($l_x = l_z = w/4 = 0.318$ mm). The transverse basis function is precalculated for the same definition ($l_x = w/4 = 0.318$ mm) and used as one basis function which is a sum of a number of rooftop functions with precalculated coefficients, as a result 24 basis functions become sufficient for the same circuit. It is emphasised that the plot of S–parameters in figure 3.13 clearly shows the agreement of a set of rooftop functions to a precalculated transverse basis function on a wide frequency band over the frequency range 1 GHz to 20 GHz, although the precalculated basis function has been calculated at a single spot frequency.

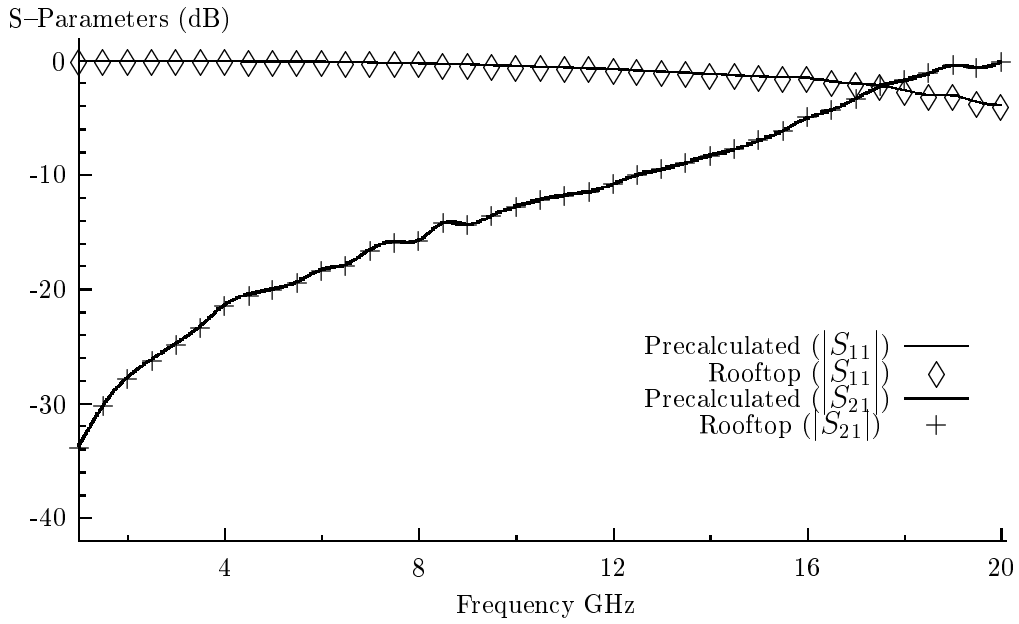

Figure 3.13: Plot of S–parameters's magnitude for the microstrip gap discontinuity comparing basis function sets

3.8.3 Region Basis Function

The use of region basis functions allows further inclusion of *a priori* knowledge of current distribution. In this section, several precalculated region basis functions are applied to microstrip circuits and results are compared with the results yielded by the use of rooftop functions and of precalculated transverse basis functions.

3.8.3.1 Microstrip Line Region Basis Function

The straight microstrip line with no discontinuity is the simplest region and a microstrip line in a finite length shown in figure 3.14 is the simplest microwave circuit to test the proposed region basis function discussed in section 3.5.4. The microstrip line in figure 3.14 is of length 6 mm, and of width 1.272 mm on a substrate of thickness 1.272 mm. The permittivity and permeability are 10 and 1 respectively.

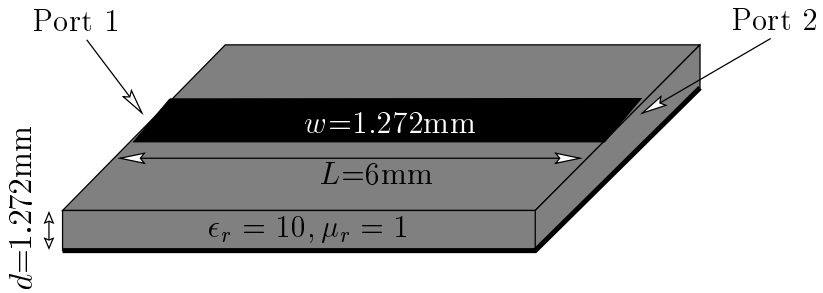

Figure 3.14: Outlook of the microstrip line in finite length

Three sets of S–parameter results are plotted in figure 3.15. These are the results calculated by using 36 rooftop functions for each current components, the results calculated by utilising precalculated transverse basis functions in which case the number of basis functions required are reduced to 6 for the same grid size ($l_x = w/4$ and $l_z = L/7$) and the results calculated by using the single proposed microstrip line region basis function given in section 3.5.4. As seen in equations 3.13 and 3.14, the precalculated current wave function is an analytical function with a precalculated wave number and thus different than the precalculated functions in [4, 5].

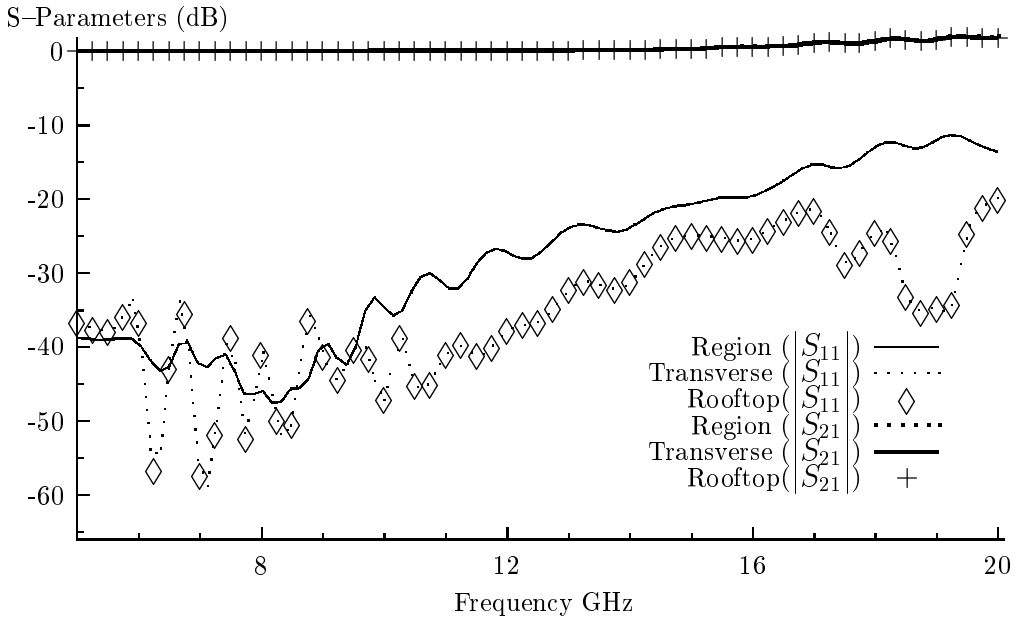

Figure 3.15: S–parameters' magnitude for the microstrip line

The accuracy of the analysis is a function of the number of basis functions used, because at high frequencies a large number of rooftop functions or a large number of line modes are required to accurately model the unknown current distribution on the microstrip line. It must be emphasised that a single microstrip line region basis function may give more accurate results than coarse rooftop functions at high operating frequencies.

3.8.3.2 Resonant Mode : Edge–coupled Filter

As illustrated in figure 3.16, the filter consists of a central microstrip resonator and two feedlines of length 12.72 mm and width 1.272 mm. The substrate has thickness 1.272 mm, relative permittivity 10 and relative permeability 1. The edge–coupled filter is analysed using rooftop functions, precalculated transverse functions and resonant mode region basis functions.

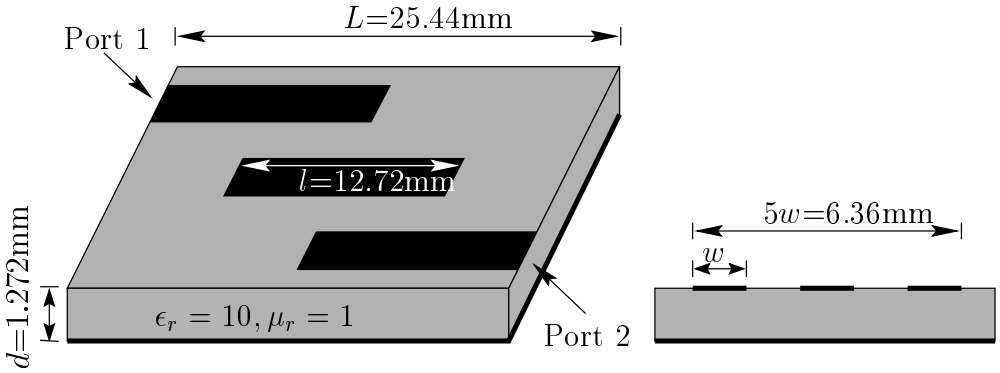

Figure 3.16: Microstrip edge–coupled filter

For the resonant mode analysis,

- The transverse current distributions on the microstrip resonator and feedlines are precalculated by using the two–dimensional version of the technique.
- The longitudinal current distribution corresponding to the resonant modes have been precalculated using the three–dimensional version of the technique, but it

is not necessary to have an excitation. The resonant frequency is found by seeking the operating frequency which makes the determinant of the impedance matrix identically zero. The resonant mode current distribution is calculated as an eigenvalue solution of the resonant frequency and stored in the data library. In the 3–D analysis, the precalculated transverse current function can also be utilised. The resulting resonant mode current distributions are shown in figure 3.17.

- The complete structure is then analysed using two different models. For the model 1, the longitudinal current distributions on the feedlines are assumed to be the same as the current on the resonator as in equations 3.17, 3.18 and shown in figure 3.17. But this does not include all modes existing on the feedlines. Therefore in model 2, the resonant modes are used only for the middle strip and the precalculated transverse basis function as well as rooftop functions are used for the feedlines in the longitudinal directions. The results from these two models are compared to those obtained from modelling the entire metallisation with rooftop functions and to those obtained using rooftop functions in the longitudinal direction and precalculated basis functions in the transverse direction.

Note that for model 1 and 2 only one basis function is required to fully describe the strip resonator over the frequency range of interest. In total 114 basis functions (57 x and 57 z components) are required for the same structure, if only precalculated transverse basis functions are used. In contrast to this, 342 rooftop functions (171 x and 171 z components) would be required in the basic method in which rooftop functions are used as sub–domain basis functions for equivalent accuracy for the same rooftop sizes ($l_x = 0.318$ mm and $l_z = 0.636$ mm). This allows a large saving in computer memory and computational time per frequency. Figure 3.18 shows the results for magnitude of S–parameters plotted against operating frequency. Model 2 agrees more closely with the basic rooftop, the precalculated transverse basis function calculation and measured data [13].

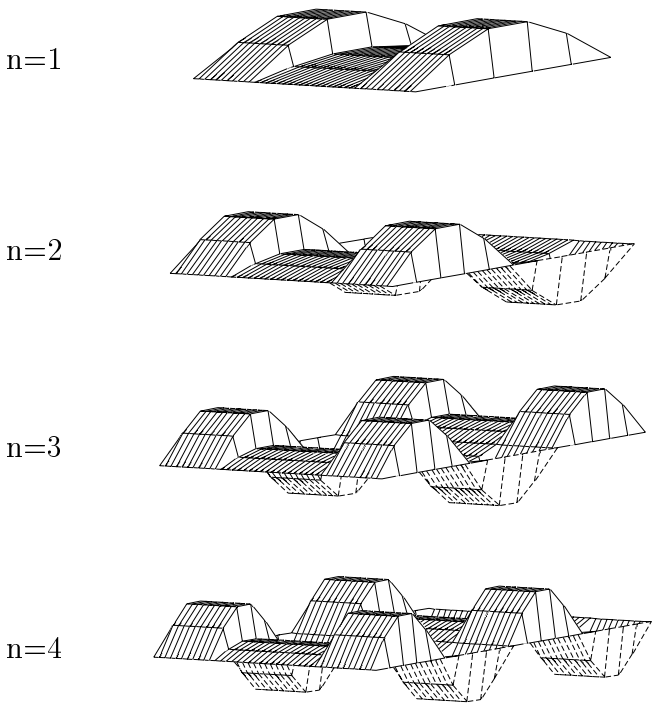

Figure 3.17: Current distributions for the first four resonant modes of a strip resonator

3.8.4 Sub–gridding

As mentioned in section 3.4.1, the grid sizes must be identical in order to exploit the benefit of using the Fast Fourier transform (FFT) for shielded planar microwave circuits [4]. A major difference between the boxed and the open case is that in the former, the discrete Fourier transform is employed, whereas for the latter, the continuous transform is required. Therefore the benefits exploited by using the FFT are not available. In this implementation sub–gridding is employed for the analysis of complex metallisation patterns. The sub–gridding is used in the sense that the size of the rooftop functions are defined as functions of their location. Fine rooftops are used next to the discontinuity. Moreover the precalculated current basis functions are used

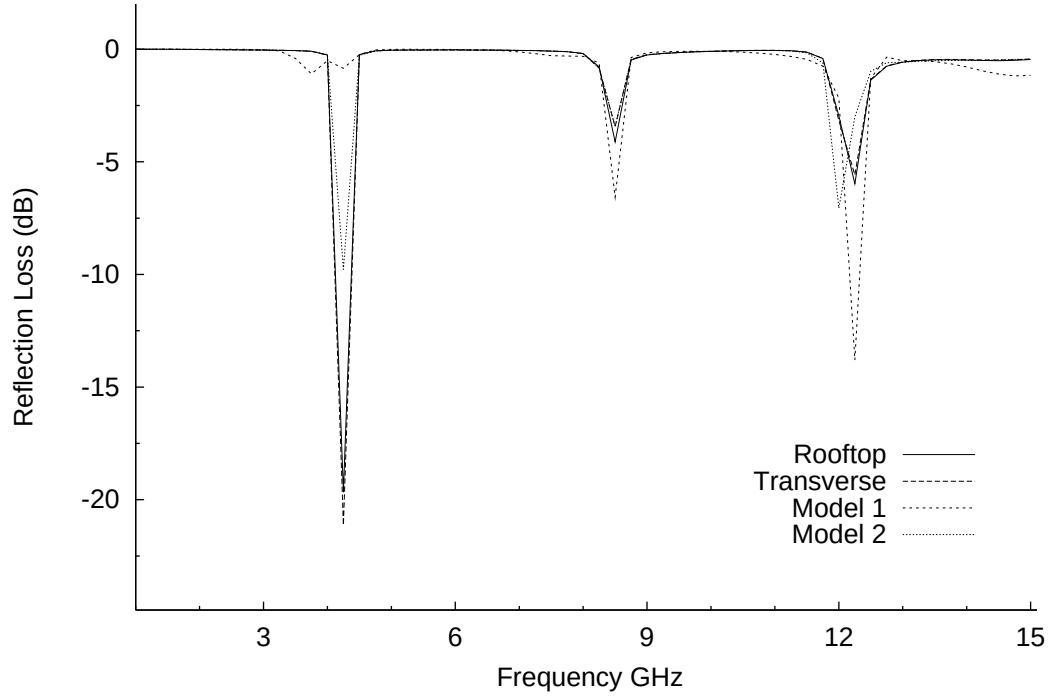

(a) Magitude of S_{11}

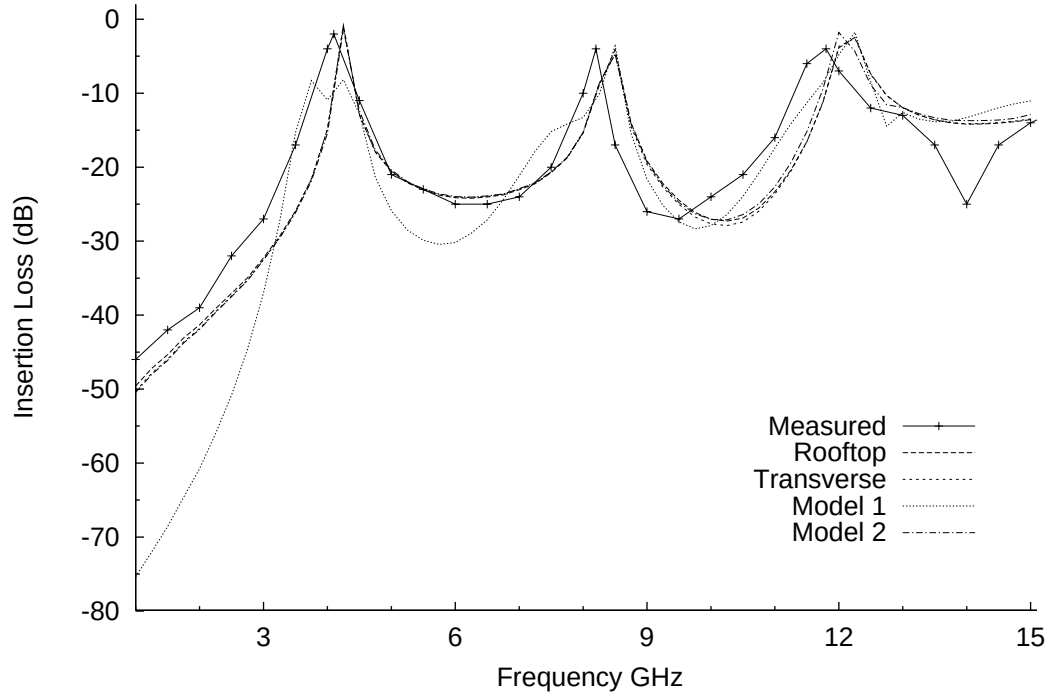

(b) Magitude of S_{21}

Figure 3.18: Plot of S–parameters' magnitude for the edge–coupled filter, comparing basis function sets

where only slow changes in the current distribution occur. As a test of confidence, the microstrip step discontinuity shown in figure 3.19 is taken as an example structure. The planar circuit in figure 3.19 is completely open on a substrate of thickness 1.272 mm and relative permittivity 10. The other dimensions are given in figure 3.19.

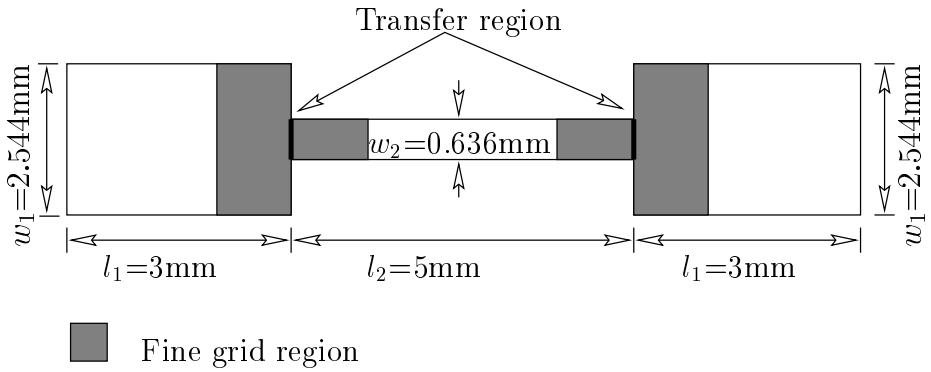

Figure 3.19: Microstrip step discontinuity

Three sets of S–parameter results are plotted in figure 3.20. To illustrate the convergence pattern, the circuit in figure 3.19 is analysed by using fine rooftop functions, which are 162 in total (81 x and 81 z components) for the definition ($l_x = 0.318$ mm and $l_z = 0.5$ mm), for the entire metallisation pattern. For the coarse grid analysis, only three microstrip line region basis functions and two transfer current basis functions which are fine rooftop functions overlap into neighbouring regions are required. In the sub–grid analysis, the benefits of using precalculated region basis functions are exploited and almost same accuracy has been achieved with only 42 current basis functions (21 x and 21 z components). For this analysis, fine rooftops are used to model current distribution in the shaded area of length 1 mm for each region. The current basis function required for an accurate analysis are reduced by 74% and the results are found almost identical to the results by the fine grid analysis.

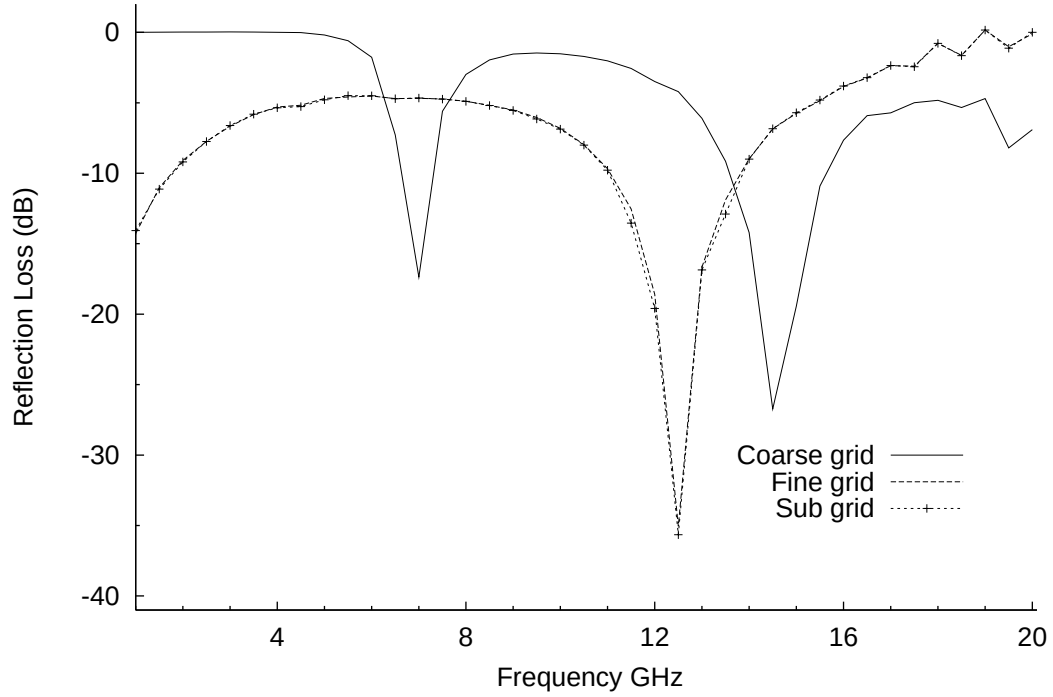

(a) Magitude of S_{11}

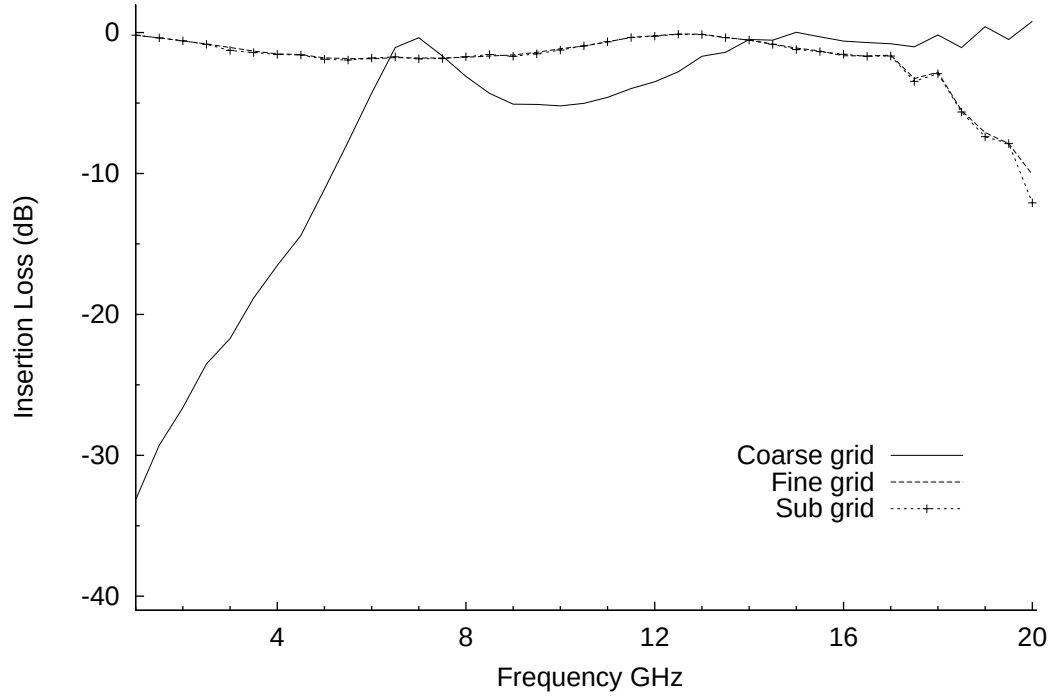

(b) Magitude of S_{21}

Figure 3.20: Plot of S–parameters' magnitude for the step discontinuity

3.9 Summary

The choice of the current basis functions to model the unknown current distribution has been discussed. The class of current basis functions used in this thesis has been given along with their drawbacks. The overlapping sub–domain rooftop functions in both directions have been described and compared to the other implementations in the literature. The rooftop functions in this thesis have been defined as functions of their locations to allow sub–gridding. The analysis of complex circuits by dividing the metallisation into "regions" has been discussed and the set of basis functions for these regions have been described. The example region basis functions such as the microstrip line region, microstrip resonator and precomputed discontinuity functions have been described. To demonstrate and verify the proposed enhancements, the numerical results for a series of two and three–dimensional example microwave circuits have been presented. It has been shown that the precalculated region basis function and sub–gridding schemes can achieve over 70% saving in the number of basis functions required without limiting the generality and accuracy of the method.

References

[1] T. Itoh and R. Mittra, "Spectral–domain approach for calculating the dispersion characteristics of microstrip lines," *IEEE Transaction on Microwave Theory and Technique*, pp. 496–499, July 1973.

[2] T. Itoh and R. Mittra, "A technique for computing dispersion characteristics of shielded microstrip lines," *IEEE Transaction on Microwave Theory and Technique*, pp. 896–898, October 1974.

[3] T. Itoh, "Analysis of microstrip resonators," *IEEE Transaction on Microwave Theory and Technique*, vol. 22, pp. 946–952, November 1974.

[4] C. J. Railton and S. A. Meade, "Fast rigorous analysis of shielded planar filters," *IEEE Transaction on Microwave Theory and Technique*, vol. 40, pp. 978–985, May 1992.

[5] S. A. Meade and C. J. Railton, "Efficient implementation of the spectral domain method including precalculated corner basis functions," *IEEE Transaction on Microwave Theory and Technique*, vol. 42, pp. 1678–1684, September 1994.

[6] R. W. Jackson, "Full–wave, finite element analysis of irregular microstrip discontinuities," *IEEE Transaction on Microwave Theory and Technique*, vol. 37, pp. 81–89, January 1989.

[7] H. H. Balik and C. J. Railton, "Sub–gridding in the spectral domain method for the analysis of planar circuits and antennas," in *3rd International conference on telecommunications in modern satellite, cable and broadcasting services*, pp. 592–595, October 1997.

[8] J. C. Rautio and R. F. Harrington, "An electromagnetic time–harmonic analysis of shielded microstrip circuits," *IEEE Transaction on Microwave Theory and Technique*, vol. 35, pp. 726–729, August 1987.

[9] R. W. Jackson and D. M. Pozar, "Full–wave analysis of microstrip open–end and gap discontinuities," *IEEE Transaction on Microwave Theory and Technique*, vol. 33, pp. 1036–1042, October 1985.

[10] W. P. Harokopus and P. B. Katehi, "Characterisation of microstrip discontinuities on multilayer dielectric substrates including radiation losses," *IEEE Transaction on Microwave Theory and Technique*, vol. 37, pp. 2058–2066, December 1989.

[11] S. A. Meade, *The Rapid and Rigorous Mathematical Modelling of Passive Planar Microwave Circuits*. PhD thesis, University of Bristol, March 1994.

[12] T. Itoh and W. Menzel, "A full–wave analysis method for open microstrip structures," *IEEE Transactions on Antennas and Propagation*, vol. 29, pp. 63–67, January 1981.

[13] T. Shibata, T. Hayashi, and T. Kimura, "Analysis of microstrip circuits using three–dimensional full–wave electromagnetic field analysis in the time domain," *IEEE Transaction on Microwave Theory and Technique*, vol. 36, pp. 1064–1070, June 1988.

Chapter 4

Impedance Matrix Calculation

4.1 Introduction

The Spectral Domain Method has been shown in the previous chapters to be an accurate full–wave model for passive open planar microwave circuits. The SDM analysis requires the definition of the unknown current distribution on the metallisation of the circuit. The minimisation of the number of basis functions required is crucial to the efficiency of the technique, therefore, sub–gridding, the inclusion of *a priori* knowledge of current distribution by using precalculated current basis functions and re–mapping of precalculated basis function are employed in this present implementation. Details were discussed in chapter 3.

Another requirement of SDM is repeated calculation of the impedance matrix elements at each spot frequency. This calculation requires a two–dimensional continuous integration over an infinite surface, which is computationally intensive. The speed of the impedance matrix calculation is a function of the two–dimensional integration and the number of the impedance matrix elements to be integrated. Therefore the enhancements are divided into two sub–divisions. These are the enhancements to speed up the numerical integration and the enhancements to reduce the number of the impedance matrix elements to be integrated. The minimisation of the number of the impedance matrix elements is completely different from the minimisation of the number of the current basis functions required. The latter case reduces the size of the impedance matrix, whereas the former reduces the number of distinct impedance matrix elements for the same size impedance matrix.

An efficient adaptive truncation for the impedance matrix integration shown in equation 2.10, which is over an infinite surface due to open structure, is presented in this chapter. This limits the numerical integration to finite computer resources by using the features of the current basis function. In addition the integration step sizes of the numerical integration are also defined as functions of the Fourier transform variables as will be explained in section 4.2.2. The present implementation uses the asymptotic

form of the Green's function [1] in the calculation of the frequency–independent part of the impedance matrix, resulting in a much smaller two–dimensional numerical integration to be calculated for each spot frequency. It must be remembered that the efficient truncation of the integration has already been employed, and as a result, special care must be taken to determine the integration range of the frequency–dependent part of the impedance matrix. The above enhancements are implemented to speed up the two–dimensional numerical integration for the impedance matrix calculation.

The *location vector* calculation is an enhancement which reduces the number of impedance matrix elements to be calculated. This technique is employed in the region where identical grid sizes are used. In this region, the rooftop functions are defined identical apart from a shift in origin. By this definition, the rooftop function can be split into two parts: the first part is identical for each rooftop and independent of its location, and the second part is a vector which represents its location.

Because the sizes of rooftop functions are not identical in this implementation of SDM, the above location vector calculation is not applicable to the entire impedance matrix. For the entire impedance matrix elements which are the products of the rooftop and the precalculated functions, the symmetry in both the impedance matrix and the Green's function is exploited.

One enhancement presented here cannot completely be classified one way or the other: it is actually a combination of two types of enhancements mentioned above. It reduces the number of the impedance matrix elements in one dimension and hence speeds up overall numerical integration. The effects of the loss in the dielectric substrate are also included into the analysis, by replacing ϵ_r by $\epsilon_r(1 - j \tan\delta)$ where $\tan\delta$ is the loss tangent of the dielectric substrate.

The enhanced SDM is applied to the analysis of a microstrip line for the effective permittivity to show the numerical convergence of the adaptive integration and the use of the asymptotic form of the Green's function. The microstrip line has also been

analysed for several loss tangents to observe the effects of the dielectric loss.

4.2 Adaptive Integration

To find the impedance matrix, equation 2.10 must be repeatedly calculated for each matrix element. This requires a two–dimensional numerical integration and special care must be taken, because the dyadic Green function has several poles [2, pages 335–340]. These poles (in practical cases, only one [3]) correspond to surface waves for an open structure and are located in between $|k_0|$ and $|\sqrt{\epsilon_r \mu_r} k_0|$. The poles have no imaginary parts if the dielectric substrate is lossless.

There are two possible ways to include such effects as described in the literature. The first way is to determine the exact pole location by using one of the numerical root–finding techniques such as the Newton–Rhapson, which is well–explained in any numerical analysis text book, then to skip the poles and to include the effect of the poles as explained in [4]. The main disadvantage of this technique is the need to calculate the location of the poles for each spot frequency. A second and more efficient technique is introduced in [5] for the polar co–ordinate systems. This has been adopted to fit the cartesian co–ordinate system used in this implementation.

In a line integration, the result is independent of the chosen path [6, page 409]. The technique used here is based on changing the integration path to a new path on which no poles exist. As the poles are located between $|k_o|$ and $|\sqrt{\epsilon_r \mu_r} k_0|$ as shown in figure 4.1, a contour integration path which skips this region obtained by shifting the integration path by 5% of k_0, as shown in figure 4.1. The value of 5% has been chosen from the author's experience, and the effects of poles are included in the analysis.

In a numerical integration procedure, there are two parameters which have the greatest effects. These parameters are discussed in the following sections and enhancements are described.

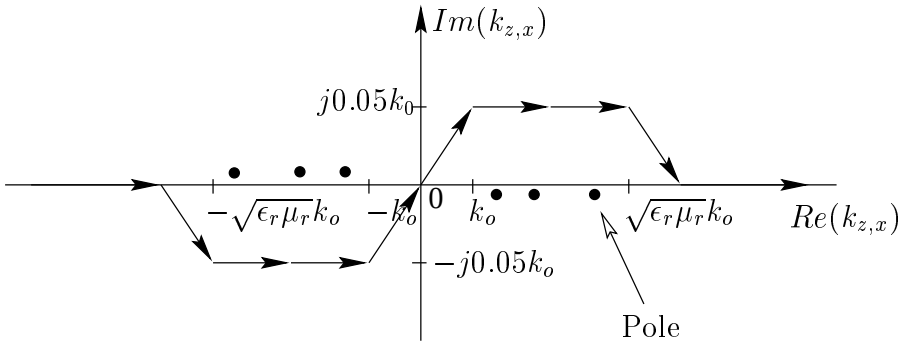

Figure 4.1: Complex integration path

4.2.1 Adaptive Integration Range

To find the unknown current distribution on the complex metallisation of the circuit, the unknown coefficients must be calculated. The Method of Moments (MoM) is commonly used to calculate these coefficients and this requires an integration over an infinite surface as a result of the open domain [3]. A suitable place for termination of the integration must be defined, to limit the infinite integration to finite computer resources. Although the choice of truncation was mentioned in [4], the exact position of the truncation was not given. In this thesis, the location of the truncation is defined using a feature of the sub–domain basis functions which are rooftop functions.

As mentioned previously, a rooftop function is defined as two separable functions, a triangle function in the direction of current flow and a step function in the direction perpendicular to flow. The Fourier transform of the rooftop function is given in equations 3.3, 3.4 and shown in figure 4.2. As shown in figure 4.2, the Fourier transforms of the components of the rooftop function become very small after just a few cycles. The integration over a just a few cycles has been found and proved to give accurate results instead of the integration over an infinite range.

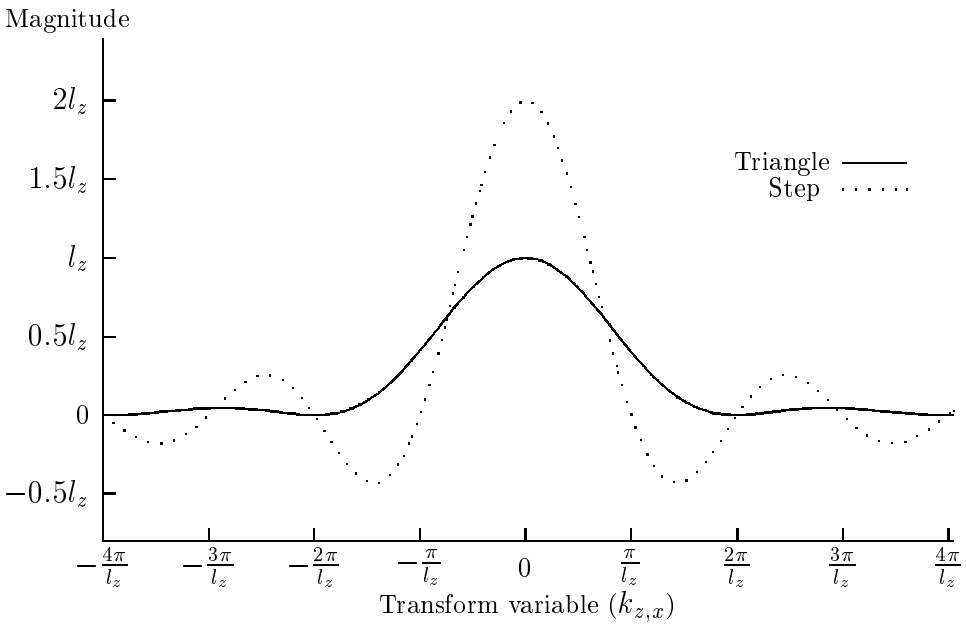

Figure 4.2: Fourier transform of a rooftop function components

4.2.2 Adaptive Integration Step

The peak value of each cycle decays exponentially as seen in figure 4.2, therefore to choose the integration step to be a function of the transform variables (k_x, k_z) is meaningful. To integrate the impedance matrix elements efficiently the following idea is used: use a fine step in the large amplitude variation areas and a coarse step for small amplitude variations. The accuracy of this method is comparable to that of using only fine steps.

In figure 4.3, max is the truncation position which is described in section 4.2.1 and the integration step as a function of the transform variables is given by;

$$h(k_{x,z}) = h_{max} e^{\ln(\frac{h_{min}}{h_{max}})\frac{|k_{x,z}|}{\max}} \tag{4.1}$$

As seen in equation 4.1 and figure 4.3, fine integration steps are used for the small values of the Fourier transform variables and coarse steps are used for large values of

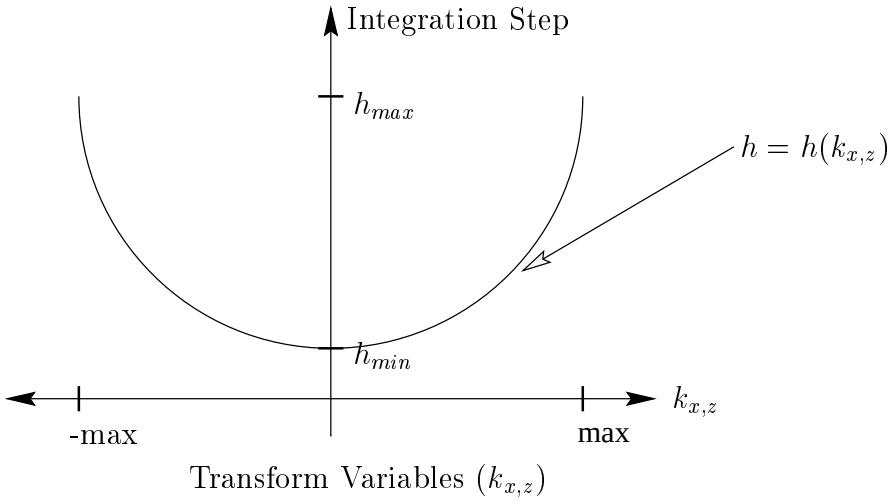

Figure 4.3: Adaptive integration step

the Fourier transform variables.

4.3 Asymptotic Form of Green's Function

4.3.1 Definition

The dyadic Green's function is defined by Itoh [2] for partly shielded microstrip line and has been adopted for open planar circuits by taking the finite thickness of the free space to infinity ($h \rightarrow \infty$; h : space between top cover and the circuit plane). The present implementation is restricted to two layers, to test the proposed enhanced features; multiple dielectric layers will be considered with enhancements in chapter 7.

The spectral domain form of the Green's function (**G** in equation 2.5) is a function of the Fourier transform variables (k_z and k_x in equation 2.6), thickness of dielectric substrate and substrate parameters (ϵ_r and μ_r) as well as operating frequency. Therefore any improvement in efficiency in calculating the terms of the Green's function will result in a significant reduction in the run–time required.

The calculation of the full Green's function is relatively computationally intensive, therefore the derivation of a simple asymptotic form of the function is desirable. This is a function which is valid for large values of k_z and k_x. Such a function is presented by Railton and Rozzi [7]

$$\mathbf{G}^{\infty}(k_x, k_z) = \lim_{k_x, k_z \to \infty} \mathbf{G}(k_x, k_z) \tag{4.2}$$

The asymptotic form of the Green's function is similar to the one which has been presented by Railton [8] for shielded planar structures, but modified to be applicable to open planar microwave circuits. For large values of k_x and k_z , two approximations can be made. These are

$$\gamma_i = \sqrt{k_x^2 + k_z^2 - k_i^2} \approx \sqrt{k_x^2 + k_z^2} \tag{4.3}$$

$$Coth\gamma_2 d \approx 1 \tag{4.4}$$

The asymptotic form of the Green's function for large k_x and k_z derived in appendix C.1 is given by:

$$\mathbf{G}_{st}^{\infty} = h_1 \mathbf{K}_{st1}^{\infty} + h_2 \mathbf{K}_{st2}^{\infty} \tag{4.5}$$

where

$$\begin{aligned}
h_1 &= -\frac{j}{\omega\epsilon_0(1+\epsilon_r)} & h_2 &= \frac{j\omega\mu_0\mu_r}{(1+\mu_r)} \\
\mathbf{K}_{zz1}^{\infty} &= \frac{k_z^2}{\sqrt{k_x^2+k_z^2}} & \mathbf{K}_{zz2}^{\infty} &= \frac{k_z^2}{\sqrt{(k_x^2+k_z^2)^3}} \\
\mathbf{K}_{zx1}^{\infty} &= -\frac{k_x k_z}{\sqrt{k_x^2+k_z^2}} & \mathbf{K}_{zx2}^{\infty} &= \frac{k_x k_z}{\sqrt{(k_x^2+k_z^2)^3}} \\
\mathbf{K}_{xz1} &= \mathbf{K}_{zx1} & \mathbf{K}_{xz2} &= \mathbf{K}_{zx2} \\
\mathbf{K}_{xx1}^{\infty} &= \frac{k_x^2}{\sqrt{k_x^2+k_z^2}} & \mathbf{K}_{xx2}^{\infty} &= \frac{k_x^2}{\sqrt{(k_x^2+k_z^2)^3}}
\end{aligned} \tag{4.6}$$

with $\omega = 2\pi f$ and ϵ_r, μ_r the relative permittivity and permeability of the electric substrate respectively.

The functions $\mathbf{K}^{\infty}_{sti}$ ($s, t = z$ or x; $i = 1, 2$) are just functions of k_x and k_z and thus are independent of frequency and metallisation pattern. The constants h_i ($i = 1, 2$) need only be calculated once per frequency, as they are independent of k_x and k_z.

4.3.2 Calculation of Impedance Matrix

The reduction of the number of calculations is the core of this research, because of the repeated impedance matrix calculation required. The impedance matrix given in chapter 2 ($\mathbf{Z}_{st}$ in equation 2.10) is redefined as:

$$\mathbf{Z}_{st} = \int_{-max_z}^{max_z} \int_{-max_x}^{max_x} \mathbf{w}_t(k_x, k_z)\mathbf{G}(k_x, k_z, d, \omega)\mathbf{J}_s(k_x, k_z)dk_x dk_z \tag{4.7}$$

Thus the integration over an infinite surface is replaced by a double integration over just a few cycles of Fourier transform of the rooftop function components. The truncation of the infinite integration is given in detail in section 4.2.1.

Using the asymptotic form of the Green's function as given by equation 4.5 the impedance matrix in equation 3.8 is now split into two parts:

$$\begin{aligned}\mathbf{Z}_{st} = &\int_{-max_z'}^{max_z'} \int_{-max_x'}^{max_x'} \mathbf{w}_t(k_x, k_z) \left[\mathbf{G}(k_x, k_z, d, \omega) - \mathbf{G}^{\infty}(k_x, k_z)\right] \mathbf{J}_s(k_x, k_z)dk_x dk_z \\ &+ \mathbf{Z}^{\infty}_{st}\end{aligned} \tag{4.8}$$

where the asymptotic part of impedance matrix is given by:

$$\mathbf{Z}^{\infty}_{st} = \int_{-max_z}^{max_z} \int_{-max_x}^{max_x} \mathbf{w}_t(k_x, k_z)\mathbf{G}^{\infty}(k_x, k_z)\mathbf{J}_s(k_x, k_z)dk_x dk_z \tag{4.9}$$

The algorithm thus splits the formulation of the impedance matrix into two continuous integrations. The first one is truncated as governed by two conditions in equations 4.3 and 4.4. The second integration is larger, but is calculated using relatively simple asymptotic Green's function expressions.

With reference to equation 4.5, the asymptotic impedance matrix $\mathbf{Z}_{st}^{\infty}$ can be expressed as:

$$\mathbf{Z}_{st}^{\infty} = h_1 \mathbf{Z}_{st1}^{\infty} + h_2 \mathbf{Z}_{st2}^{\infty} \tag{4.10}$$

where

$$\mathbf{Z}_{st1}^{\infty} = \int_{-max_z}^{max_z} \int_{-max_x}^{max_x} \mathbf{w}_t(k_x, k_z) \mathbf{K}_{st1}^{\infty}(k_x, k_z) \mathbf{J}_s(k_x, k_z) dk_x dk_z \tag{4.11}$$

$$\mathbf{Z}_{st2}^{\infty} = \int_{-max_z}^{max_z} \int_{-max_x}^{max_x} \mathbf{w}_t(k_x, k_z) \mathbf{K}_{st2}^{\infty}(k_x, k_z) \mathbf{J}_s(k_x, k_z) dk_x dk_z \tag{4.12}$$

h_i and $\mathbf{K}_{sti}^{\infty}$ $(s, t = x \text{ or } z;\ i = 1, 2)$ are defined for the asymptotic form of the Green's function in equation 4.5.

Following section 4.3.1, $\mathbf{Z}_{st1}$ and $\mathbf{Z}_{st2}$ are only functions of Fourier transform variables and independent of the operating frequency and dielectric substrate parameters and therefore need to be calculated only once per metallisation pattern. Thus the algorithm allows the frequency, permittivity, permeability and substrate thickness to be changed without requiring $\mathbf{Z}_{st1}$ and $\mathbf{Z}_{st2}$ to be re–calculated. Moreover only the first integration in equation 4.8 and simple h_i $(i = 1, 2)$ are repeatedly calculated for each spot frequency, but it is emphasised that the integration range has been efficiently truncated by using the features of the rooftop function's components. Therefore special care must be taken to determine the truncation location of the numerical integration of the dyadic Green's function by satisfying equations 4.3 and 4.4. Since it has been found and illustrated in section 4.2.1 that the numerical integration of the impedance matrix elements over a just a few cycles of the Fourier transform of the rooftop function's components gives accurate results, instead of integrating

over an infinite surface, the conditions given in equations 4.3 and 4.4 then become inapplicable. Therefore the conditions 4.3 and 4.4 must be checked for each spot frequency and terminate the use of the asymptotic form of the Green's function when anyone of equations 4.3 and 4.4 is not satisfied.

4.4 Location Vector Calculation

Although the dimensions of the rooftop functions in this thesis are functions of their locations, so that a finer rooftop is used in the region where rapid change in current distribution takes place, all rooftop functions in any one region are identical apart from a shift in origin. Therefore $R_n(r)$ in equation 3.6 can be separated into two functions as

$$\mathbf{R}_n(r) = \mathbf{J}_n(l_x, l_z)\mathbf{P}_n(r) \tag{4.13}$$

where $\mathbf{P}_n$ is the function of the location of the n^{th} rooftop, whereas $\mathbf{J}_n$ is a function of the dimensions of the rooftop, but independent of its location as follows,

$$\begin{aligned} \mathbf{P}_n &= e^{j(k_x x_n + k_z z_n)} = e^{j(k_x p l_x + k_z q l_z)} \\ \mathbf{J}_{xn}(k_x, k_z) &= \frac{4}{k_x^2 k_z l_x}(1 - \cos(k_x l_x))\sin(k_z l_z) \\ \mathbf{J}_{zn}(k_x, k_z) &= \frac{4}{k_x k_z^2 l_z}\sin(k_x l_x)(1 - \cos(k_z l_z)) \end{aligned} \tag{4.14}$$

l_x, l_z are grid sizes and x_n, z_n, which are functions of p, q are the origin of the n^{th} rooftop function. The set of functions $\mathbf{P}_n(r)$ are referred to as the location vector. The maximum values of p, q are P, Q which are the total number of the rooftop functions required for the region of interest. The Method of Moments is the technique used to find the unknown coefficients of the current basis functions. A set of weighting functions, which are identical to the set of basis functions for the metallisation of the circuit, are required. Therefore the impedance matrix elements for the region where

the sizes of the grids are identical are given by

$$\mathbf{Z}_{st}(p,q) = \int_{-\infty}^{\infty}\int_{-\infty}^{\infty}(\mathbf{J}_s\mathbf{J}_t\mathbf{G}_{st})\mathbf{P}_s\mathbf{P}_t dk_x dk_z \qquad s,t = x,z \tag{4.15}$$

To facilitate the solution and speed up the impedance matrix calculation, the impedance matrix of the region of interest is divided into four quadrants as,

$$\mathbf{Z} = \begin{bmatrix} \mathbf{Z}_{zz}(p,q) & \mathbf{Z}_{zx}(p,q) \\ \mathbf{Z}_{xz}(p,q) & \mathbf{Z}_{xx}(p,q) \end{bmatrix} \tag{4.16}$$

In equation 4.16, only half of the zz, of xx and zx are required to be calculated if symmetry is used alone (given in detail in section 4.5.1). After substitution of 4.14 into 4.15, the impedance matrix elements (in equation 4.15) differ from each other by their integer numbers (p and q in equation 4.14). It has been found that the first line alone of each quarter of the matrix is sufficient to find whole region of interest in the impedance matrix by using re–defined rooftops. The impedance matrix elements, as a function of the integer numbers (p,q) can be written as,

$$\mathbf{Z}_{st}(p,q) = \int_{-\infty}^{\infty}\int_{-\infty}^{\infty}(\mathbf{J}_s\mathbf{J}_t\mathbf{G}_{st})\sum_{p=0}^{(P-1)} e^{jk_x pl_x}\sum_{q=0}^{(Q-1)} e^{jk_z ql_z} \tag{4.17}$$

and the rest are calculated by;

$$\mathbf{Z}_{st}(-p,q) = \mathbf{Z}_{st}(p,q) \qquad \mathbf{Z}_{st}(p,-q) = \mathbf{Z}_{st}(p,q) \tag{4.18}$$

$$\mathbf{Z}_{st}(-p,q) = -\mathbf{Z}_{st}(p,q) \qquad \mathbf{Z}_{st}(p,-q) = -\mathbf{Z}_{st}(p,q) \tag{4.19}$$

Equation 4.18 is used to calculate the first and fourth quadrants of the impedance matrix and equation 4.19 is used for the second quadrant. This technique gives great savings in computer run–time, especially for complex circuits. The total number of impedance matrix elements for the region of interest are $(2PQ)^2$ whereas the number

of impedance matrix elements required to be calculated by using the method proposed here are only 3PQ.

4.5 Symmetry

4.5.1 Symmetry in Impedance Matrix

The minimisation of the number of the impedance matrix elements required to be calculated is crucial to achieve an efficient implementation. Therefore symmetries in the impedance matrix calculation are taken advantage of the algorithm in a similar manner to [3]. As illustrated in figure 4.4 the square impedance matrix is divided into four quadrants which are $\mathbf{Z}_{zz}, \mathbf{Z}_{zx}, \mathbf{Z}_{xz}$ and $\mathbf{Z}_{xx}$. As a result of the Method of Moments, the following symmetries apply:

$$\mathbf{Z}_{zz}(n,m) = \mathbf{Z}_{zz}(m,n) \qquad \text{similarly for } \mathbf{Z}_{xx}$$
$$\mathbf{Z}_{xz} = (\mathbf{Z}_{zx})^T$$

where $\mathbf{Z}_{st}(n,m)$ represents the product of nth weighting function with mth basis function.

Therefore the algorithm requires half of the impedance matrix shown in figure 4.4 plus the $n = m$ diagonal to be calculated. The rest of the impedance matrix elements are found by using the symmetries.

Extra symmetries can be applied to $\mathbf{Z}_{zx}$, if the procedure is Galerkin's and the basis functions are rooftop functions with identical dimensions. In this case, the location vector calculation given in detail in section 4.4 is more efficient than the use of symmetry. The symmetry in the impedance matrix is favoured when precalculated current basis functions and sub–gridding of the metallisation are used to define the

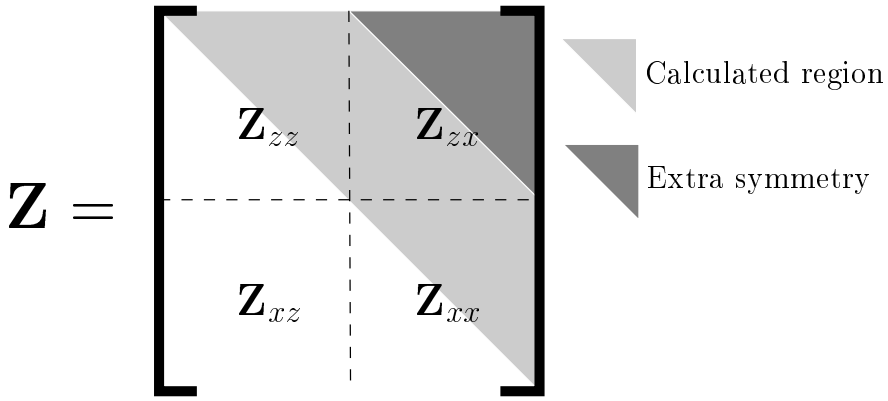

Figure 4.4: Schematic of impedance matrix symmetries

unknown current distribution of the metallisation of the circuit. It must be emphasised that the symmetry in $\mathbf{Z}_{zx}$, is not used because the rooftops are in identical size and the procedure is Galerkin's.

4.5.2 Symmetry in Green's Function

As seen in equation 4.6 and [2], both dyadic and asymptotic form of the Green's function are either odd or even symmetrical such as

$$\mathbf{G}_{st}(k_x,k_z) = \mathbf{G}_{st}(-k_x,-k_z) \;=\; \mathbf{G}_{st}(-k_x,k_z) = \mathbf{G}_{st}(k_x,-k_z) \qquad s=t \quad (4.20)$$

$$\mathbf{G}_{st}(k_x,k_z) = \mathbf{G}_{st}(-k_x,-k_z) \;=\; -\mathbf{G}_{st}(-k_x,k_z) = -\mathbf{G}_{st}(k_x,-k_z) \qquad s\neq t \quad (4.21)$$

where $s,t = x,z$. These features are exploited for the calculation of $\mathbf{Z}_{st}$ in equation 4.8. In this implementation the Green's function is calculated for only one quarter of the integration range ($k_x \geq 0$ and $k_z \geq 0$) and the rest are derived by using the equations 4.20, 4.21.

4.6 Enhancement for Numerical Integration

In the previous sections, modifications to speed up the impedance matrix calculation and to reduce the number of impedance matrix elements have been discussed. The improvement introduced in this section is actually a combination of these two kinds of enhancements. The speed of the calculation of the impedance matrix elements is increased by reducing the number of the impedance matrix elements to be calculated in one dimension. As mentioned previously, the first step of the analysis is to expand the unknown current distribution as a set of known current basis functions with unknown coefficients, as given in equation 2.8. The known current basis functions which can be either sub–domain or precalculated functions are defined as two separate functions for each direction as:

$$\begin{aligned} \mathbf{J}_s(k_x,k_z) &= \sum_{n=1}^{N} a_{sn}\mathbf{J}_{sn}(k_x,k_z) \\ &= a_{sn}\left(\sum_{nx=1}^{N_x}\mathbf{J}_{snx}(k_x)\sum_{nz=1}^{N_z}\mathbf{J}_{snz}(k_z)\right) \qquad n=1..N \end{aligned} \tag{4.22}$$

and the Method of Moments requires a set of weighting functions, which is identical to the set of current basis functions if the procedure is Galerkin's, defined by:

$$\begin{aligned} \mathbf{w}_t(k_x,k_z) &= \sum_{n=1}^{N}\mathbf{w}_{tn}(k_x,k_z) \\ &= \sum_{nx=1}^{N_x}\mathbf{w}_{tnx}(k_x)\sum_{nz=1}^{N_z}\mathbf{w}_{snz}(k_z) \qquad n=1..N \end{aligned} \tag{4.23}$$

where $N = N_xN_z$. $\mathbf{J}_s$ and $\mathbf{w}_t$ in equation 2.10 can be replaced by equations 4.22 and 4.23, then the impedance matrix elements become;

$$\begin{aligned} \mathbf{Z}_{st}(n,m) = \int_{-\infty}^{\infty}\int_{-\infty}^{\infty} &\left(\sum_{n=1}^{N}\mathbf{w}_{tn}(k_x,k_z)\right)\mathbf{G}(k_x,k_z,d,\omega) \\ &\left(\sum_{m=1}^{N}\mathbf{J}_{sm}(k_x,k_z)\right)dk_xdk_z \end{aligned} \tag{4.24}$$

With reference to equations 4.22 and 4.23, equation 4.24 can be rearranged as;

$$\mathbf{Z}_{st}(n,m) = \int_{-\infty}^{\infty} \left[\int_{-\infty}^{\infty} \left(\sum_{nx=1}^{N_x} \mathbf{w}_{tnx}(k_x) \right) \mathbf{G}(k_x, k_z, d, \omega) \left(\sum_{mx=1}^{N_x} \mathbf{J}_{smx}(k_x) \right) dk_x \right] \left(\sum_{nz=1}^{N_z} \mathbf{w}_{tnz}(k_z) \right) \left(\sum_{mz=1}^{N_z} \mathbf{J}_{smz}(k_z) \right) dk_z \tag{4.25}$$

The integration thus splits into two dependent integrations, but the number of integrands are independent for each integration in one dimension. The run–time for the impedance matrix calculation is a function of the number of current basis functions used in both directions and can be formulated as;

$$\frac{N_z(2N_xN_z + 1)}{(2N_x + 1)} \tag{4.26}$$

To illustrate the efficiency of the proposed technique, a simple microstrip line of finite length as shown in figure 4.5 is taken as an example. The dimensions of the circuit are not considered because the basic idea of the enhancement is discussed instead of presenting numerical results.

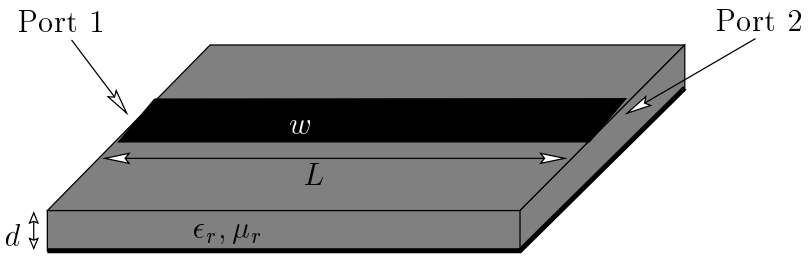

Figure 4.5: Microstrip line

A total of 57 rooftop functions are required for the analysis which does not use any precalculated current basis functions in either direction for the definition ($l_x = w/4, l_z = L/20$). Therefore N in equations 4.22 and 4.23 is 57. The size of the impedance matrix is double of the number of current basis functions and $N(2N + 1)$, which is 6555, the impedance matrix elements need to be calculated for each spot frequency

if symmetries in the impedance matrix are used. But the rooftop functions are two separable functions and the integration can be split into two dependent parts. In this case $(N1(2N1+1)$, which is 21, sub–impedance matrix elements are required to be calculated and 6555 impedance matrix elements are derived by facilitating 21 sub–impedance matrix elements. If precalculated current basis functions are used, the savings in computer memory and run–rime are even greater. In the author's experience, this enhancement gives up to 99% saving for the one dimensional integration and up to 90% for overall integration.

It must be noted that as the current basis functions are defined as two separable functions, the values of the current basis functions at each integral point are only calculated once and used during numerical integration for the entire frequency range.

4.7 Inclusion of Loss in Dielectric Substrate

The relative permittivity (ϵ_r) of a dielectric substrate is a real number if the substrate is lossless. Loss in a dielectric material may occur because of a finite conductivity (σ) or by damping effects [9]. In this case ϵ_r is a complex number and the imaginary part is always negative. A positive imaginary part implies energy creation instead of energy loss. The complex permittivity is given by

$$\epsilon_r = \epsilon_r^{'} - j(\epsilon_r^{''} + \frac{\sigma}{\omega}) \tag{4.27}$$

where $\epsilon_r^{''} + \frac{\sigma}{\omega}$ may be considered as the imaginary part of the permittivity or $\omega\epsilon_r^{''} + \sigma$ as the total conductivity. The loss tangent of a dielectric medium is defined by:

$$\tan\delta = \frac{\epsilon_r^{''} + \frac{\sigma}{\omega}}{\epsilon_r^{'}} \tag{4.28}$$

and the complex relative permittivity of a dielectric substrate can be written by using

the loss tangent ($\tan\delta$) as;

$$\epsilon_r^{loss} = \epsilon_r(1 - j\tan\delta) \tag{4.29}$$

Any measurement of $\tan\delta$ always includes the effects of the finite conductivity. At microwave frequencies, however $\epsilon_r^{''}$ is usually much larger than $\frac{\sigma}{\omega}$. In this implementation, the dielectric losses are included by replacing ϵ_r by $\epsilon_r(1 - j\tan\delta)$.

4.8 Numerical Convergence

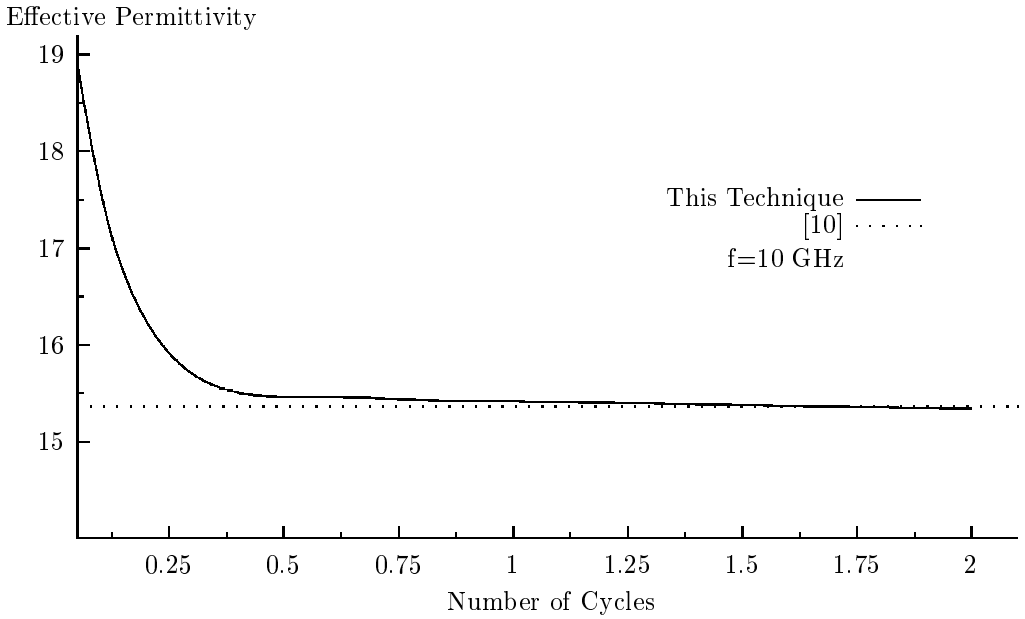

Figure 4.6: Effective permittivity of the open microstrip line

To illustrate the convergence pattern, results are presented for the example of two–dimensional open microstrip line of width 1.27 mm on a substrate of thickness 1.27 mm and of permittivity 20. In figure 4.6, the effective permittivity versus the number of cycles of the Fourier transform of the rooftop function included in the numerical integration is plotted. It is evident that relative convergence for this example has

been reached when $N_c \geq 1$ (N_c is the number of cycles). The exact value of N_c required for convergence is problem dependent, but is usually of the order of 1 even for more complicated three–dimensional structures.

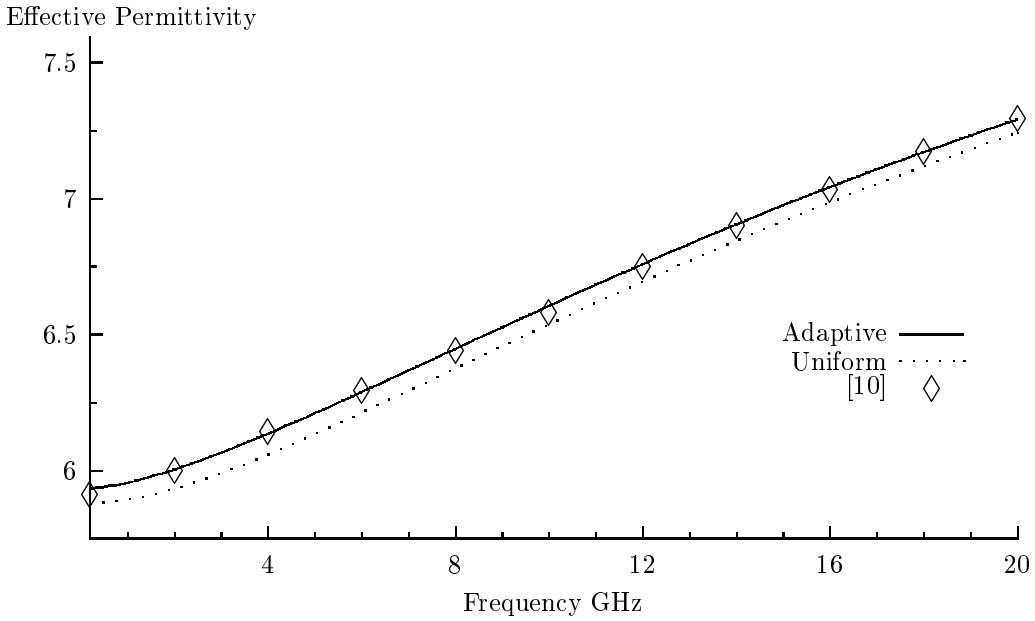

Figure 4.7: Effective permittivity of the open microstrip line

The convergence pattern for the adaptive integration step size is shown in figure 4.7 for the same structure. First the microstrip line has been modelled using the adaptive integration step as a function of the Fourier transform variables. Latter, it has been modelled using uniform integration steps while keeping the number of integration steps unchanged. Both results are compared with the published results by Itoh [10]. Even though identical number of integration steps are used, the accuracy is improved by using the adaptive integration technique as illustrated in figure 4.7.

The numerical convergence of this technique is also dependent on the integration range of the dyadic and asymptotic parts of the impedance matrix calculation in equations 4.7, 4.8 and 4.9. To illustrate this, the convergence pattern results are presented for the two–dimensional microstrip line of width 3.17 mm on a substrate of thickness 3.04 mm and of relative permittivity 11.7. In Figure 4.8, the effective

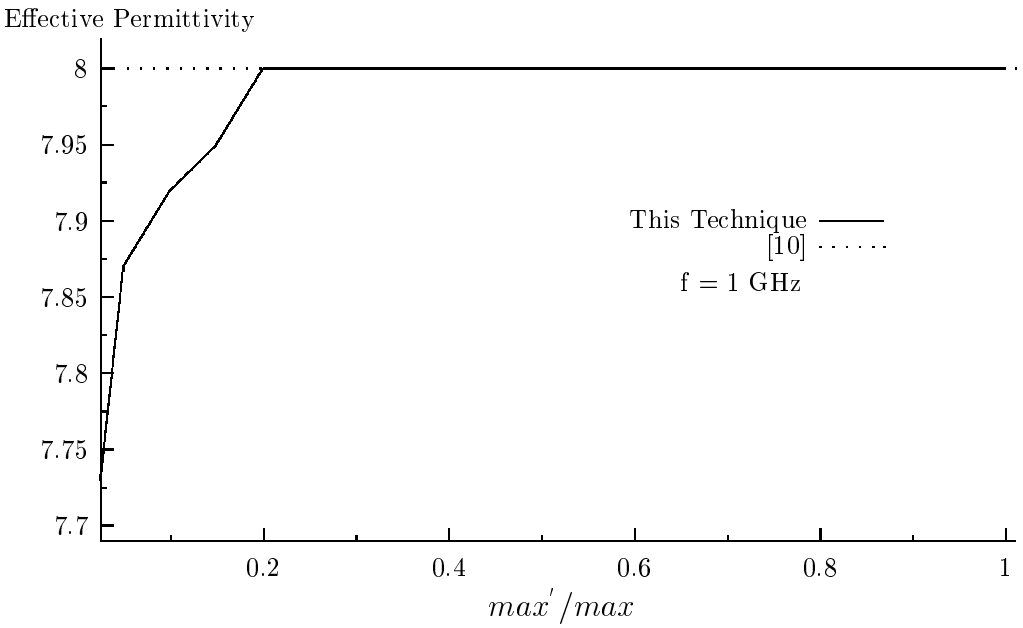

Figure 4.8: Numerical convergence of effective permittivity

permittivity versus the ratio of max' and max, given in equations 4.7, 4.8 and 4.9, is plotted. Since the numerical integration is over one cycle, max is given by;

$$max = \frac{2\pi}{l_x} \tag{4.30}$$

where $l_x = w/4$. max' is the integration range of the asymptotic part of the impedance matrix and a function of the operating frequency. It is evident that relative convergence for this example has been reached when ratio ≤ 0.2, that is a small percentage error compared to large values of the ratio. The exact value of ratio is problem dependent and determined by the conditions given in equations 4.3 and 4.4.

4.9 Loss in Dielectric Substrate

To illustrate the effects of the loss in the dielectric substrate, first results are presented for an example microstrip line whose dimensions are quoted in second part of

section 4.8 with the aid of two–dimensional version of the technique. In figure 4.9 a series of curves are plotted for several loss tangents of a dielectric substrate of which relative permittivity is 11.7. It is evident that the chance in the effective permittivity is inversely proportional to the loss tangent of the dielectric substrate in the region, which is between 1 GHz and 20 GHz, as shown in figure 4.9, but in the region, which is above 20 GHz, the loss in the substrate is less dependent on the effective permittivity.

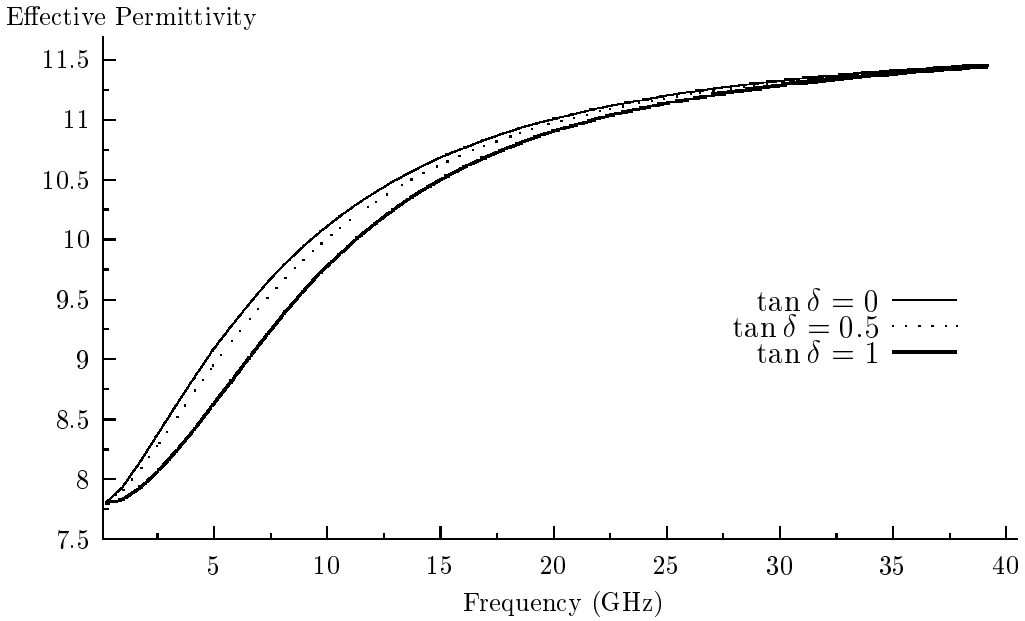

Figure 4.9: Effective permittivity of the microstrip line for different loss tangents of the dielectric substrate

Secondly, S–parameter results are presented for a simple microstrip line, which has been modelled in section 3.8.3.1, for different loss tangents. In this model, a precalculated transverse basis function is used in the direction perpendicular to current flow, whereas a current wave with a precalculated wave number is used in the direction of propagation. As illustrated in figure 4.10, S_{21} is almost unity for the substrate without any loss, because there is neither discontinuity nor loss in the circuit. This is no longer valid for the microstrip line with dielectric loss. Even though there is no singularity in the microstrip line, the S_{21} is not around unity, this is because the energy is lost in the lossy microstrip line. The loss is proportional to the loss tangent

of the dielectric substrate as illustrated in figure 4.10. The energy loss also increases as the operating frequency increases.

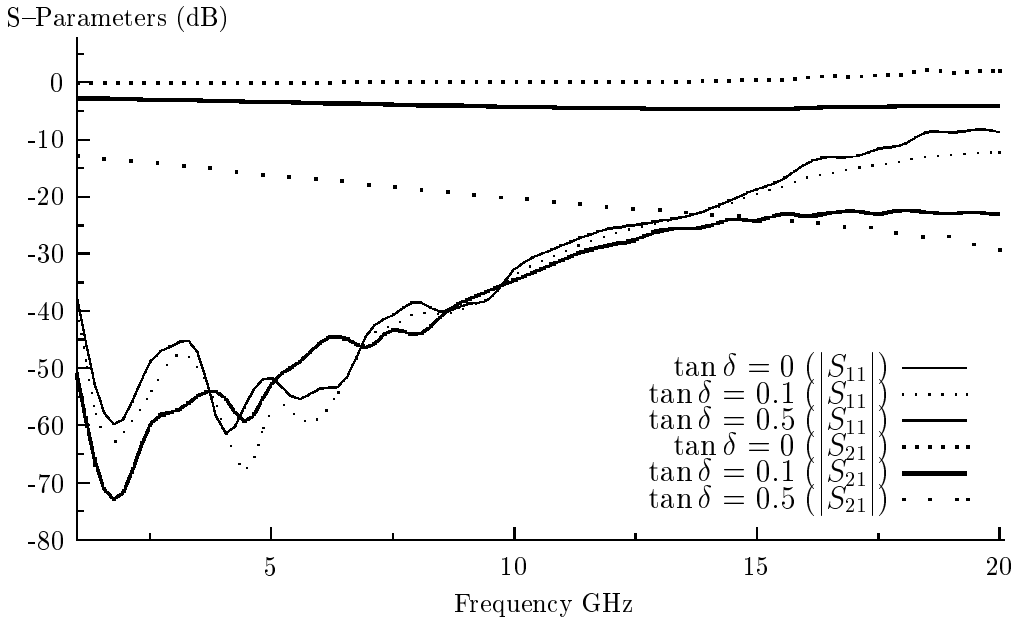

Figure 4.10: S–parameters' magnitude for the microstrip line with different loss tangents of the dielectric substrate

4.10 Summary

In this chapter, enhancements to improve the calculation of the impedance matrix have been described. The adaptive integration technique, which includes an adaptive truncation and an adaptive numerical integration step size has been proposed, to speed up the impedance matrix integration. The asymptotic form of the Green's function, which splits the impedance matrix into frequency dependent and asymptotic parts has been adopted for open planar microwave circuits. The location vector calculation has been introduced and applied in the region where identical grid sizes are used, to reduce the number of the impedance matrix elements to be calculated. The nature of the basis function which is to be defined as two separable functions for each

direction has been exploited to improve the numerical two–dimensional integration. Moreover the loss in the dielectric substrate has been included into the analysis and its effect has been illustrated on the simple microstrip structures.

References

[1] C. J. Railton and S. A. Meade, "Fast rigorous analysis of shielded planar filters," *IEEE Transaction on Microwave Theory and Technique*, vol. 40, pp. 978–985, May 1992.

[2] T. Itoh, *Numerical Techniques for Microwave and Millimeter–Wave Passive Structures*. John Willey and Sons, 1989.

[3] R. W. Jackson, "Full–wave, finite element analysis of irregular microstrip discontinuities," *IEEE Transaction on Microwave Theory and Technique*, vol. 37, pp. 81–89, January 1989.

[4] D. M. Pozar, "Input impedance and mutual coupling of rectangular microstrip antennas," *IEEE Transaction on Antennas and Propagation*, vol. 30, pp. 1191–1196, November 1982.

[5] E. H. Newman and D. Forrai, "Scattering from a microstrip patch," *IEEE Transaction on Antennas and Propagation*, vol. 35, pp. 245–251, March 1987.

[6] E. Kreyszing, *Advanced Engineering Mathematics*. Jhon Willy, 5. ed., 1983.

[7] C. J. Railton and T. Rozzi, "Complex modes in boxed microstrip," *IEEE Transaction on Microwave Theory and Technique*, vol. 36, pp. 865–873, May 1988.

[8] C. J. Railton and J. P. McGeehan, "A rigorous and computationally efficient analysis of microstrip for use as an electro–optic modulator," *IEEE Transaction on Microwave Theory and Technique*, vol. 37, pp. 1099–1103, July 1989.

[9] R. E. Collin, *Foundations for Microwave Engineering*. McGraw-Hill, 1992.

[10] T. Itoh and R. Mittra, "Spectral–domain approach for calculating the dispersion characteristics of microstrip lines," *IEEE Transaction on Microwave Theory and Technique*, pp. 496–499, July 1973.

Chapter 5

Efficient Excitation Modelling for Open Planar Circuits

5.1 Introduction

The ultimate goal of the work described in this thesis is to develop a fast, efficient technique in order to calculate the frequency response of open planar microwave circuits. Throughout this thesis, the circuits are represented by N–port network parameters. The scattering parameters, otherwise called S–parameters, are utilised but can be transformed to other representations by using standard formulae. While the S–parameter results of several circuits have been plotted, to verify the enhancements given in the earlier chapters, the derivation of S–parameters, which utilise an efficient excitation modelling introduced here for open planar circuits, is given in detail.

For the shielded planar microwave circuits, the S–parameters at a spot frequency are derived by Meade [1, chapter 5] from the solution of the matrix equation (equation 2.9), i.e. the set of coefficients define the unknown surface current distribution for an excitation configuration defined by the excitation vector ($\mathbf{V}_t$ in equation 2.9). This implementation cannot simply be applied to open structures without further modifications, because there are no side walls where the tangential electric field is identically zero.

A method was introduced by Jackson [2, 3] in 1985 for open planar structures, but his technique, in contrast to the method described here, is not efficient and requires a large number of extra sub–domain basis functions at relatively low frequencies, therefore a method is needed to yield accurate results in the whole microwave region and must be effective in remedying this deficiency.

To simplify the excitation, the circuit is represented as a black box and feedlines are connected to the ports of the circuit as shown in figure 5.1. The excitation problem now becomes the definition of the unknown current distribution on the metallisation of the entire system, which consists of a microwave circuit with feedlines connected to the ports. Definition of the unknown surface current distribution on the metallisation of the circuit (a black box in figure 5.2) is discussed in detail in chapter 3. A set of basis

functions are required to define the unknown current distribution on the feedlines, in order to complete the algorithm.

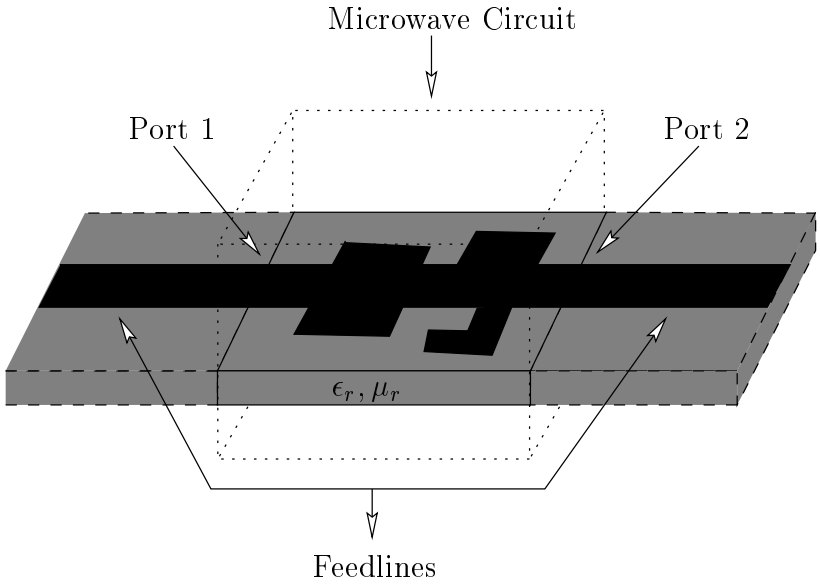

Figure 5.1: Illustration of excitation of the two port microwave circuit

Following [3], it is assumed that the fundamental microstrip mode is propagated on the feedline for which a travelling current wave has been chosen as a basis function. With this choice, the S–parameters of the circuit can be directly derived from the coefficients of the travelling waves used. But the use of the travelling wave as a current basis function on the feedline causes a current discontinuity in the interface between the port and feedline. In order to overcome this difficulty and to reach an accurate solution, a function, which is named by the author as the *compensation* function, is introduced for the interface between the port of the circuit and the adjacent feedline, instead of truncating the cosine (real part) portion one–quarter of wavelength from a zero of the sine (imaginary part) [2,3].

The length of the feedline is theoretically infinite, but in practice is an integer number of half wavelengths of the travelling current wave. In this implementation, the travelling current wave which is directed into the input port is called the incident current wave and that directed out of the input port is called the reflected current

wave. The transmitted current wave is the travelling current wave emanating from the output port as illustrated in figure 5.2.

The basic philosophy of the excitation, shown in figure 5.2, is that the incident current wave with a unit amplitude comes from infinity and goes into the input port. Some of the current travels through the circuit towards the output port, and some of the current reflects from the input port.

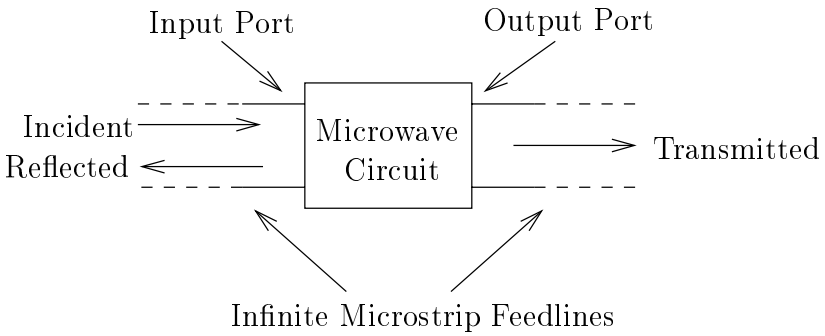

Figure 5.2: Illustration of excitation of the two port microwave circuit in closed form

In summary, the main steps of the algorithm can be itemised as follows;

- Connect the feedlines to the ports of the circuit. The width of the feedline must be identical to the width of the corresponding port
- Define the unknown current distribution on the metallisation of the circuit as a set of known current basis functions with unknown coefficients
- Use the sum of an incident current wave with unit amplitude and a reflected current wave with unknown amplitude for the feedline connected to the input port and a transmitted current wave with unknown amplitude for the feedline connected to output port as current basis functions
- Use the *compensation* function at the interface between the black box and adjacent feedline in order to transmit the full effects of the excitation into the circuit

- Apply the Method of Moments to eliminate the electric field components and solve the matrix equation, i.e. the set of unknown current coefficients which defines the unknown current distribution for the incident current wave with unit amplitude
- Calculate the S–parameters using the reflected and transmitted current wave coefficients.
- Repeat this procedure for each spot frequency, to find the S–parameters of the circuit for the frequency range of interest .

In the following sections, the efficient excitation modelling for open planar circuits is described in detail and compared with available techniques. Examples are also given to highlight the efficiency of the proposed technique.

5.2 Excitation Modelling

Because of their open structures, special care must be taken to include the effects of the excitation model into the analysis of open planar microwave circuits. Figure 5.3 shows the general three–dimensional open planar microwave circuit which is considered to be a black box in figure 5.2 and of which a set of current basis functions, described in detail in chapter 3, are used to define the unknown surface current distribution.

Circuits in this thesis are excited by connecting semi–infinite feedlines whose widths are identical to the joining ports, therefore the excitation has been simplified to the definition of the unknown current distribution of the system. The fundamental microstrip mode is assumed to propagate on each feedline and thus a travelling current wave is chosen as a current basis function. Derivations of the incident, reflected and transmitted current waves by using the travelling current wave in the direction of

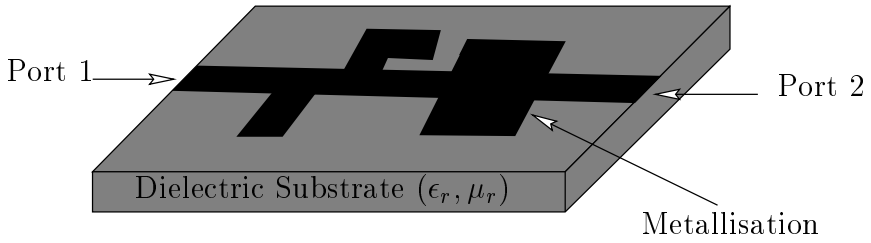

Figure 5.3: General 3–D open planar microwave circuit

propagation in the space domain are given by;

$$J_i(z) = \begin{cases} e^{-jk_n(z-z_i)} & -L + z_i \leq z \leq z_i \\ 0 & \text{otherwise} \end{cases}$$
$$J_r(z) = \begin{cases} -a_r e^{jk_n(z-z_i)} & -L + z_i \leq z \leq z_i \\ 0 & \text{otherwise} \end{cases} \quad (5.1)$$
$$J_t(z) = \begin{cases} a_t e^{-jk_n(z-z_o)} & z_o \leq z \leq L + z_o \\ 0 & \text{otherwise} \end{cases}$$

where k_n is the precalculated wavenumber of the infinite microstrip line of width identical to the feedline, L is the length of the feedline and z_s $(s = i, o)$ is the offset of the port from the origin. The wave number of each spot frequency is precalculated using the two–dimensional version of the technique, which is given in detail in appendix B, and stored in a data file, in order to use when it is required. The letters i, t, r indicate the incident, transmitted and reflected current waves respectively and the unknown coefficients a_r, a_t are coefficients of the reflected and transmitted current waves, which are used to calculate the S–parameters of the microwave circuit at each spot frequency. These waves are assumed to flow in the z direction and can be derived for the x direction by changing z to x in equation 5.1. The ports are assumed to be at the origin and can be shifted. The sum of the incident and reflected current waves is the current basis function of the feedline connected to the input port and a reflected current wave is defined as a current basis function for the feedline connected

to the output port in the direction of current flow as,

$$\begin{aligned} J_{input} &= J_i + J_r \\ &= (1 - a_r)\cos(k_n(z - z_i)) - j(1 + a_r)\sin(k_n(z - z_i)) \end{aligned} \tag{5.2}$$

$$\begin{aligned} J_{output} &= J_t \\ &= a_t[\cos(k_n(z - z_o)) - j\sin(k_n(z - z_o))] \end{aligned} \tag{5.3}$$

Note that these functions are in the space domain and Fourier transforms are required in the Spectral Domain Method. The Fourier transforms of the current basis functions of the feedlines as defined in equation 5.1 and derived in appendix D.1 are given by;

$$\mathbf{J}_i(k_n, k_z) = \frac{2}{k_z - k_n}\sin\left((k_z - k_n)\frac{L}{2}\right)e^{-j(k_z - k_n)\frac{L}{2}}e^{jk_z z_i} \tag{5.4}$$

$$\mathbf{J}_r(k_n, k_z) = \frac{2}{k_z + k_n}\sin\left((k_z + k_n)\frac{L}{2}\right)e^{-j(k_z + k_n)\frac{L}{2}}e^{jk_z z_i} \tag{5.5}$$

$$\mathbf{J}_t(k_n, k_z) = \frac{2}{k_z - k_n}\sin\left((k_z - k_n)\frac{L}{2}\right)e^{j(k_z - k_n)\frac{L}{2}}e^{jk_z z_o} \tag{5.6}$$

where L is the length of the feedline, which theoretically extends to infinity, but will yield accurate results if it is an integer number of half wavelengths [2,3]. The current basis functions for the feedlines in both directions in the spectral domain are defined by;

$$\begin{aligned} \mathbf{J}_{input}(k_x, k_n, k_z) =& [\mathbf{g}_z^{in}(k_x) + j\mathbf{g}_x^{in}(k_x)]\mathbf{J}_i(k_n, k_z) + \\ & a_r[\mathbf{g}_z^{in}(k_x) - j\mathbf{g}_x^{in}(k_x)]\mathbf{J}_r(k_n, k_z) \end{aligned} \tag{5.7}$$

$$\mathbf{J}_{output}(k_x, k_n, k_z) = a_t[\mathbf{g}_z^{o}(k_x) + j\mathbf{g}_x^{o}(k_x)]\mathbf{J}_t(k_n, k_z) \tag{5.8}$$

where functions $\mathbf{g}_z^{in}, \mathbf{g}_x^{in}, \mathbf{g}_z^{o}$ and $\mathbf{g}_x^{o}$ are the sum of the Fourier transforms of the rooftop functions with previously calculated coefficients by the two–dimensional version of the technique (given in detail in appendix B).

The definition of the current basis functions for the feedlines connected to the ports of the circuit is described as shown in figure 5.4. As shown in equations 5.2, 5.3 and in

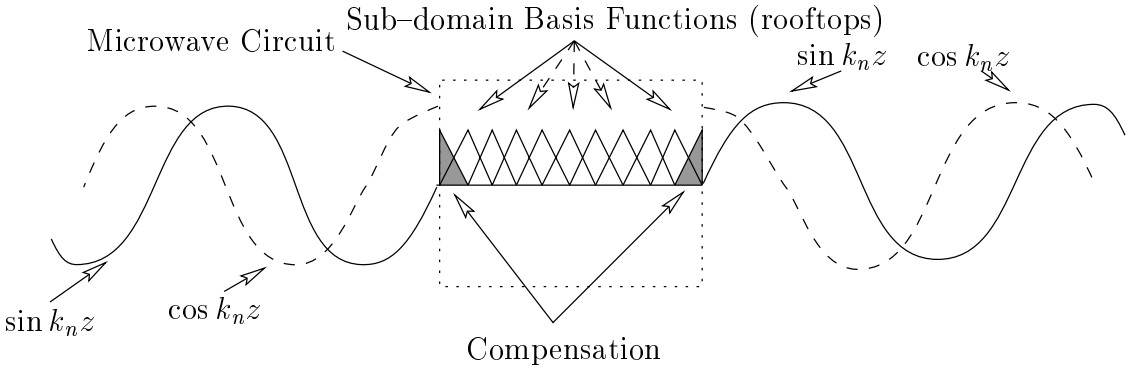

Figure 5.4: Illustration of the excitation in the direction of current flow

figure 5.4, the current basis functions of the feedlines have real ($\cos k_n z$) and imaginary ($\sin k_n z$) parts. The real part causes current discontinuities in the direction of current flow, because the triangle function as a rooftop function component is identically zero at the interface between the port and the adjacent feedline, whereas $\cos(k_n z)$ has a finite value. The problem is the same in the direction perpendicular to current flow, because in this case the step function as a rooftop function component has a finite value, whereas $\sin(k_n z)$ is identically zero. Therefore extra basis functions are still required in each interface between the port and adjacent feedline for the correct solution. These functions are introduced and referred to by the author as *compensation* functions which are shown in figure 5.5. The compensation functions are defined for the input port in the space domain by:

$$J_z(z) = \begin{cases} 1 - \frac{z - z_i}{l_z} & z_i \leq z \leq z_i + l_z \\ 0 & \text{otherwise} \end{cases} \tag{5.9}$$

$$J_x(z) = \begin{cases} \frac{z - z_i}{l_z} & z_i \leq z \leq z_i + l_z \\ 0 & \text{otherwise} \end{cases} \tag{5.10}$$

and for the output port;

$$J_z(z) = \begin{cases} 1 + \frac{z - z_o}{l_z} & z_o - l_z \leq z \leq z_o \\ 0 & \text{otherwise} \end{cases} \tag{5.11}$$

$$J_x(z) = \begin{cases} -\frac{z - z_o}{l_z} & z_o - l_z \leq z \leq z_o \\ 0 & \text{otherwise} \end{cases} \tag{5.12}$$

where l_z is the size of the compensation functions in the direction of propagation.

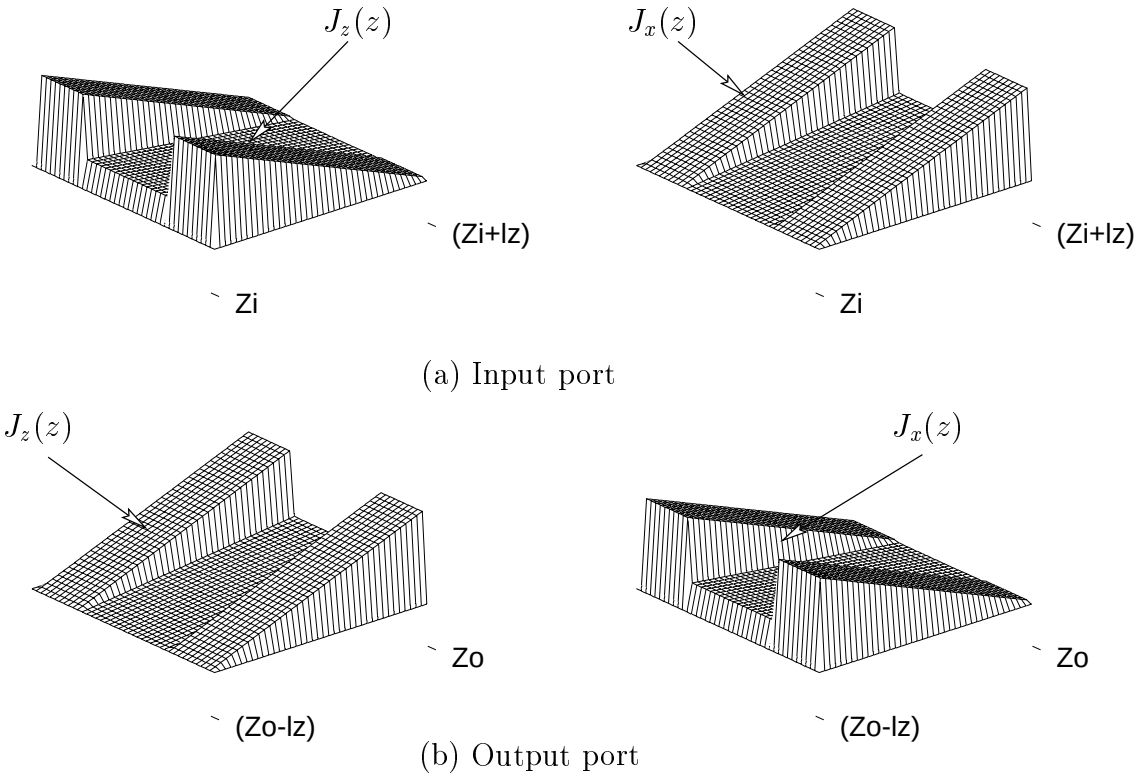

Figure 5.5: Compensation functions for the input and output ports

$J_z(z)$ in equation 5.9 and figure 5.5(a) transfers the effect of the cosine portion of the incident current wave in the direction of current flow, whereas $J_x(z)$ in equation 5.10 and figure 5.5(a) transfers the effect of the sine portion of the incident current wave in the direction perpendicular to the current flow. Similarly $J_z(z)$ in equation 5.11 and figure 5.5(b) transfers the current wave to the output port in the direction of

propagation whereas $J_x(z)$ in equation 5.12 and figure 5.5(b) transfers the current wave in the transverse direction.

As illustrated in figure 5.5, the compensation function is actually a semi–rooftop function with an offset from the origin to either $-z$ or $+z$ directions and the missing portion of the rooftop function has been completed by the current waves. Fourier transforms of the half rooftop functions are given by;

$$\mathbf{J}_{left}(k_z) = \frac{1}{k_z^2 l_z}[(1-\cos(k_z l_z)) + j(\sin(k_z l_z) - k_z l_z)] \tag{5.13}$$

$$\mathbf{J}_{right}(k_z) = \frac{1}{k_z^2 l_z}[(1-\cos(k_z l_z)) - j(\sin(k_z l_z) - k_z l_z)] \tag{5.14}$$

where $\mathbf{J}_{left}$ and $\mathbf{J}_{right}$ indicate the Fourier transform of the left and right hand side of a rooftop function. The derivation of the compensation functions from the left and right hand side of the rooftop function for the input port are given by;

$$\mathbf{J}_z(k_z) = \mathbf{J}_{right}(k_z) e^{jk_z z_i} \tag{5.15}$$

$$\mathbf{J}_x(k_z) = \mathbf{J}_{left}(k_z) e^{jk_z(z_i + l_z)} \tag{5.16}$$

and for the output port, they are given by;

$$\mathbf{J}_z(k_z) = \mathbf{J}_{left}(k_z) e^{jk_z z_o} \tag{5.17}$$

$$\mathbf{J}_x(k_z) = \mathbf{J}_{right}(k_z) e^{jk_z(z_o - l_z)} \tag{5.18}$$

The identical precalculated basis functions ($\mathbf{g}_z^{in}, \mathbf{g}_x^{in}, \mathbf{g}_z^{o}$ and $\mathbf{g}_x^{o}$ in equation 5.8) are used for the components of the compensation functions in the transverse direction. Including all current basis functions of the entire system, the total current is expressed

as:

$$\mathbf{J}_{total} = \mathbf{J}_{box}(k_x, k_z) + \sum_{n=1}^{N} (a_{pn}\mathbf{J}_{port_n}(k_x, k_n k_z) + a_{cn}\mathbf{J}_{comp_n}(k_x, k_z)) \tag{5.19}$$

where N is the number of ports, $\mathbf{J}_{box}$ refers to the basis functions of the actual open circuit and $\mathbf{J}_{port_n}$ is either the sum of the incident and reflected current wave or the transmitted current wave. To calculate the S–parameters of the circuit, a_{pn} must be known. The Method of Moments is employed to eliminate the electric field components and to find the unknown coefficients. Weighting functions are then required: $\mathbf{J}_{box}$ and $\mathbf{J}_{comp_n}$ are used. A total of N weighting functions must be defined to complete the algorithm. A triangle function which straddles the lines separating the port and the feedline, is used in the direction of current flow and precalculated basis functions are applied in the direction perpendicular to current flow. After application of the Method of Moments, the matrix equation yields,

$$[\mathbf{Z}][\mathbf{I}] = [0] \tag{5.20}$$

Because two travelling waves, which are the incident current wave with unit amplitude and the reflected current wave with unknown amplitude, are used for the feedline connected to the input port of the circuit, $\mathbf{Z}$ is not a square matrix and contains unknown coefficients, as well as the known unit amplitude. The column of the impedance matrix corresponding to the incident current wave products has been moved to the right hand side of the equation and the equation 5.20 becomes,

$$[\mathbf{Z}]_n[\mathbf{I}]_n = [\mathbf{Z}]_i \tag{5.21}$$

where $\mathbf{Z}_n$ consists of the elements related to unknown current basis functions and $\mathbf{Z}_i$ is the column matrix containing the elements related to incident current waves. Any root–finding procedure can be applied to solve equation 5.21 and the unknown coefficients can be found. The S–parameters of the N–port circuit are actually the

coefficients of the reflected and the transmitted current waves.

It is emphasised that the asymptotic form of the Green's function given in detail in section 4.3.1 is utilised to split the impedance matrix into frequency–dependent and frequency–independent parts, but the current basis function for the feedline in equation 5.1 is a function of wave number, which is a function of operating frequency. Therefore the asymptotic form of the Green's function can only be applied to the impedance matrix elements related to the products of current basis functions of the circuit. However, numerical enhancements introduced in section 4.6 are used to reduce the number of impedance matrix elements required and to speed up the two–dimensional integration.

5.3 Comparison with other Excitation Modellings

Excitation modelling has been implemented by Meade [1] for a general shielded planar structure, as shown in figure 5.6. In this technique, a source is defined by setting the corresponding element to a finite value and all others to zero:

$$\mathbf{V}_t = \begin{cases} \sum_{q=1}^{Q} 4(l_z)^2 aba_{pq} & \text{for each basis function at input port} \\ 0 & \text{otherwise} \end{cases} \tag{5.22}$$

where a_{pq} is the relative weighting coefficient of the q^{th} component of the p^{th} basis function, l_z is the grid size in z direction and a and b are the dimensions of the box. The $4(l_z)^2$ term was derived from the width of the weighting function and the ab term is a scaling factor for the Green's function.

The matrix equation 2.9 is then solved for the set of current coefficients and the embedded Y–parameters are calculated. The S–parameters are derived by the standard

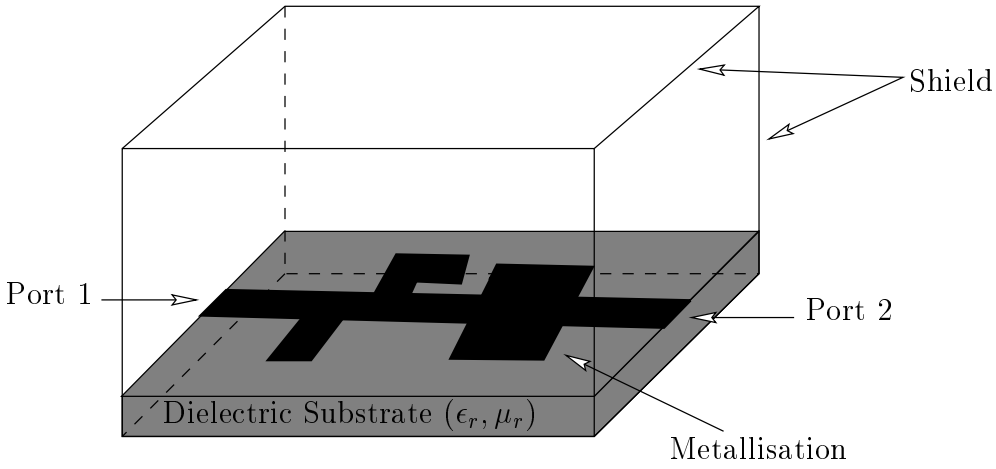

Figure 5.6: General 3–D shielded microwave circuit

formula expressed in matrix form as,

$$\mathbf{S} = (\mathbf{Y} + \mathbf{I})^{-1}(\mathbf{Y} - \mathbf{I}) \tag{5.23}$$

It is not possible to apply this technique to the planar open structure, because no side walls exist in the circuit, and so the tangential electric field can not be assumed to be identically zero. Moreover, the effects of port/feedline arrangement are dominant to the resulting S–parameters, therefore Meade has also introduced a de–embedding algorithm to minimise the effects of the port/feed arrangement [4]. The extraction of the S–parameters from the *a priori* knowledge of the surface current distribution is achieved by applying transmission line theory to the feedlines. The precalculated line mode basis functions are used to model the current standing wave set up on the feedlines. The de–embedding algorithm relies on the presence of a current standing wave minimum on the input line. This can only be guaranteed when the line length $L \geq \lambda_g/2$ so the frequency range of the technique has a lower limit which is a function of the transmission line length and the guide wavelength. Thus, the de–embedding algorithm is problem dependent and hence not valid for the wide frequency range of interest.

Jackson [2] has introduced a method to calculated S–parameters of gap–discontinuities in 1985 and applied to irregular shaped microstrip structures [3] in 1989. The technique described here was initially inspired by his work, but his technique is not efficient at relatively low frequencies, just like Meade's technique mentioned above. Because the cosine portion of the travelling wave is believed to cause numerical difficulties and it is truncated one–quarter of a guide wavelength from a zero of the sine. The length of the truncation is a function of the operating frequency. At low frequencies, its length becomes larger than the entire circuit's dimension, and a large number of extra rooftop functions are required otherwise the cosine portion of the current wave reflects before reaching the input port.

These are the limitations and drawbacks of existing excitation modellings. The technique introduced here does not have either lower limit or truncation, and therefore it is valid over a wide microwave frequency band and does not require a large number of rooftop functions at low frequencies.

5.4 Evaluation of Efficient Excitation Modelling

The Excitation modelling is initially inspired by the the method described by Jackson [2] and developed by remedying the deficiency which occurs at relatively low frequencies. The evaluation of the efficient excitation mechanism is shown in figure 5.7. As mentioned above, the feedlines are connected to the ports of the circuit and travelling current waves are used as current basis functions for these feedlines. The cosine portion of the z–directed current wave is assumed to cause a longitudinal current discontinuity and numerical difficulties in [2,3] and is truncated one–quarter guide wavelength from a zero of the sine, but this truncation also gives undefined regions as illustrated by the shaded areas in figure 5.7(a). An attempt was made to minimise the effects of these undefined regions by shifting the current wave so that it terminates in the middle of the finite element grid, instead of at the port and by using

extra rooftops to complete the truncated region. This shifting of the current wave can cover the shaded regions only if the frequency is high enough so that the grid size is bigger than the length of the truncation, which is a function of the frequency, without using extra rooftops. Hence at low frequencies, where the truncation length is even larger than the entire circuit's dimension, and it is impossible to cover this region by using a single rooftop function and a large number of rooftop functions are necessary. There is no point in using a large number of rooftop functions when they are unnecessary.

The second step of the evaluation is to use a travelling current wave without truncation. The termination is still in the middle of the finite element grid, instead of at port as shown in figure 5.7(b). In this case, extra rooftop functions are not required, because there is no truncation of the current wave. But, at the port, the coefficient of the rooftop function must be identical to the sum of the incident and reflected current waves, because there is no discontinuity in the interface between the port and feedline. However the shaded area is defined twice which causes numerical difficulties and a current discontinuity.

The solution to the problem outlined above is to shift the current wave back, so that it terminates at the port of the circuit. In this case, as shown in figure 5.7(c) the cosine portion of the current wave has a finite value, whereas the rooftop function in the direction of current flow is identically zero. Therefore, the cosine portion of the incident current wave reflects from the input port, because the current at the input port must be identically zero (shaded area in figure 5.7(c)). So this is not the solution to the problem.

The final step of the evaluation and efficient excitation mechanism is shown in figure 5.7(d). There is neither truncation of the cosine portion of current wave nor shifting the current wave to terminate in the middle of the finite element grid. In order to transmit the effect of the cosine portion of the current wave in the direction of current flow and the effect of the sine portion of the current wave in the direction

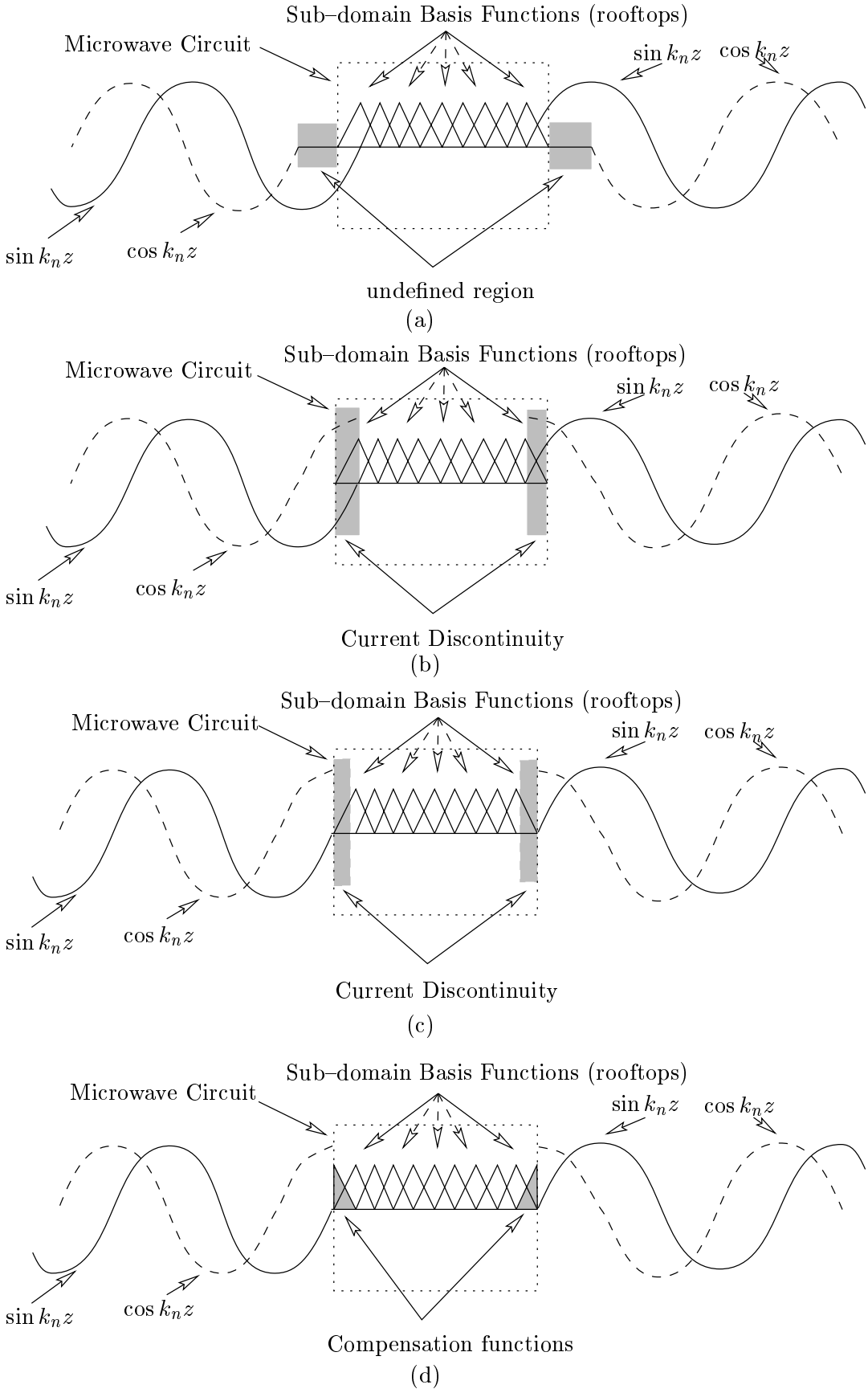

Figure 5.7: Evaluation of efficient excitation modelling

perpendicular to current flow, the compensation functions are used at the interface between the feedline and port of the circuit.

5.5 Numerical Results

It must be noted that, no extra rooftop functions are used to complete the truncated portion of the current wave to use identical number of basis functions in each model and to illustrate the improvement in the accuracy for identical number of basis functions.

5.5.1 Microstrip Line

To demonstrate the evaluation of the excitation and the improvement in the accuracy, a microstrip line without any discontinuity has been analysed as a test structure. The reason for this choice is that its S–parameters are very easy to predict.

The microstrip line in figure 5.8 is of length 2.8 mm, of width 0.7 mm on the substrate thickness 0.381 mm, relative permittivity 11.7 and relative permeability 1. The dimensions of the circuit have been intentionally chosen by the author to be relatively small, in order to highlight the deficiency of the Jackson's technique and to illustrate the improvement in the accuracy.

Four sets of S–parameter results are plotted in figure 5.9. These are the results calculated by using 42 rooftop functions in total for the definition ($l_x = w/4 = 0.157$ mm and $l_z = L/8 = 0.35$ mm). First the test structure is analysed by using truncated travelling current waves for excitation. The minimum operating frequency in the analysis is 1 GHz and the corresponding length of the truncated cosine portion is 26.25 mm, which is 75 times bigger than the overlapping rooftop size, which is 0.35 mm in the direction of propagation. For the maximum operating frequency of 20

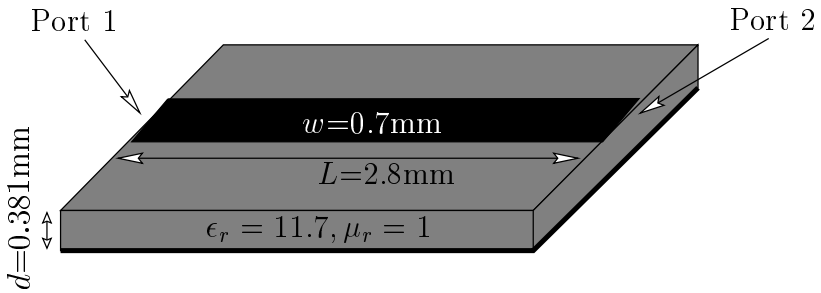

Figure 5.8: Finite microstrip line test structure

GHz, the corresponding length of the truncated portion is 1.25 mm, which is still more than 3 times bigger than the rooftop size. Therefore the cosine portion of the incident current wave never reaches to the input port of the circuit in this frequency range and the circuit behaves like an open–end discontinuity as shown in figure 5.9. To get the same accuracy by Jackson's technique for this frequency range, up to 888 extra rooftop functions are required. So Jackson's technique is not efficient for this type of small circuit in this frequency range. Even though the second and third steps of the evaluation of the excitation give slight improvement without requiring extra rooftops, they are still not suitable excitation modelling techniques for the open structures over the entire microwave region.

In the end, the introduced excitation modelling is used for the analysis of the test structure, and the improvement in the accuracy is highlighted in figure 5.9. In this model, the effects of excitation are transferred into the circuit without any loss. The S_{21} is almost zero, whereas S_{11} is negative large value as they have been predicted.

5.5.2 Edge–Coupled Filter

In order to further prove the accuracy of the excitation modelling introduced here, it is applied to the analysis of the microstrip edge–coupled filter shown in figure 3.16. The edge–coupled filter is viewed by author as an important circuit to illustrate the

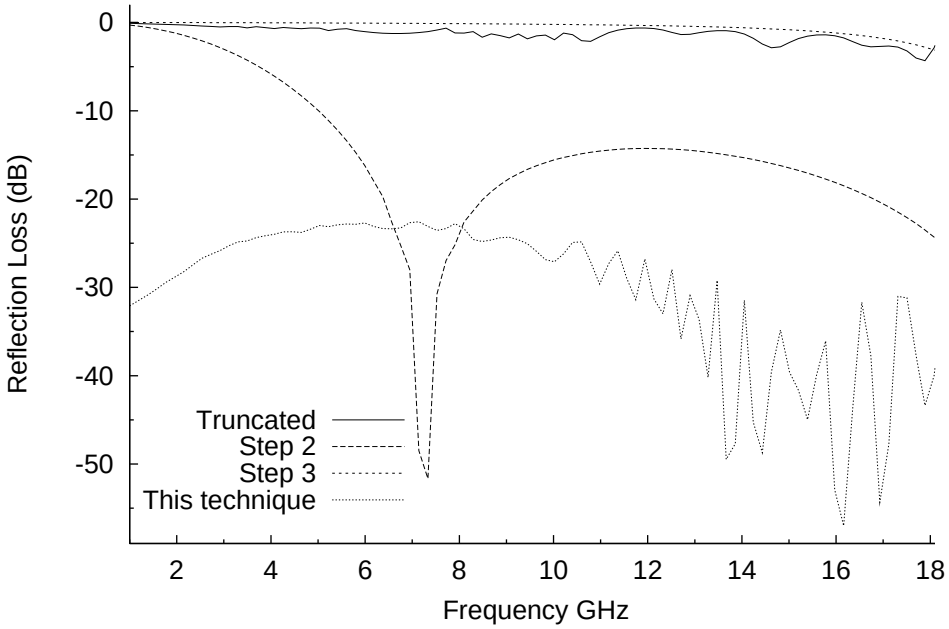

(a) Magnitude of S_{11}

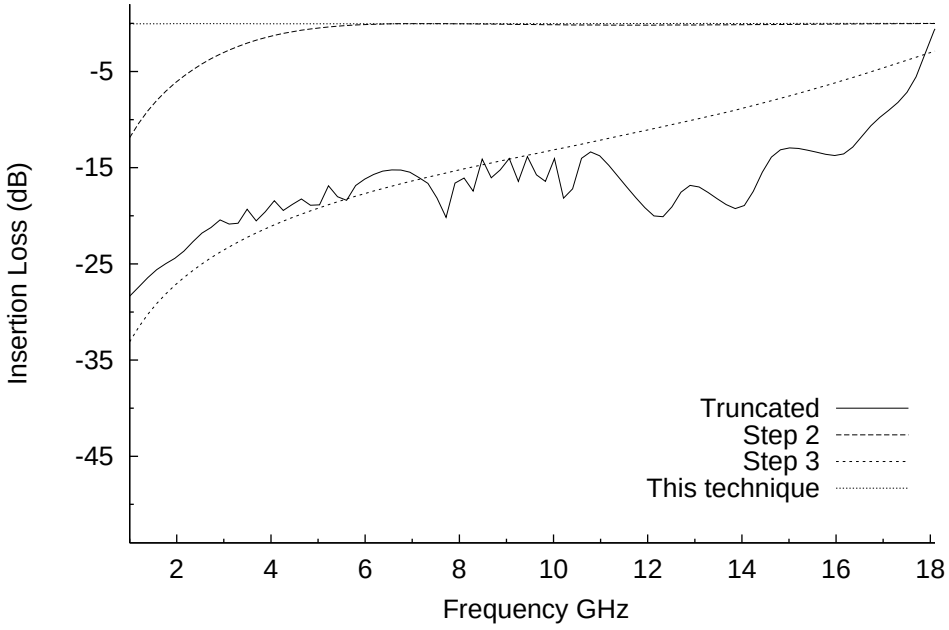

(b) Magnitude of S_{21}

Figure 5.9: Magnitude of S–parameters for the open microstrip line illustrating the evaluation of the excitation modelling

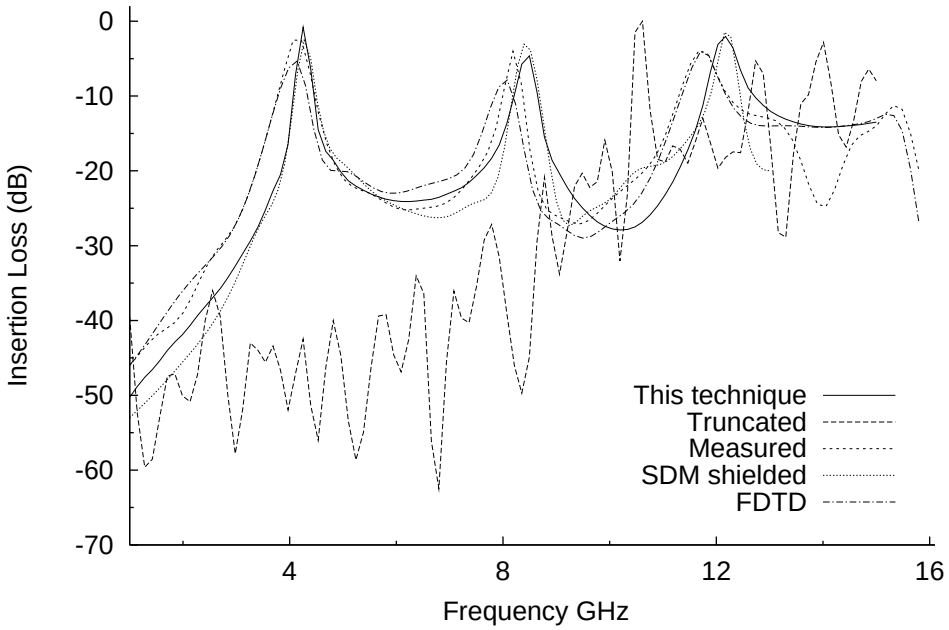

Figure 5.10: Magnitude of S–parameters for the edge–coupled filter

improvement in the accuracy, because in the literature, results are available from measurements performed by Shibata *et al* [5], from FDTD performed by Paul *et al* [6] and from SDM shielded performed by Railton *et al* [7]. The dimensions of the circuit are given in section 3.8.3.2.

As seen in figure 5.10, there is a clear agreement between the introduced excitation modelling and the published results for SDM shielded and FDTD as well as with measured data. Furthermore, problems caused by box mode broadband using the method of [7] have been eliminated. The use of travelling current waves with truncation yields completely meaningless results, this is because the minimum operation frequency is 1 GHz with the corresponding length of the truncated cosine portion being 29.14 mm. This is almost 46 times bigger than the size of the rooftop in the direction of the propagation for the definition ($l_x = w/4 = 0.318$ mm and $l_z = l/20 = 0.636$ mm). The maximum operating frequency, which is 15 GHz, is still not sufficient to cover the missing portion without extra rooftops. For the maximum operation frequency

the length of the truncated portion is 1.78 mm and still almost 3 times bigger than the rooftop size. Again for the same accuracy by Jackson's technique requires up to 540 extra rooftops (270 x and 270 z components) to complete the missing portions

It must be noted that, the Jackson technique was used as described in his paper [2,3] and shown to be accurate. However his technique is accurate only if the missing portion is completed with a large number of rooftops. At low frequencies, a large number of rooftop functions are required to complete the missing portion.

5.6 Summary

In this chapter, an efficient excitation algorithm to extract the circuit S–parameters from the known surface current distribution has been discussed. It has been shown that the introduced excitation modelling is effective in remedying all deficiencies of available excitation modellings in the literature. The accuracy of the technique was compared with published results with the aid of numerical examples of a microstrip line and the edge–coupled filter. It is emphasised that, the number of extra rooftops required to complete the missing portion are not "several" as quoted in [3], but a huge number of rooftop functions are required to yield accurate solution at low frequencies.

References

[1] S. A. Meade, *The Rapid and Rigorous Mathematical Modelling of Passive Planar Microwave Circuits*. PhD thesis, University of Bristol, March 1994.

[2] R. W. Jackson and D. M. Pozar, "Full–wave analysis of microstrip open–end and gap discontinuities," *IEEE Transaction on Microwave Theory and Technique*, vol. 33, pp. 1036–1042, October 1985.

[3] R. W. Jackson, "Full–wave, finite element analysis of irregular microstrip discontinuities," *IEEE Transaction on Microwave Theory and Technique*, vol. 37, pp. 81–89, January 1989.

[4] S. A. Meade and C. J. Railton, "Efficient extraction of s–parameters from the spectral domain method for passive planar microwave circuits," in *24 th. European Microwave Conference*, pp. 1084–1089, September 1994.

[5] T. Shibata, T. Hayashi, and T. Kimura, "Analysis of microstrip circuits using three–dimensional full–wave electromagnetic field analysis in the time domain," *IEEE Transaction on Microwave Theory and Technique*, vol. 36, pp. 1064–1070, June 1988.

[6] D. L. Paul, E. M. Daniel, and C. J. Railton, "Fast finite difference time domain method for the analysis of planar microstrip circuits," in *21st European Microwave Conference*, pp. 303–308, September 1991.

[7] C. J. Railton and S. A. Meade, "Fast rigorous analysis of shielded planar filters," *IEEE Transaction on Microwave Theory and Technique*, vol. 40, pp. 978–985, May 1992.

Chapter 6

Analysis of Complex Microwave Circuits

6.1 Introduction

Chapter 3 has discussed the minimisation of current basis functions, which are required to define the unknown current distribution on the complex metallisation pattern, whereas in chapter 4 the calculation of the impedance matrix has been improved by introducing significant enhancements. Chapter 5 has introduced a novel efficient excitation modelling technique for open planar microwave circuits by remedying the deficiency of the Jackson's technique [1, 2]. As mentioned in section 5.3, the cosine portion of the current wave was truncated one quarter wavelength from a zero of the sine assuming that it caused numerical difficulties, and this truncated portion was completed using an extra set of rooftop functions. The so–called compensation function has been introduced in section 5.2 to be used at the interface between the port and adjacent feedline in order to transmit the full effect of excitation without requiring truncation and the use of the extra set of rooftop functions.

In this chapter, the total improvement in the complex circuit analysis will be discussed. To do this, the improvement gained by each enhancement will be given in percentage, instead of run–time requirement on the computer. Because the run–time is computer dependent and the speed of the analysis is a function of CPU and memory of the computer as well as computer load.

6.2 Microstrip Step

The microstrip step, shown in figure 6.1 has been modelled in section 3.8.4 and published in [3]. The aim to repeat this is to demonstrate the total improvement in the analysis. In section 3.8.4, the sub–gridding was used to define the unknown surface current distribution but the effects of the enhancements introduced in chapter 4 and of the efficient excitation modelling given in chapter 5 have not been taken into account.

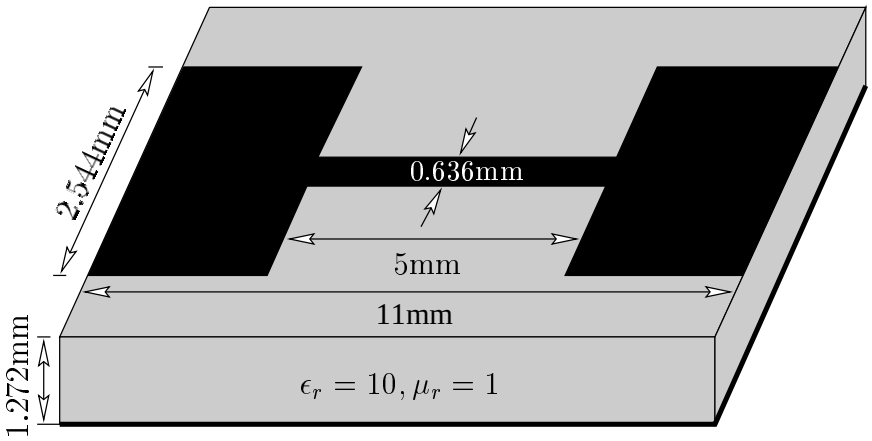

Figure 6.1: Outlook of the microstrip step discontinuity

As mentioned in chapter 3, the analysis of a complex microwave circuit is based on dividing the circuit into regions where the current distribution is easy to determine. Therefore, the circuit shown in figure 6.1 is divided into 7 regions as illustrated in figure 6.2.

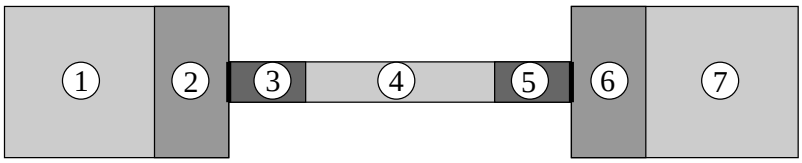

Figure 6.2: Plan evaluation of the microstrip step discontinuity shoving regions

The set of basis functions for the model in figure 6.2 is summarised below:

- Regions 1,4 and 7 :

  3 precalculated current waves as defined by equations 3.13 and 3.14

- Regions 2,3,5 and 6 :

  16 rooftop current basis functions ($l_x = 0.318$ mm and $l_z = 0.5$ mm)

- Ports :

  The sum of an incident and reflected current wave for the input port and a

transmitted current wave for the output port as defined by equations 5.2 and 5.3

- Transfer :
  - 2 compensation functions in the interfaces between the port and feedline as defined by equations 5.15, 5.16 for the input port and 5.17, 5.18 for the output port
  - 2 rooftop functions to join two regions ($l_x = 0.318$ mm and $l_z = 0.5$ mm)

The total number of current basis functions required to model the unknown current on the metallisation of the circuit is 42 (21 x and 21 z components) in contrast to 162 (81 x and 81 z components) as given in detail in section 3.8.4. The current basis functions required for accurate modelling are reduced by 74%. A truncated current wave and an extra set of rooftop functions to complete this truncated portion as used by Jackson [2] are employed to excite the open circuit of interest. The minimum operating frequency is 1 GHz and the corresponding length of the truncated portion is 27.7 mm, which is 55 times bigger than the rooftop function size. For the maximum operating frequency of 20 GHz, the corresponding length of the truncation is 1.25 mm, which is still 2.5 times bigger than the rooftop size. To complete the missing portion in order to get accurate results, up to 1512 extra rooftop functions (756 x and 756 z components) are required. In this thesis, however a novel compensation function has been introduced and the effect of excitation has been successfully transferred into the circuit of interest by using two for each port. Therefore, 4 compensation functions (2 x and 2 z components) for 2–port circuit are enough in contrast to 1512 extra rooftops and the saving is 99.7% at 1 GHz.

The adaptive integration technique given in detail in section 4.2 is used to calculate the impedance matrix elements. A coarse integration step which is 4 times bigger than the fine integration step is chosen. With this choice, the speed of the calculation is increased 4 times compared with the use of uniform integration steps. In addition, in section 4.6 the feature of the current basis function which is to be two

separable functions in each direction is exploited. 903 impedance matrix elements must be integrated in each direction if the enhancement in section 4.6 is not used. 18 basis functions (9 x and 9 z components) are used in x direction and 903 impedance matrix elements can be derived from 171 sub–impedance matrix elements. Therefore the impedance matrix elements needed to be integrated are reduced by 81% in one dimension. The improvement by using the symmetry of the Green's function also gives 10% improvement. The S–parameter results were plotted in figure 3.20.

6.3 Edge–Coupled Filter

The edge–coupled filter shown in figure 3.16 has been modelled in section 3.8.3.2 to test the similarity of the results given by precalculated current basis function and a set of rooftop function. The filter has also been analysed in section 5.5.2 to illustrate the accuracy of the proposed excitation modelling technique. It is mentioned here to combine these two enhancements and to illustrate the total improvement in percentage of computer resources.

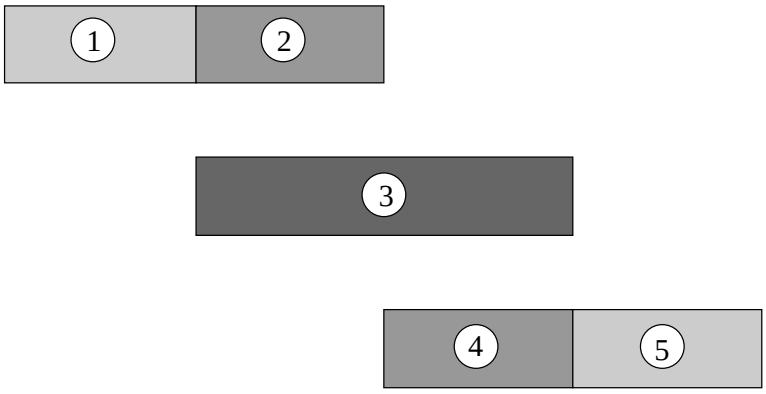

Figure 6.3: Plan evaluation of the microstrip edge–coupled filter shoving regions

The edge–coupled filter has been divided into 5 regions as shown in figure 6.3. The set of basis functions for the model in figure 6.3 is summarised below:

- Regions 1 and 5 :

  2 precalculated current waves as defined by equations 3.13 and 3.14

- Regions 2 and 4 :

  18 precalculated transverse basis functions in the direction perpendicular to current flow and rooftop functions in the direction of propagation as given in detail in section 3.8.2

- Region 3 :

  1 precalculated transverse basis function in the direction perpendicular to current flow and resonance mode current basis function in the direction of propagation as given in detail in section 3.8.3.2 and shown in figure 3.17

- Ports :

  The sum of an incident and reflected current wave for the input port and a transmitted current wave for the output port as defined by equations 5.2 and 5.3

- Transfer :

  - 2 compensation functions in the interfaces between ports and feedlines as defined by equations 5.15, 5.16, 5.17 and 5.18
  - 2 rooftop functions to join two regions ($l_x = 0.318$ mm and $l_z = 0.636$ mm)

The total number of current basis functions required for this metallisation is 46 in total in contrast to 342. The current basis functions required for accurate modelling are reduced by 86%. The truncated current wave as given in detail in section 5.3 and an extra set of rooftop functions to complete this truncated portion are used to excite the edge–coupled filter. The minimum operating frequency is 1 GHz and the corresponding length of the truncated portion is 29.14 mm, which is almost 46 times bigger than the rooftop size. For the maximum operating frequency of 15 GHz, the corresponding length of truncation is 1.78 mm, which is still almost 3 times bigger than the rooftop size. To complete the missing portion in order to get accurate results, 540 extra rooftop functions are required at 1 GHz. In this model, the compensation

functions have been used and the effect of excitation has been successfully transferred into the circuit.

The adaptive integration technique has been employed to calculate the impedance matrix elements. A coarse integration step is 4 times longer than the fine integration step so, the speed of the calculation is increased 4 times compared with the use of uniform integration step. 6 basis functions are used in x direction and 1081 impedance matrix elements can be derived from 21 sub–impedance matrix elements. Therefore the impedance matrix elements needed to be integrated are reduced by 98% in one dimension. The improvement by using the symmetry of the Green's function also gives 10% improvement. The S–parameter results were shown in figures 3.18 and 5.10. The run–time on HP700 workstations is around 1 minute to calculate S–parameters at each spot frequency. This is slightly bigger than the calculation time reported in [4] for the shielded edge–coupled filter. This is because of having more current basis functions and of excitation problem. The current wave in a length of a number of half wavelength which is a function of operating frequency. This length is bigger at low frequency and its Fourier transform is finer. Therefore fine integration steps are required to model.

6.4 Simple Low–Pass Filter

Measurement results are available for the microstrip low–pass filter [5] shown in figure 6.4. This filter is analysed to demonstrate the total improvement in this implementation and to compare the calculated results to available measurement data. The dimensions and parameters of the dielectric substrate are given in figure 6.4.

The low–pass filter has been divided into 7 regions as shown in figure 6.5. The set of basis functions for the model in figure 6.5 is summarised below:

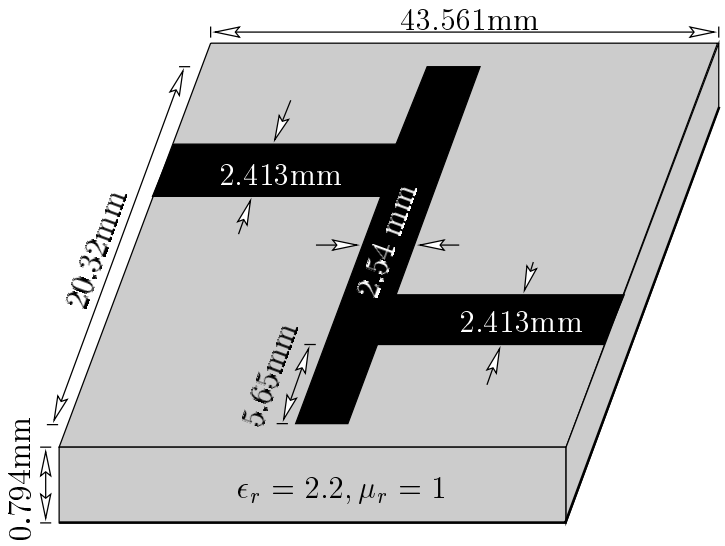

Figure 6.4: Low–pass filter detail

- Regions 1 and 7 :

  2 precalculated current waves as defined by equations 3.13 and 3.14

- Regions 2 and 6 :

  18 rooftop current basis functions ($l_x = 0.60325$ mm and $l_z = 0.60325$ mm)

- Region 3 :

  57 rooftop current basis functions ($l_x = 0.635$ mm and $l_z = 0.635$ mm)

- Regions 4 and 5 :

  12 rooftop current basis functions ($l_x = 0.635$ mm and $l_z = 1.27$ mm)

- Ports :

  The sum of an incident and reflected current wave for the input port and a transmitted current wave for the output port as defined by equations 5.2 and 5.3

- Transfer :

  – 2 compensation functions in the interfaces between ports and feedlines as defined by equations 5.15, 5.16, 5.17 and 5.18

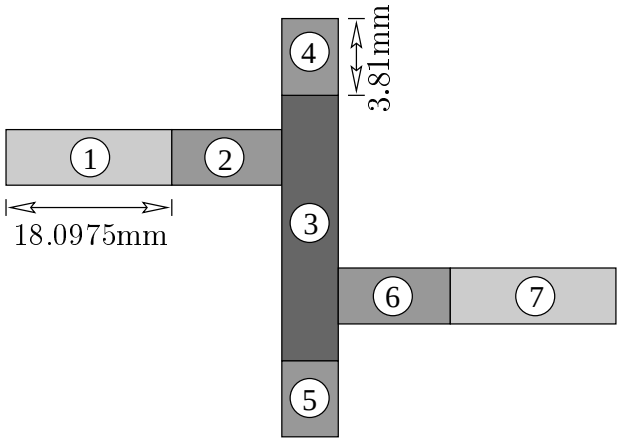

Figure 6.5: Plan evaluation of the microstrip low–pass filter shoving regions

– 18 rooftop functions to join two regions ($l_x = 0.60325$ mm and $l_z = 0.60325$ mm in horizontal direction and $l_x = 0.635$ mm and $l_z = 0.635$mm in vertical directions)

The total number of current basis functions required for this analysis is 214 (107 x and 107 z components) in total in contrast to 594. The current basis functions required for accurate modelling are reduced by 64%. The truncated current wave as given in detail in section 5.3 and an extra set of rooftop functions to complete this truncated portion are used to excite the open circuit of interest. The minimum operating frequency is 2 GHz and the corresponding length of the truncated portion is 27.42 mm, which is 45 times bigger than the rooftop size. For the maximum operating frequency of 20 GHz, the corresponding length of truncation is 2.6925 mm, which is still 4 times bigger than the rooftop size. To complete the missing portion in order to get accurate results, 528 extra rooftop functions are required to analyse at 1 GHz. With the use of the compensation functions, 4 functions are enough instead of using the truncated current wave and 528 extra rooftop functions.

The adaptive integration given in detail in section 4.2 is also used to calculate the impedance matrix elements. A coarse integration step is 4 times longer than the fine integration step. With this choice, the speed of the calculation is increased 4

times compared with the use of uniform integration steps. 66 basis functions are used in x direction and 23005 impedance matrix elements can be derived from 2211 sub–impedance matrix elements. Therefore the impedance matrix elements needed to be integrated are reduced by 90.4% in one dimension. The improvement by using the symmetry of the Green's function also gives 5% improvement. The S–parameter results are plotted in figures 6.6. As seen in figure 6.6, the calculated results and measurements are in very good agreement.

6.5 Summary

This chapter has presented results for the SDM implementation compared to calculated and measured data available in the literature for open planar passive microwave circuits to illustrate the total improvement in the analysis. The efficiency of the method is highlighted by computation time improvement in percentage for spot frequency S–parameters.

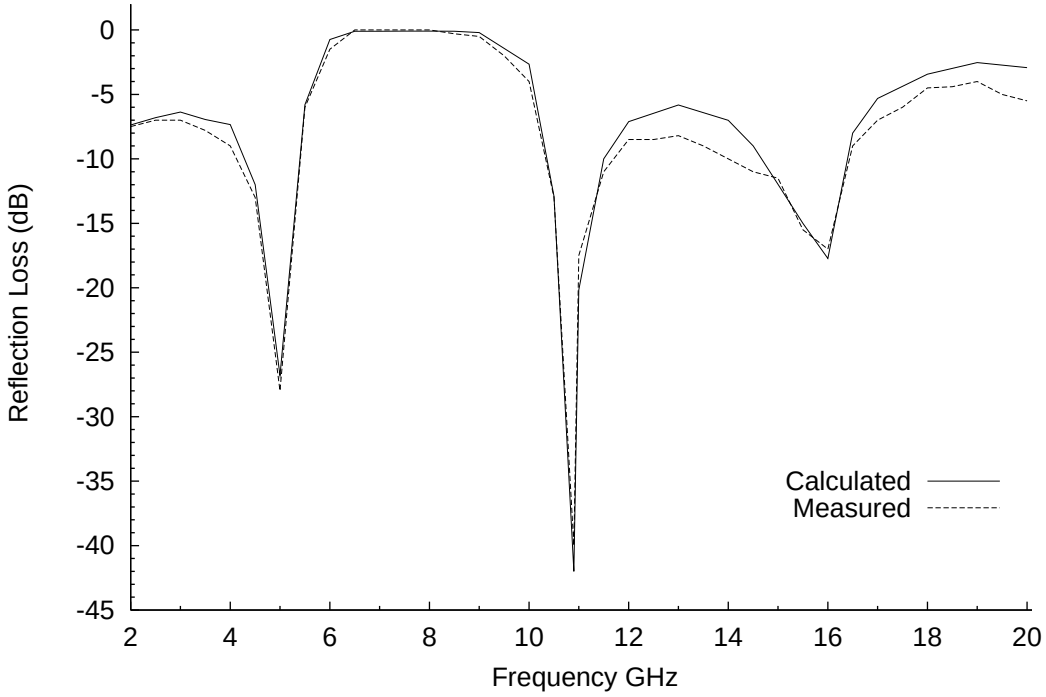

(a) Magnitude of S_{11}

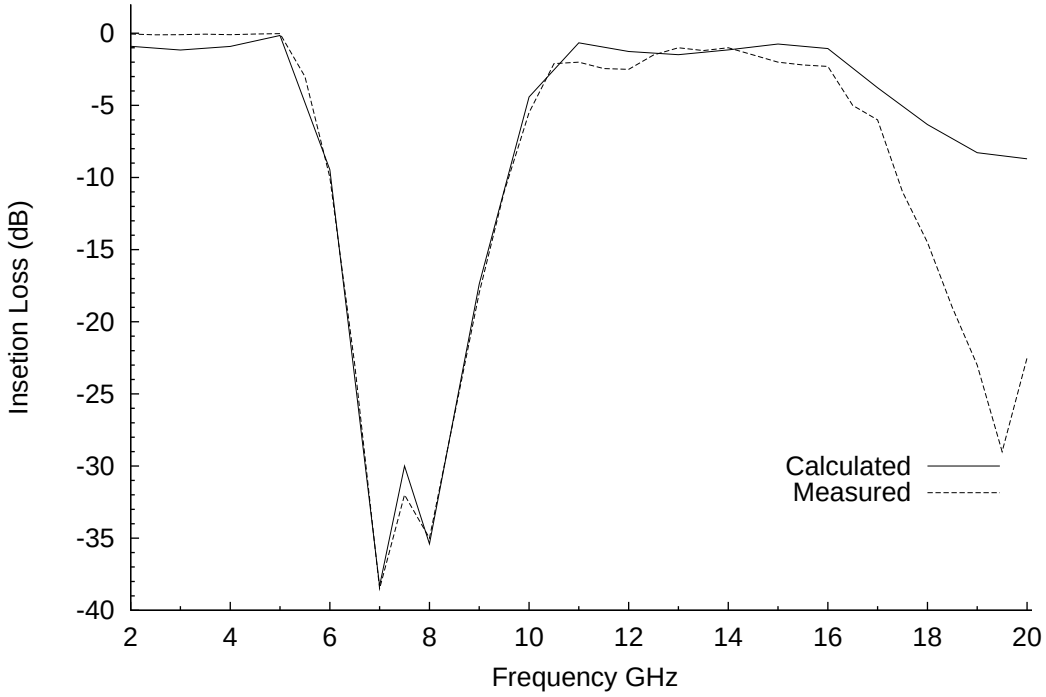

(b) Magnitude of S_{21}

Figure 6.6: Plot of S–parameters' magnitude for the low–pass filter

References

[1] R. W. Jackson and D. M. Pozar, "Full–wave analysis of microstrip open–end and gap discontinuities," *IEEE Transaction on Microwave Theory and Technique*, vol. 33, pp. 1036–1042, October 1985.

[2] R. W. Jackson, "Full–wave, finite element analysis of irregular microstrip discontinuities," *IEEE Transaction on Microwave Theory and Technique*, vol. 37, pp. 81–89, January 1989.

[3] H. H. Balik and C. J. Railton, "Sub–gridding in the spectral domain method for the analysis of planar circuits and antennas," in *3rd International conference on telecommunications in modern satellite, cable and broadcasting services*, pp. 592–595, October 1997.

[4] C. J. Railton and S. A. Meade, "Fast rigorous analysis of shielded planar filters," *IEEE Transaction on Microwave Theory and Technique*, vol. 40, pp. 978–985, May 1992.

[5] D. M. Sheen, S. M. Ali, M. D. Abdouzahra, and J. A. Kong, "Application of the three–dimensional finite-difference time–domain method of the analysis of planar microstrip circuits," *IEEE Transaction on Microwave Theory and Technique*, vol. 38, pp. 849–857, July 1990.

Chapter 7

Analysis of Multilayer Structures

7.1 Introduction

The preceding chapters have presented an efficient technique, which has been implemented for fast rigorous analysis of two layered open planar microwave circuits. An arbitrary shape embedded in a multilayer medium allows for more versatile design with higher density. Because of this, multilayer microstrip is often used in the design of microstrip components which operate at high levels of RF power, or in the design of overlay microwave couplers. The application of the technique to the analysis of multilayer structures will be examined. In this chapter, only circuits with multiple dielectric substrates are considered as a multilayer structure; a general N–layered circuit is shown in figure 7.1. Circuit with multiple conductor layers are not examined in this thesis.

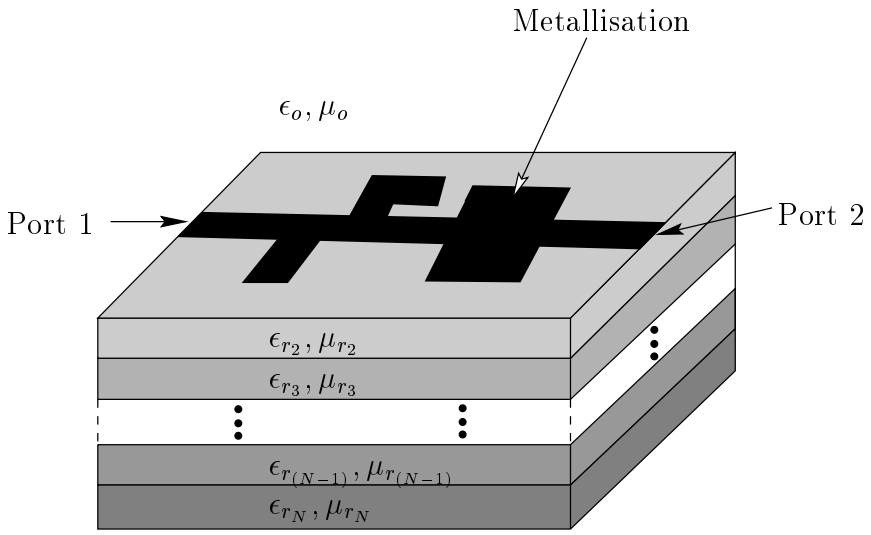

Figure 7.1: General 3–D multilayered microwave circuit

The Green's function in the spectral domain is commonly derived for the multilayer circuit of interest by using one of two different formulation precesses. First, the Green function can be directly derived by solving Maxwell's equations in the spectral domain, with suitable boundary conditions [1–3], but extending this procedure for multiple dielectric layers becomes too complicated [2]. In [4], a generalised spectral

domain Green's function is derived in terms of suitable components of vector electric and magnetic potentials. With these vector potentials, the boundary conditions were simplified into equivalent transmission line problems in the spectral domain, as in [5]. The solutions were then simplified to solving a *standard* form containing only two layers, by the use of iterative solutions. The effect of other layers is taken into account via the reflected and transmitted coefficients, which are functions of the parameters of the other layers (thickness, dielectric permittivity and permeability). Despite these simplifications, the technique is found by the author to be still complicated and not favourable to this implementation.

Itoh [5] presented a simple method, called the immitance approach, for deriving the dyadic Green's functions for a microstrip line and applied this to the analysis of a microstrip resonator [6] in 1981. Itoh used the transverse equivalent circuit concept in the spectral domain, in conjunction with a simple coordinate transformation rule. The author has chosen Itoh's immitance approach to derive Green's function for multilayer structures and the formulation process is given in detail in this chapter.

The asymptotic form of the Green's function for the multilayer structure is derived for the large value of Fourier transform variables by using the immitance approach. Numerical results are plotted for multilayer structures to verify the accuracy of the derivation and the effect of multilayering with the aid of a microstrip line and a microstrip resonator.

7.2 Derivation of Dyadic Green's Function

The immitance approach was presented by Itoh [5] in 1980, for deriving the dyadic Green's functions of printed transmission lines, by decoupling the TE and TM components. An application of this method was presented by Itoh and Menzel [6], which allows the analysis of planar resonator antennas. It is based on the transverse equi-

valent circuit concept, as applied in the spectral domain, in conjunction with a simple co–ordinate transformation rule. Although the method may be applied to other printed circuit structures, a simple microstrip resonator shown in figure 7.2 is used for the formulation.

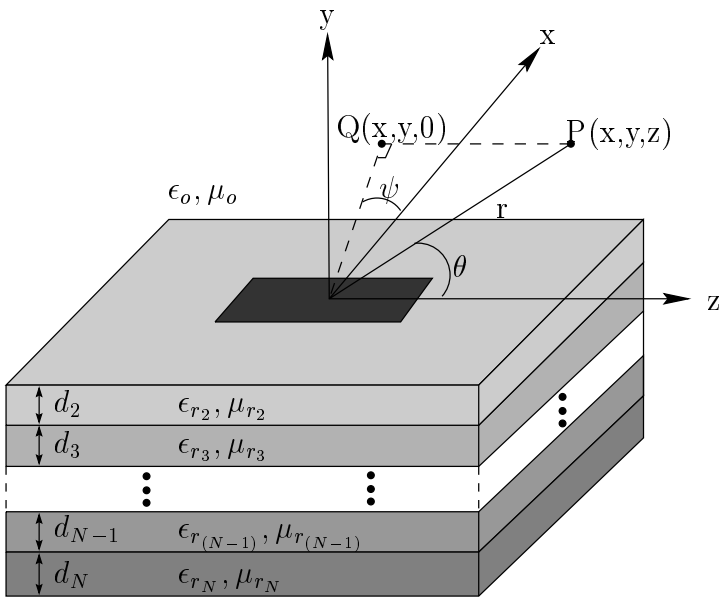

Figure 7.2: Cross–section of a multilayered microstrip resonator

The basic concept of the immitance approach can be understood if the inverse transform of the Fourier transform in equation 7.1 for the field is examined.

$$\phi(x,z) = \frac{1}{(2\pi)^2} \int_{-\infty}^{\infty} \int_{-\infty}^{\infty} \boldsymbol{\phi}(k_x, k_z) e^{-j(k_x x + k_z z)} dk_x dk_z \tag{7.1}$$

From this expression, all field components are a superposition over k_x and k_z of inhomogeneous (in y) plane waves which are propagating in the direction of θ from the z–axis , where $\theta = \cos^{-1}\left(\frac{k_z}{\sqrt{k_x^2+k_z^2}}\right)$. For each θ, waves may be decomposed into TM–to–y $(\mathbf{E}_y, \mathbf{E}_v, \mathbf{H}_u)$, and TE–to–y $(\mathbf{H}_y, \mathbf{H}_v, \mathbf{E}_u)$ where the coordinates v and u are

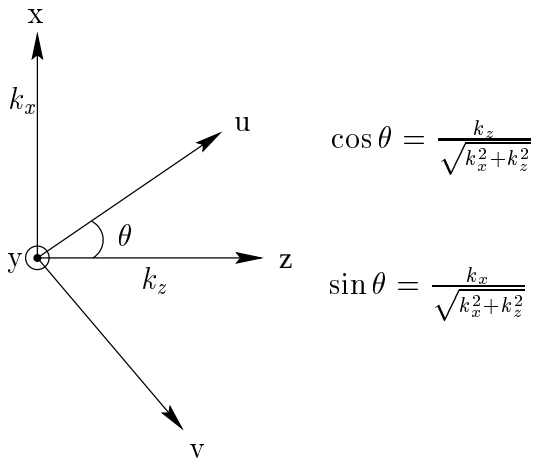

Figure 7.3: Co–ordinate transformation

as shown in figure 7.3 and related with (x, z) via

$$u = z\sin\theta - x\cos\theta \tag{7.2}$$

$$v = z\cos\theta + x\sin\theta \tag{7.3}$$

The current $\mathbf{J}_v$ creates only the TM fields, because it is concerned with $\mathbf{H}_u$ and likewise $\mathbf{J}_u$ creates the TE fields. Therefore, an equivalent circuit for the TM and TE fields can be drawn, as shown in figure 7.4. The characteristic impedance in each region is given by;

$$\mathbf{Z}_{TM_i} = \frac{\mathbf{E}_v}{\mathbf{H}_u} = \frac{\gamma_i}{j\omega\epsilon_i} \tag{7.4}$$

$$\mathbf{Z}_{TE_i} = -\frac{\mathbf{E}_u}{\mathbf{H}_v} = \frac{j\omega\mu_i}{\gamma_i} \tag{7.5}$$

$$\gamma_i = \sqrt{k_x^2 + k_z^2 - k_i^2} \tag{7.6}$$

where $i = 1..N$ and $k_i^2 = \omega^2\mu_i\epsilon_i$. The γ_i is the propagation constant in the y direction in the i^{th} region. All boundary conditions for the TM and TE waves are incorporated in the equivalent circuits. The electric fields $\mathbf{E}_v$ and $\mathbf{E}_u$ are continuous at $y = 0$ and

given by;

$$\mathbf{E}_v(k_x, k_z, 0) = \mathbf{Z}_e(k_x, k_z, 0)\mathbf{J}_v(k_x, k_z, 0) \tag{7.7}$$

$$\mathbf{E}_u(k_x, k_z, 0) = \mathbf{Z}_h(k_x, k_z, 0)\mathbf{J}_u(k_x, k_z, 0) \tag{7.8}$$

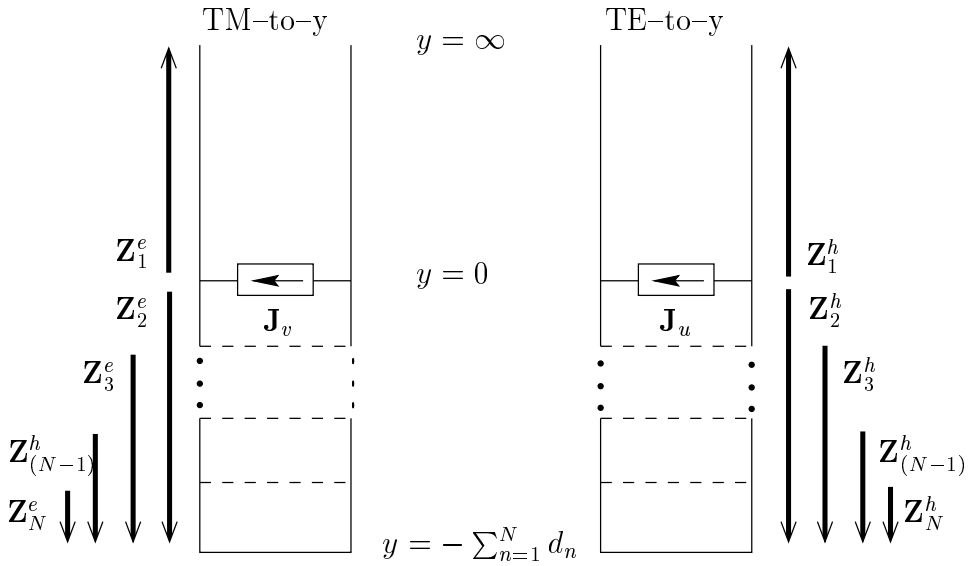

Figure 7.4: Equivalent transmission lines for the TM and TE fields

$\mathbf{Z}_e$ and $\mathbf{Z}_h$ are the input impedances looking into the equivalent circuits at $y = 0$ and are given by;

$$\mathbf{Z}_e(k_x, k_z, d) = \left(\frac{1}{\mathbf{Z}_1^e} + \frac{1}{\mathbf{Z}_2^e}\right)^{-1} \tag{7.9}$$

$$\mathbf{Z}_h(k_x, k_z, d) = \left(\frac{1}{\mathbf{Z}_1^h} + \frac{1}{\mathbf{Z}_2^h}\right)^{-1} \tag{7.10}$$

where $\mathbf{Z}_1^e$ and $\mathbf{Z}_2^e$ are input impedances looking into the corresponding regions at $y = 0$ in the TM equivalent circuit, whereas $\mathbf{Z}_1^h$ and $\mathbf{Z}_2^h$ are those impedances in the TE circuit. The definition of $\mathbf{Z}_1^e$ and $\mathbf{Z}_1^h$ are;

$$\mathbf{Z}_1^e = \mathbf{Z}_{TM_1} \qquad \mathbf{Z}_1^h = \mathbf{Z}_{TE_1} \tag{7.11}$$

As seen in figure 7.4, a transmission line is terminated by another transmission line of different characteristic impedance. Therefore conventional transmission line theory can be used to find the $\mathbf{Z}_2^e$ and $\mathbf{Z}_2^h$ as

$$\begin{aligned}
\mathbf{Z}_{N-1}^e &= \mathbf{Z}_{TM_{(N-1)}} \frac{\mathbf{Z}_N^e \coth \gamma_{N-1} d_{N-1} + \mathbf{Z}_{TM_{(N-1)}}}{\mathbf{Z}_{TM_{(N-1)}} \coth \gamma_{N-1} d_{N-1} + \mathbf{Z}_N^e} \\
\mathbf{Z}_{N-1}^h &= \mathbf{Z}_{TE_{(N-1)}} \frac{\mathbf{Z}_N^h \coth \gamma_{N-1} d_{N-1} + \mathbf{Z}_{TE_{(N-1)}}}{\mathbf{Z}_{TE_{(N-1)}} \coth \gamma_{N-1} d_{N-1} + \mathbf{Z}_N^h} \\
&\vdots = \vdots \\
\mathbf{Z}_2^e &= \mathbf{Z}_{TM_2} \frac{\mathbf{Z}_3^e \coth \gamma_2 d_2 + \mathbf{Z}_{TM_2}}{\mathbf{Z}_{TM_2} \coth \gamma_2 d_2 + \mathbf{Z}_3^e} \\
\mathbf{Z}_2^h &= \mathbf{Z}_{TE_2} \frac{\mathbf{Z}_3^h \coth \gamma_2 d_2 + \mathbf{Z}_{TE_2}}{\mathbf{Z}_{TE_2} \coth \gamma_2 d_2 + \mathbf{Z}_3^h}
\end{aligned} \tag{7.12}$$

where

$$\mathbf{Z}_N^e = \frac{\mathbf{Z}_{TM_N}}{\coth \gamma_N d_N} \qquad \mathbf{Z}_N^h = \frac{\mathbf{Z}_{TE_N}}{\coth \gamma_N d_N}$$

The final part of the immitance approach formulation is to map from the (u, v) to (x, z) co–ordinate system for the spectral wave corresponding to each θ given by k_x and k_z. Because of the coordinate transform in equations 7.2 and 7.3, $\mathbf{E}_x$ and $\mathbf{E}_z$ are linear combination of $\mathbf{E}_u$ and $\mathbf{E}_v$. Similarly $\mathbf{J}_x$ and $\mathbf{J}_z$ are superpositions of $\mathbf{J}_u$ and $\mathbf{J}_v$. When the above notations are applied, the Green's function elements are found to be:

$$\mathbf{G}_{zz} = N_z^2 \mathbf{Z}_e + N_x^2 \mathbf{Z}_h \tag{7.13}$$

$$\mathbf{G}_{zx} = N_x N_z (-\mathbf{Z}_e + \mathbf{Z}_h) \tag{7.14}$$

$$\mathbf{G}_{xz} = \mathbf{G}_{zx} \tag{7.15}$$

$$\mathbf{G}_{xx} = N_x^2 \mathbf{Z}_e + N_z^2 \mathbf{Z}_h \tag{7.16}$$

where N_x and N_z are transforming ratios given by;

$$N_x = \frac{k_x}{\sqrt{k_x^2 + k_z^2}} \qquad N_z = \frac{k_z}{\sqrt{k_x^2 + k_z^2}} \tag{7.17}$$

Note that $\mathbf{Z}^e$ and $\mathbf{Z}^h$ are functions of $k_x^2 + k_z^2$ and the ratio of k_x and k_z enters through N_x and N_z.

7.3 Asymptotic Form of Green's function

The Green's function which has been derived in section 7.2 by the use of the immitance approach, is computationally complex and this complexity increases with the number of layers. There is however a possibility to use the asymptotic form of the Green's function, which has been shown to be effective for two layer structures in section 4.3.1. For large transform variables (k_x and k_z), the original Green's function for a multilayer structure converges to the Green's function of a simple two layer structure. For this, they must satisfy the conditions which are given by;

$$\gamma_i = \sqrt{k_x^2 + k_z^2 - k_{max}^2} \approx \sqrt{k_x^2 + k_z^2} \tag{7.18}$$

$$Coth\gamma_{ij} d_{min} \approx 1 \tag{7.19}$$

where $k_{max} = \max(k_i)$ and $d_{min} = \min(h_i)$.

So, for the large Fourier transform variables, all multilayer structures are equivalent to the structure containing the immediate two layers, extended to infinity, on each side of the strip. The reason for this is that large values of transform variables account for the reactive field of the source, which is a localised effect.

With the above argument, the asymptotic form of the Green's function of multilayered structures can be directly obtained from the asymptotic form of the Green's function

for two layer structure, which is given in detail in section 4.3.1 as;

$$\mathbf{G}_{st}^{\infty} = h_1 \mathbf{K}_{st1}^{\infty} + h_2 \mathbf{K}_{st2}^{\infty} \tag{7.20}$$

where

$$\begin{aligned}
h_1 &= -\frac{j}{\omega\epsilon_0(1+\epsilon_{r_2})} & h_2 &= \frac{j\omega\mu_0\mu_r}{(1+\mu_{r_2})} \\
\mathbf{K}_{zz1}^{\infty} &= \frac{k_z^2}{\sqrt{k_x^2+k_z^2}} & \mathbf{K}_{zz2}^{\infty} &= \frac{k_z^2}{\sqrt{(k_x^2+k_z^2)^3}} \\
\mathbf{K}_{zx1}^{\infty} &= -\frac{k_x k_z}{\sqrt{k_x^2+k_z^2}} & \mathbf{K}_{zx2}^{\infty} &= \frac{k_x k_z}{\sqrt{(k_x^2+k_z^2)^3}} \\
\mathbf{K}_{xz1} &= \mathbf{K}_{zx1} & \mathbf{K}_{xz2} &= \mathbf{K}_{zx2} \\
\mathbf{K}_{xx1}^{\infty} &= \frac{k_x^2}{\sqrt{k_x^2+k_z^2}} & \mathbf{K}_{xx2}^{\infty} &= \frac{k_x^2}{\sqrt{(k_x^2+k_z^2)^3}}
\end{aligned} \tag{7.21}$$

with $\omega = 2\pi f$ and ϵ_{r2}, μ_{r2} the relative permittivity and permeability of the electric substrate next to the strip respectively. It must be noted that the first layer is free–space because of the open structure.

The functions $\mathbf{K}_{sti}^{\infty}$ $(s,t = z \text{ or } x;\ i = 1,2)$ are just functions of k_x and k_z and thus are independent of frequency and metallisation pattern. The constants h_i $(i = 1,2)$ need only be calculated once per frequency, as they are independent of k_x and k_z.

An important point to be considered for the spectral domain integration of the impedance matrix elements is the treatment of the surface wave poles. It can be easily proven that all the poles of the Green's function lie between k_o and $\sqrt{\epsilon_{rmax} * \mu_{rmax}} k_o$. The same technique given in section 4.2 is used for the impedance matrix elements integration.

7.4 Numerical Examples

To verify the accuracy of the Green's function which has been derived by the use of the immitance approach, the simple two layer microstrip line of width 1.27 mm on a substrate of thickness 1.27 mm and of permittivity 8.875 is taken as a test structure. The microstrip line is analysed for the effective permittivity by the existing two dimensional version of the technique, then the substrate is divided into three, assuming that the structure is now a four layer microstrip line with identical substrate parameters. The effective permittivities are plotted in figure 7.5 and compared with published data [7].

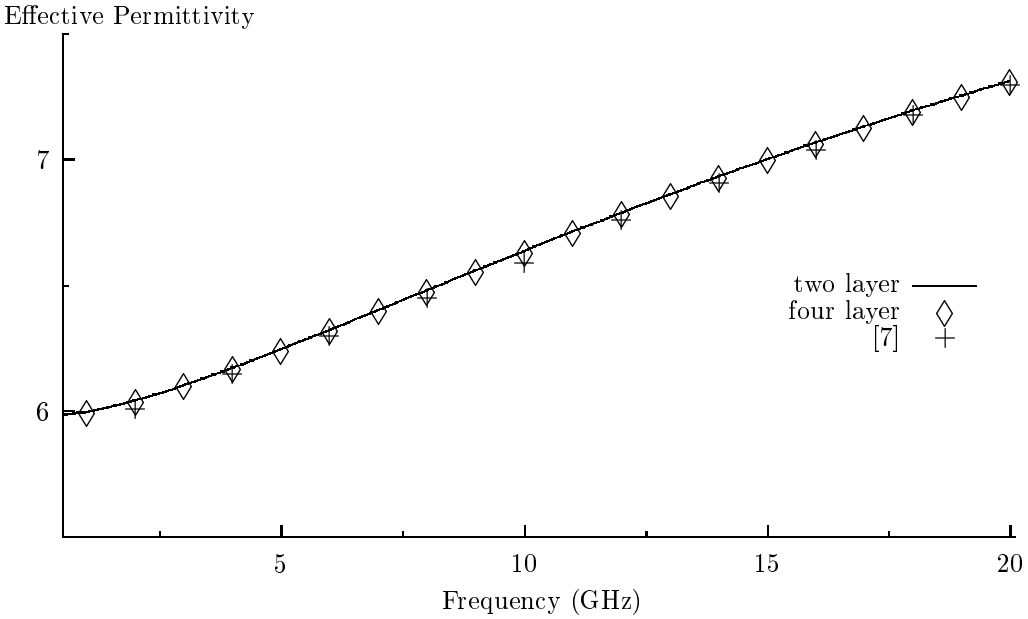

Figure 7.5: Illustration of an accuracy of the immitance approach

To further test the accuracy of the Green's function which has been derived by the immitance approach, results are compared with the simple closed–form expression for the effective dielectric constant of a microstrip on a two layer substrate [8]. The geometry of the two substrate layer microstrip used in the present test is shown in figure 7.6.

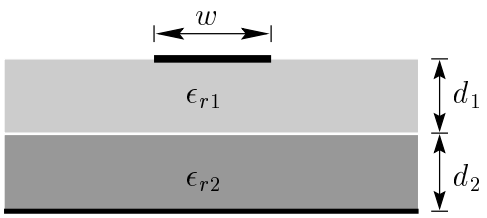

Figure 7.6: Geometry of coupled microstrip with two substrate layers

Following [8], the total height of the substrate layers, $d_{tot} = d_1 + d_2$, is held constant and the design formula uses the following as design parameters:

- ratio of the width to total height, w/d_{tot}
- the height ratio, $d_r = d_2/d_{tot}$
- the dielectric constant, ϵ_{r1} and ϵ_{r2}
- the effective dielectric permittivities of the single layer cases, $\epsilon_{reff}(d_r = 0)$ and $\epsilon_{reff}(d_r = 1)$

Figure 7.7 shows the effective dielectric permittivity as a function of the height ratio for different dielectric constants of the lower substrate. The results are compared with published data [8]. In figure 7.7, a linear normalisation is used, described by;

$$\epsilon_{reff(norm)}(d_r) = \epsilon_{reff}(d_r) - \epsilon_{reff}(0) - d_r\left[\epsilon_{reff}(1) - \epsilon_{reff}(0)\right] \tag{7.22}$$

where $\epsilon_{reff}(0)$ and $\epsilon_{reff}(1)$ are the effective permittivity for the single substrate cases given by;

$$\begin{aligned} \epsilon_{reff}(0) &= \epsilon_{reff} \qquad d_r = 0 \\ \epsilon_{reff}(1) &= \epsilon_{reff} \qquad d_r = 1 \end{aligned} \tag{7.23}$$

As shown in figures 7.5 and 7.7, the immitance approach is shown to be an accurate

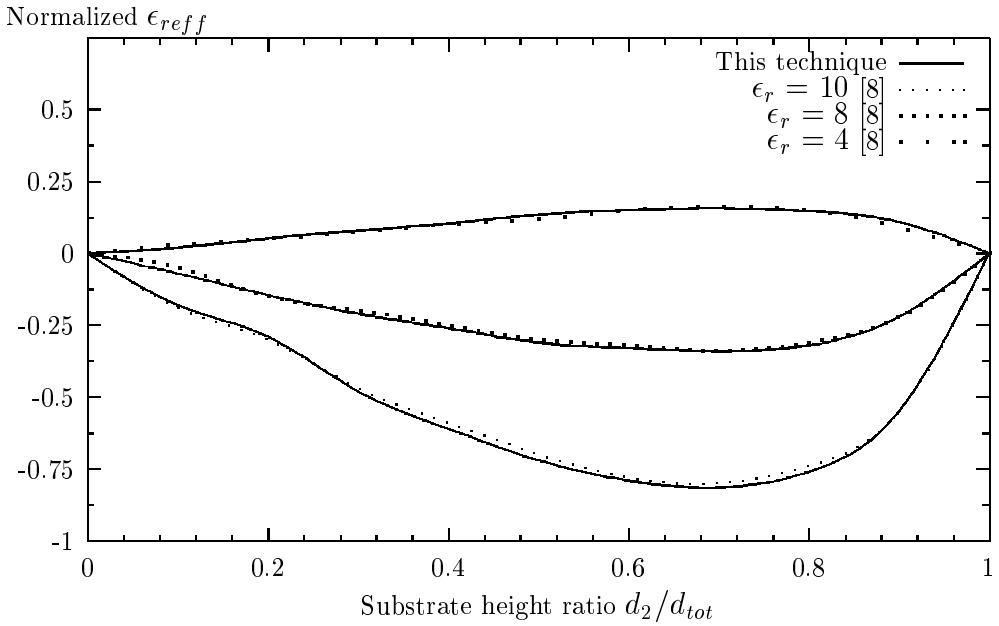

Figure 7.7: ϵ_{reff} of a microstrip on a two layer substrate normalised using equation 7.22 as a function of the substrate height ratio for different values of ϵ_{r2} ($w/d_{tot} = 1$ and $\epsilon_{r1} = 6$)

way to find the Green's function for multilayer structures.

To observe the effects of the order of dielectric substrates with different parameters, the microstrip line of width 1 mm is modelled and a series of results are plotted in figure 7.8. In the analysis, each layer thickness has been chosen to be 0.25 mm.

As shown in figure 7.8, the order of the dielectric layers is very effective. At low frequencies the value of the effective permittivity is determined by the relative permittivity of the substrate next to the strip. It is clearly shown in figure 7.8 that the parameters of substrate next to the ground plane is effective on the increment of the effective permittivity from one frequency point to another.

Further illustrate the effects of multilayering, a simple three layer microstrip resonator of width 1 mm and of length 8 mm as shown in figure 7.9 is modelled and the table 7.1 has been prepared. The calculation of the resonant frequency is given in [1, 6]. As

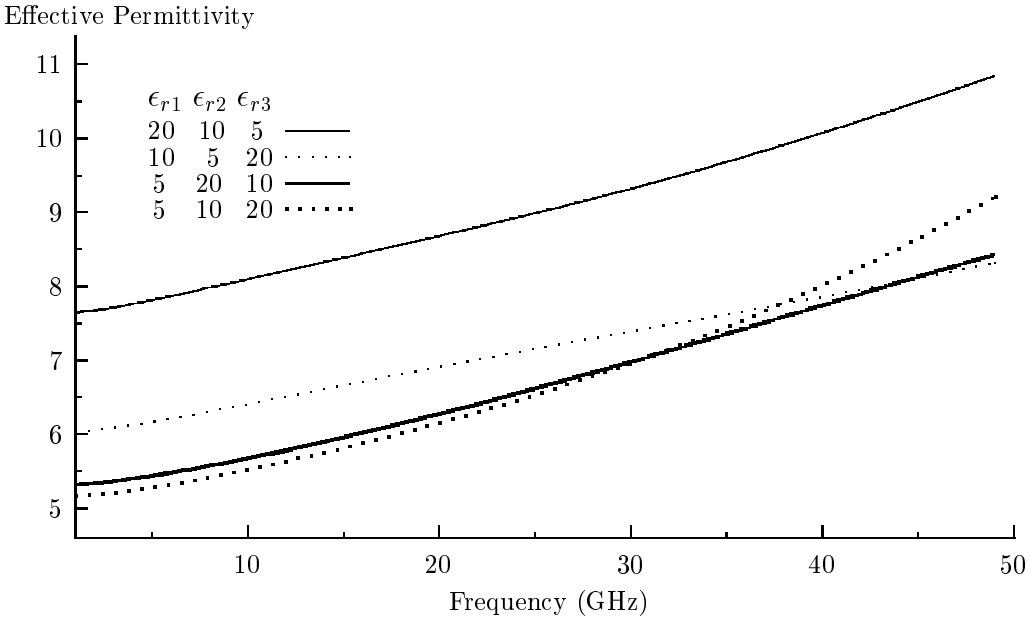

Figure 7.8: Illustration of the effects of multilayering on effective permittivity

shown in table 7.1 that, the order of the dielectric layers is dominant on the resonant frequency. The resonant frequency is inversely proportional to the value of parameters of dielectric substrate next to the conducting strip.

ϵ_{r2} \ ϵ_{r1}		d_1=0.636mm		
		20	10	5
d_2=0.636mm	20	3.05+j1.70$10^{-3}$	3.93+j6.71$10^{-3}$	5.13+j1.85$10^{-2}$
	10	3.38+j3.81$10^{-3}$	4.24+j8.77$10^{-3}$	5.40+j2.06$10^{-2}$
	5	3.83+j6.44$10^{-3}$	4.70+j1.27$10^{-2}$	5.82+j2.28$10^{-2}$

Table 7.1: Illustration of the effects of multilayering on resonant frequency (GHz)

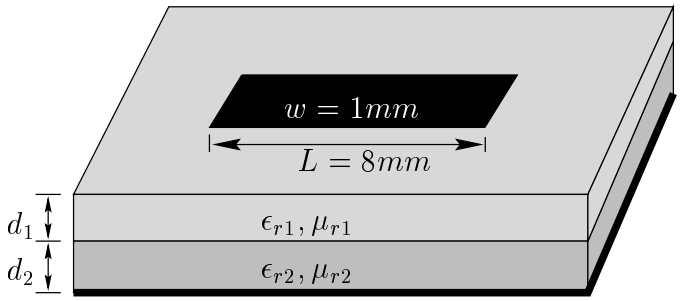

Figure 7.9: Two layer microstrip resonator

7.5 Summary

This chapter discusses the derivation of the Green's function for the multi dielectric layer structures. To verify the derivation, the simple microstrip line which has been previously analysed in the literature is modelled by the two dimensional version of the technique. The effects of multilayering on the effective permittivity of a microstrip line and the resonant frequency of a microstrip resonator have been illustrated by modelling corresponding structure.

References

[1] T. Itoh, "Analysis of microstrip resonators," *IEEE Transaction on Microwave Theory and Technique*, vol. 22, pp. 946–952, November 1974.

[2] J. B. Davies and D. Mirshekar-Syahkal, "Spectral domain solution of arbitrary coplanar transmission line with multilayer substrate," *IEEE Transaction on Microwave Theory and Technique*, vol. 25, pp. 143–146, February 1977.

[3] D. M. Pozar, "General radiations for a phased array of printed antennas derived from infinite current sheets," *IEEE Transaction on Antennas and Propagation*, vol. 33, pp. 498–504, May 1985.

[4] N. K. Das and D. M. Pozar, "A generalised spectral–domain Green's function for multilayer dielectric substrates with application to multilayer transmission lines," *IEEE Transaction on Microwave Theory and Technique*, vol. 35, pp. 326–335, March 1987.

[5] T. Itoh, "Spectral domain immitance approach for dispersion characteristics of generalized printed transmission lines," *IEEE Transaction on Microwave Theory and Technique*, vol. 28, pp. 733–736, July 1980.

[6] T. Itoh and W. Menzel, "A full–wave analysis method for open microstrip structures," *IEEE Transactions on Antennas and Propagation*, vol. 29, pp. 63–67, January 1981.

[7] T. Itoh and R. Mittra, "Spectral–domain approach for calculating the dispersion characteristics of microstrip lines," *IEEE Transaction on Microwave Theory and Technique*, pp. 496–499, July 1973.

[8] J. P. K. Gilb and C. A. Balanis, "Closed–form expressions for the design of microstrip lines with two substrate layers," in *IEEE MTT–S INT. Microwave Symp.*, pp. 1005–1008, 1993.

Chapter 8

Conclusions and Future Work

8.1 Summary

The aim of this research has been to develop a technique for the efficient, fast, rigorous and accurate analysis of passive open planar microwave circuits. It is also possible to apply this implementation to the planar antennas.

The lower frequency bands can provide only limited amount of spectrum for radio–borne services such as cellular telephones and wireless local area networks and are already heavily used. As the operating frequency is moved upward to less used frequency bands with more available bandwidth, the approximations, which simplify the complicated equations describing the operation of microwave circuits, are no longer valid. Therefore it is necessary to use full–wave analysis in order to fulfil present demands.

Currently several methods are reported in the literature applied to planar transmission line problems and discontinuity analysis, as discussed in chapter 2. The Spectral Domain Method (SDM) which is based on solving the coupled integral equation in the spectral domain has been chosen by the author to meet these requirements. The SDM is very popular but has been criticised for being computationally intensive, due to the need for the analytical preprocessing. This feature imposes certain restrictions on the applicability of the technique, but allows the development of an interactive design tool. The general formulation of SDM has been given in detail in section 2.3.3.

The choice of basis functions, which define the unknown current distribution on the metallisation of the circuit, is crucial to the efficiency of the technique. The current basis functions must be chosen to approximate the unknown current distribution as closely as possible, otherwise a large number of basis functions are required for convergence. Chapter 3 discussed the class of current basis functions used in this thesis. The implementation of an arbitrary metallisation pattern requires sub–domain basis functions which are the rooftop functions described in section 3.4. As has been discussed, the rooftop function differs from that commonly implemented. The use of

the rooftop function has been improved by introducing sub–gridding in the spectral domain. The sub–gridding is used in the sense that the rooftop functions are defined as functions of their locations.

The precalculated basis function which was introduced by Railton and Meade [1, 2] has been defined either as a linear combination of rooftop functions with precalculated coefficients, or as a current wave function with a precalculated propagation constant. It has been noted in chapter 3 that there is no restriction of geometry and the size of the rooftop function which is necessary in [1, 2] to exploit the benefits of using FFT.

This thesis approaches the problem by sub–dividing a complex circuit metallisation into areas which are bounded by the presence of a discontinuity. The term *region* has been defined to describe such an area and the set of basis functions which fully describe the region is called the *region basis function*. The derivation of region basis functions has been described for a number of example regions in section 3.5.

The SDM method is a frequency domain technique and requires the repeated impedance matrix calculation at each frequency point of interest. This is in contrast to methods such as the FDTD and TLM, which give the time domain response of the circuit, which can then be transformed to a wide band frequency response for a single run of the algorithm. In chapter 4, the enhancements in order to reduce the number of impedance matrix elements calculated at each spot frequency and in order to speed up the two–dimensional continuous integration have been introduced. The adaptive integration technique, which consists of an adaptive truncation of the integration range and an adaptive integration step has been introduced to limit the two–dimensional continuous integration over an infinite surface to finite computer resources.

The implementation of asymptotic functions as described in section 4.3.1 and of the location vector calculation as described in section 4.4 have been discussed. The symmetry in both the Green's function and the impedance matrix has also been

exploited. Further enhancement, discussed in section 4.6, has been introduced in order to reduce the number of the impedance matrix elements calculated in one dimension in order to speed up the overall numerical integration.

Throughout this thesis, the circuits have been represented by N–port network parameters, i.e. S–parameters. Chapter 5 has presented an improved form of excitation modelling which remedies the problems in the currently available methods, and provides a more efficient implementation. The current wave function without any form of truncation has been used to excite the open microwave circuit of interest. The compensation function has been introduced in section 5.2, to be used at the interface between the port and the feedline, in order to transmit the full effect of excitation.

In chapter 7, the derivation of the Green's function for multi dielectric layer structures has been given in detail and its asymptotic forms have been derived. The loss in the dielectric substrate has been included into analysis by replacing ϵ_r by $\epsilon_r(1 - j \tan\delta)$ where $\tan\delta$ is the loss tangent of the dielectric substrate.

8.2 Future Work

The purpose of the work described in this thesis has been to improve the efficiency of the Spectral Domain Method, to allow the fast rigorous analysis of open planar microwave circuits. As has been summarised this target has been achieved by the enhancements described in the preceding chapters.

The scope for future work to further increase the versatility of the SDM enhanced in this thesis includes the following: inclusion of conductor loss and finite conductor thickness, plus the capability to handle multiple conductor layers and 3–D metallisation.

In this implementation, the conductor has been assumed to be perfect and of infinitesimal thickness. Most of the applications meet above requirements. The inclusion of conductor loss and finite conductor thickness have been investigated by other researchers [3–8]. The 3–D metallisation structures have been analysed by Becks and Wolff [9] in the spectral domain. The technique to analyse circuits with multiple conductor layers has also been introduced in [10]. However the enhancements in this thesis have reduced the computational overheads so that interactive and the present implementation can be widened in order to include the above applications.

8.3 Concluding Remarks

The development of an passive open microwave circuit design package has been presented in this thesis. The enhanced SDM has been shown to be accurate compared to measured data and results calculated by other techniques. The work described here has achieved a reduction in computation time required of up to 90%, therefore making viable of an interactive tool which is based on a rigorous full–wave analysis technique.

References

[1] C. J. Railton and S. A. Meade, "Fast rigorous analysis of shielded planar filters," *IEEE Transaction on Microwave Theory and Technique*, vol. 40, pp. 978–985, May 1992.

[2] S. A. Meade and C. J. Railton, "Efficient implementation of the spectral domain method including precalculated corner basis functions," *IEEE Transaction on Microwave Theory and Technique*, vol. 42, pp. 1678–1684, September 1994.

[3] W. Heinrich, "Full–wave analysis of conductor losses on MMIC transmission lines," *IEEE Transaction on Microwave Theory and Technique*, vol. 38, pp. 1468–1472, October 1990.

[4] C. Shih, R. Wu, S. Jeng, and C. H. Chen, "Frequency–dependent chacteristics of open microstrip lines with finite strip thickness," *IEEE Transaction on Microwave Theory and Technique*, vol. 37, pp. 793–795, April 1989.

[5] K. M. Rahman and C. Nguyen, "Full–wave analysis of coplanar strips considering the finite strip metalisation thickness," *IEEE Transaction on Microwave Theory and Technique*, vol. 42, pp. 2177–2179, November 1994.

[6] Z. Ma, E. Yamashita, and R. Mittra, "Hybrid–mode analysis of planar transmission lines with arbitrary metalisation cross section," *IEEE Transaction on Microwave Theory and Technique*, vol. 41, pp. 491–497, March 1993.

[7] J. Kuo and T. Itoh, "Hybrid–mode computation of propagation and attenuation characteristic of parallel coupled microstrips with finite metalisation thickness," *IEEE Transaction on Microwave Theory and Technique*, vol. 45, pp. 274–280, February 1997.

[8] G. B. Stracca, "A simple evaluation of losses in thin microstrips," *IEEE Transaction on Microwave Theory and Technique*, vol. 45, pp. 281–283, February 1997.

[9] T. Becks and I. Wolff, "Analysis of 3–D metallisation structures by a full–wave spectral domain technique," *IEEE Transaction on Microwave Theory and Technique*, vol. 40, pp. 2219–2227, December 1992.

[10] M.-J. Tsai, D. Flaviis, O. Fordham, and N. G. Alexopoulos, "Modelling planar arbitrary shaped microstrip elements in multilayered media," *IEEE Transaction on Microwave Theory and Technique*, vol. 45, pp. 330–337, March 1997.

Appendix A

Fourier Transforms of Current Basis Functions

A.1 Fourier Transform of Rooftop Function

The components of a rooftop function are defined in the space domain by :

$$J_{xn}(x,z) = J_{xn}(x)J_{xn}(z) = \begin{cases} 1 - \frac{|x-x_n|}{l_x} & x_n - l_x \leq x \leq x_n + l_x \\ & z_n - l_z \leq z \leq z_n + l_z \\ 0 & \text{otherwise} \end{cases} \tag{A.1}$$

$$J_{zn}(x,z) = J_{zn}(x)J_{zn}(z) = \begin{cases} 1 - \frac{|z-z_n|}{l_z} & x_n - l_x \leq x \leq x_n + l_x \\ & z_n - l_z \leq z \leq z_n + l_z \\ 0 & \text{otherwise} \end{cases} \tag{A.2}$$

where $J_{xn}(x,z)$ and $J_{zn}(x,z)$ are the n^{th} rooftop functions for current flow in x and z directions respectively. The case for the x–directed current is considered first. Taking Fourier transforms in the x and z direction with the transform

$$\mathbf{J}_{xn}(k_x,k_z) = \int_{-\infty}^{\infty}\int_{-\infty}^{\infty} J_{xn}(x,z)e^{j(k_x x + k_z z)}dxdz \tag{A.3}$$

Since the rooftop functions are defined as two separable functions, equation A.3 can be split onto two separate integrals of the form

$$\mathbf{J}_{xn}(k_x,k_z) = \mathbf{J}_{xn}(k_x)\mathbf{J}_{xn}(k_z) = \int_{-\infty}^{\infty} J_{xn}(x)e^{jk_x x}dx \int_{-\infty}^{\infty} J_{xn}(z)e^{jk_z z}dz \tag{A.4}$$

Considering the first integral in equation A.4, the triangle function $J_{xn}(x)$ in figure A.1(a) is only defined over the interval $x_n - l_x$ to $x_n + l_x$ equal to a triangle function and is otherwise zero, therefore can be written as,

$$\begin{aligned} \mathbf{J}_{xn}(k_x) &= \int_{x_n - l_x}^{x_n + l_x} 1 - \frac{|x - x_n|}{l_x} e^{jk_x x}dx \\ &= \frac{2}{k_x^2 l_x}(1 - \cos(k_x l_x))e^{jk_x x_n} \end{aligned} \tag{A.5}$$

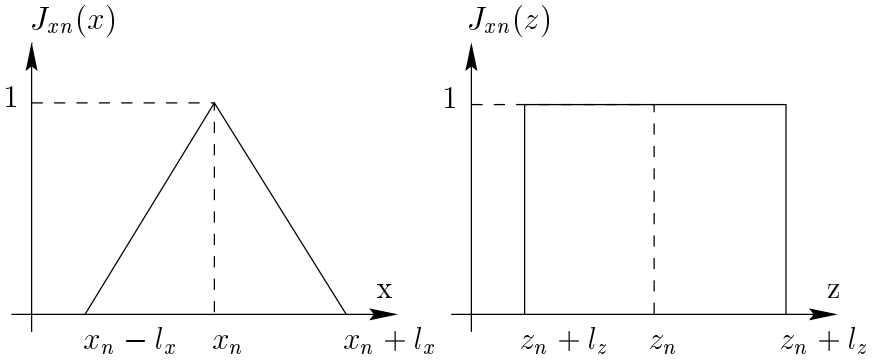

(a) Triangle function $J_{xn}(x)$ (a) Step function $J_{xn}(z)$

Figure A.1: Components of a rooftop function (x–directed rooftop)

Considering the second integral in equation A.4, the step function $J_{xn}(z)$ in figure A.1(b) is only defined over the interval $z_n - l_z$ to $z_n + l_z$ equal to unity and is otherwise zero.

$$\begin{aligned} \mathbf{J}_{xn}(k_z) &= \int_{z_n - l_z}^{z_n + l_z} 1 e^{jk_z z} dz \\ &= \frac{2}{k_z} \sin(k_z l_z) e^{jk_z z_n} \end{aligned} \tag{A.6}$$

Combining the two transforms with equation A.4, the two–dimensional Fourier transform of the x–directed rooftop basis function $J_{xn}(k_x, k_z)$ is

$$\mathbf{J}_{xn}(k_x, k_z) = \frac{4}{k_x^2 k_z l_x} (1 - \cos(k_x l_x)) \sin(k_z l_z) e^{j(k_x x_n + k_z z_n)} \tag{A.7}$$

Similarly, the two–dimensional Fourier transform of the z–directed rooftop function $\mathbf{J}_{zn}(k_x, k_z)$ can be derived as,

$$\mathbf{J}_{zn}(k_x, k_z) = \frac{4}{k_x k_z^2 l_z} \sin(k_x l_x)(1 - \cos(k_z l_z)) e^{j(k_x x_n + k_z z_n)} \tag{A.8}$$

A.2 Fourier Transform of Line Modes

The variation of the current distribution in the direction of current flow in the space domain is given by:

$$J_z(z) = \sum_{n=0}^{N} \cos(\frac{n\pi z}{L}) + \sum_{n=1}^{N} \sin(\frac{n\pi z}{L}) \tag{A.9}$$

$$J_x(z) = \sum_{n=0}^{N} \sin(\frac{n\pi z}{L}) + \sum_{n=1}^{N} \cos(\frac{n\pi z}{L}) \tag{A.10}$$

where L is the length of the microstrip line. The case for the z–directed current is considered first. Taking a Fourier transform in z direction with the transform

$$\begin{aligned} \mathbf{J}_z(k_z) &= \int_{-\infty}^{\infty} J_z(z) e^{jk_z z} dz \\ &= \sum_{n=0}^{N} \int_{-\infty}^{\infty} \cos(\frac{n\pi z}{L}) e^{jk_z z} dz + \sum_{n=1}^{N} \int_{-\infty}^{\infty} \sin(\frac{n\pi z}{L}) e^{jk_z z} dz \end{aligned} \tag{A.11}$$

Considering the fist integral in equation A.11, the cosine function is only defined over the interval $-\frac{L}{2}$ to $\frac{L}{2}$ and is otherwise zero, therefore can be written as

$$\begin{aligned} \sum_{n=0}^{N} \int_{-\infty}^{\infty} \cos(\frac{n\pi z}{L}) e^{jk_z z} dz &= \sum_{n=0}^{N} \int_{-\frac{L}{2}}^{\frac{L}{2}} \cos(\frac{n\pi z}{L}) e^{jk_z z} dz \\ &= \sum_{n=0}^{N} \frac{2(-1)^n \frac{n\pi}{L}}{(k_z^2 - (\frac{n\pi}{L})^2)} \cos(\frac{k_z L}{2}) \end{aligned} \tag{A.12}$$

Considering the second integral in equation A.11, the sine function is only defined over the interval $-\frac{L}{2}$ to $\frac{L}{2}$ and is otherwise zero, therefore can be written as

$$\begin{aligned} \sum_{n=1}^{N} \int_{-\infty}^{\infty} \sin(\frac{n\pi z}{L}) e^{jk_z z} dz &= \sum_{n=1}^{N} \int_{-\frac{L}{2}}^{\frac{L}{2}} \sin(\frac{n\pi z}{L}) e^{jk_z z} dz \\ &= \sum_{n=1}^{N} j \frac{2(-1)^n k_z}{(k_z^2 - (\frac{n\pi}{L})^2)} \cos(\frac{k_z L}{2}) \end{aligned} \tag{A.13}$$

Combining the two transforms with equation A.11, the Fourier transform of $\mathbf{J}_z$ is

$$\mathbf{J}_z(k_z) = \sum_{n=0}^{N} \frac{2(-1)^n \frac{n\pi}{L}}{(k_z^2 - (\frac{n\pi}{L})^2)} \cos(\frac{k_z L}{2}) + \sum_{n=1}^{N} j \frac{2(-1)^n k_z}{(k_z^2 - (\frac{n\pi}{L})^2)} \cos(\frac{k_z L}{2}) \tag{A.14}$$

Similarly, the Fourier transform of $\mathbf{J}_x$ can be derived as

$$\mathbf{J}_x(k_z) = \sum_{n=0}^{N} j \frac{2(-1)^n k_z}{(k_z^2 - (\frac{n\pi}{L})^2)} \cos(\frac{k_z L}{2}) + \sum_{n=1}^{N} \frac{2(-1)^n \frac{n\pi}{L}}{(k_z^2 - (\frac{n\pi}{L})^2)} \cos(\frac{k_z L}{2}) \tag{A.15}$$

A.3 Fourier Transform of Current Wave

The variation of the current distribution in the direction of current flow in the space domain is given by:

$$J_z(z) = \begin{cases} e^{-jk_n z} & \frac{L}{2} \leq z \leq \frac{L}{2} \\ 0 & \text{otherwise} \end{cases} \tag{A.16}$$

$$J_x(z) = \begin{cases} e^{-jk_n (z - \frac{\pi}{2})} & \frac{L}{2} \leq z \leq \frac{L}{2} \\ 0 & \text{otherwise} \end{cases} \tag{A.17}$$

where L is the length of the microstrip line and k_n is the precalculated wave constant. The case for the z–directed current considered first. Taking a Fourier transform in z direction with the transform

$$\begin{aligned} \mathbf{J}_z(k_z) &= \int_{-\infty}^{\infty} J_z(z) e^{jk_z z} dz \\ &= \int_{-\frac{L}{2}}^{\frac{L}{2}} e^{j(k_z - k_n)z} dz \end{aligned} \tag{A.18}$$

Considering the fist integral in equation A.11, the current wave function is only defined over the interval $-\frac{L}{2}$ to $\frac{L}{2}$ and is otherwise zero. The Fourier transform yields as,

$$\mathbf{J}_z(k_z) = \frac{2}{(k_z - k_n)} \cos(k_z - k_n) \tag{A.19}$$

Similarly, the Fourier transform of $\mathbf{J}_x$ can be derived as

$$\mathbf{J}_x(k_z) = \frac{j2}{(k_z - k_n)} \cos(k_z - k_n) \tag{A.20}$$

Appendix B

Two–Dimensional Version of SDM

B.1 Two–Dimensional Version of SDM

In this appendix, the two–dimensional formulation of SDM is used to precalculate the propagation constant k_n, and the transverse dependency of the z and x–directed currents on the microstrip is presented. The procedure is standard, but is outlined here in order to show how it fits in with the complex circuit calculation. Sinusoidal propagation is assumed in the z direction of the form $e^{-jk_z z}$ and the current distribution of the form in both directions

$$J(x,z) = e^{-jk_z z}(J_x(x)\hat{x} + J_z(x)\hat{z}) \tag{B.1}$$

where the functions J_x and J_z are now expanded so that

$$J_x(x) = \sum_{n=1}^{N} a_{xn} J_{xn}(x) \tag{B.2}$$

$$J_z(x) = \sum_{n=1}^{N} a_{zn} J_{zn}(x) \tag{B.3}$$

where

$$J_{xn}(x) = \begin{cases} 1 - \frac{|x-x_n|}{l_x} & x_n - l_x \le x \le x_n + l_x \\ 0 & \text{otherwise} \end{cases} \tag{B.4}$$

$$J_{zn}(x) = \begin{cases} 1 & x_n - l_x \le x \le x_n + l_x \\ 0 & \text{otherwise} \end{cases} \tag{B.5}$$

The electric field can be related to the surface current ($J_s(x)$) via the following integral equation in the spectral domain

$$\begin{bmatrix} \mathbf{G}_{zz} & \mathbf{G}_{zx} \\ \mathbf{G}_{xz} & \mathbf{G}_{xx} \end{bmatrix} \begin{bmatrix} \mathbf{J}_z \\ \mathbf{J}_x \end{bmatrix} = \begin{bmatrix} \mathbf{E}_z \\ \mathbf{E}_x \end{bmatrix} \tag{B.6}$$

where

$\mathbf{G}(k_x, d, k_z, \omega)$ is the dyadic Green's function in the spectral domain,
$\mathbf{J}_z$ is the Fourier transform of the z–directed surface current density,
$\mathbf{J}_x$ is the Fourier transform of the x–directed surface current density,
$\mathbf{E}$ is the Fourier transform of the electric field.

Because the calculations take place in the spectral domain, current basis functions (equation B.3) must be transformed into the spectral domain by using the Fourier transform equation which is defined as

$$\boldsymbol{\phi}(k_x) = \int_{-\infty}^{\infty} \phi(x) e^{jk_x x} dx \tag{B.7}$$

To solve equation B.1, the Method of Moments is applied. This eliminates the unknown Fourier transform of the electric field ($\mathbf{E}$) from the formulation. Inner products are now taken by using a set of weighting functions which are identical to the set of current basis functions (Procedure of Galerkin's).

$$\begin{bmatrix} \mathbf{Z}_{zz} & \mathbf{Z}_{zx} \\ \mathbf{Z}_{xz} & \mathbf{Z}_{xx} \end{bmatrix} \begin{bmatrix} a_z \\ a_x \end{bmatrix} = \begin{bmatrix} \mathbf{0} \end{bmatrix} \tag{B.8}$$

the elements of the impedance matrix $\mathbf{Z}$ are given by

$$\mathbf{Z}_{st} = \int_{-\infty}^{\infty} \mathbf{J}_t(k_x) \mathbf{G}(k_x, k_z, d, \omega) \mathbf{J}_s(k_x) dk_x \tag{B.9}$$

The matrix equation B.8 is solved for the propagation constant k_n in the z direction by an iterative search for k_z, solving for the determinant of the impedance matrix equal to zero. The set of unknown current coefficients (a_n) and thus the precalculated surface current distribution in the direction perpendicular to current flow are obtained as elements of an eigenvector for the wave constant (k_n). The set of coefficients and k_n are stored to use in the complex microwave circuit calculation.

Appendix C

Derivation of Asymptotic Form of Green's Function

C.1 Derivation of Asymptotic Form of Green's Function

For the large Fourier transform variables, these approximations can be applicable to the dyadic Green's function,

$$\begin{aligned} Coth\gamma_2 d &\approx 1 \\ \gamma_i = \sqrt{k_x^2 + k_z^2 - k_i^2} &\approx \sqrt{k_x^2 + k_z^2} \end{aligned} \tag{C.1}$$

the above approximations simply the Green's function as,

$$\begin{aligned} \mathbf{G}_{zz}^{\infty} &= \frac{1}{k_x^2 + k_z^2}(k_z^2 \mathbf{Z}_e^{\infty} + k_x^2 \mathbf{Z}_h^{\infty}) & \mathbf{G}_{zx}^{\infty} &= -\frac{k_x k_z}{k_x^2 + k_z^2}(\mathbf{Z}_e^{\infty} - \mathbf{Z}_h^{\infty}) \\ \mathbf{G}_{xz}^{\infty} &= \mathbf{G}_{zx}^{\infty} & \mathbf{G}_{xx}^{\infty} &= \frac{1}{k_x^2 + k_z^2}(k_x^2 \mathbf{Z}_e^{\infty} + k_z^2 \mathbf{Z}_h^{\infty}) \end{aligned}$$

The asymptotic form of the Green's function thus obtained can be arranged in a closed form as follows,

$$\mathbf{G}_{st}^{\infty} = h_1 \mathbf{K}_{st1}^{\infty} + h_2 \mathbf{K}_{st2}$$

where

$$
\begin{aligned}
h_1 &= -\frac{j}{\omega\epsilon_0(1+\epsilon_r)} & h_2 &= \frac{j\omega\mu_0\mu_r}{(1+\mu_r)} \\
\mathbf{K}^{\infty}_{zz1} &= \frac{k_z^2}{\sqrt{k_x^2+k_z^2}} & \mathbf{K}^{\infty}_{zz2} &= \frac{k_z^2}{\sqrt{(k_x^2+k_z^2)^3}} \\
\mathbf{K}^{\infty}_{zx1} &= -\frac{k_x k_z}{\sqrt{k_x^2+k_z^2}} & \mathbf{K}^{\infty}_{zx2} &= \frac{k_x k_z}{\sqrt{(k_x^2+k_z^2)^3}} \\
\mathbf{K}_{xz1} &= \mathbf{K}_{zx1} & \mathbf{K}_{xz2} &= \mathbf{K}_{zx2} \\
\mathbf{K}^{\infty}_{xx1} &= -\frac{k_x^2}{\sqrt{k_x^2+k_z^2}} & \mathbf{K}^{\infty}_{xx2} &= -\frac{k_x^2}{\sqrt{(k_x^2+k_z^2)^3}}
\end{aligned}
\tag{C.2}
$$

Appendix D

Excitation

D.1 Fourier Transforms of Basis Functions for Feedlines

The travelling current wave has been chosen in this thesis to be current basis functions of the feedlines. The derivations of incident reflected and transmitted current waves from the travelling wave in the direction of propagation are given in the space domain by;

$$J_i(z) = \begin{cases} e^{-jk_n(z-z_i)} & -L+z_i \leq z \leq z_i \\ 0 & \text{otherwise} \end{cases} \tag{D.1}$$

$$J_r(z) = \begin{cases} -a_r e^{jk_n(z-z_i)} & -L+z_i \leq z \leq z_i \\ 0 & \text{otherwise} \end{cases} \tag{D.2}$$

$$J_t(z) = \begin{cases} a_t e^{-jk_n(z-z_o)} & z_o \leq z \leq L+z_o \\ 0 & \text{otherwise} \end{cases} \tag{D.3}$$

The case for the incident current wave in equation D.1 is considered first. Taking the Fourier transform in the direction of propagation (z direction) with the transform

$$\mathbf{J}_i(k_x, k_z) = \int_{-\infty}^{\infty} J_i(z) e^{jk_z z} dz \tag{D.4}$$

The incident current wave is only defined over an interval $-L+z_i$ to z_i equal to a travelling wave in $+z$ direction and is otherwise zero, therefore can be written as,

$$\begin{aligned} \mathbf{J}_i(k_z) &= \int_{-L+z_i}^{z_i} e^{-jk_n(z-z_i)} e^{jk_z z} dz \\ &= \frac{2}{k_z - k_n} \sin\left((k_z - k_n)\frac{L}{2}\right) e^{-j(k_z-k_n)\frac{L}{2}} e^{jk_z z_i} \end{aligned} \tag{D.5}$$

The Fourier transform of the reflected current wave in equation D.2 is calculated by;

$$\mathbf{J}_r(k_x, k_z) = \int_{-\infty}^{\infty} J_r(z) e^{jk_z z} dz \tag{D.6}$$

The reflected current wave is defined over the identical interval to incident current wave, thus can be written as,

$$\begin{aligned} \mathbf{J}_r(k_z) &= \int_{-L+z_i}^{z_i} e^{jk_n(z-z_i)} e^{jk_z z} dz \\ &= \frac{2}{k_z + k_n} sin\left((k_z + k_n)\frac{L}{2}\right) e^{-j(k_z+k_n)\frac{L}{2}} e^{jk_z z_i} \end{aligned} \tag{D.7}$$

Similarly, the Fourier transform of the transmitted current wave in equation D.3, defined over an interval z_o to $L + z_o$, can be written as

$$\begin{aligned} \mathbf{J}_t(k_z) &= \int_{z_o}^{L+z_o} e^{-jk_n(z-z_o)} e^{jk_z z} dz \\ &= \frac{2}{k_z - k_n} \sin\left((k_z - k_n)\frac{L}{2}\right) e^{j(k_z-k_n)\frac{L}{2}} e^{jk_z z_o} \end{aligned} \tag{D.8}$$

Copy of Publications